1-1-2016

Space Solar Power Satellite Systems, Modern Small Satellites, And Space Rectenna

Corey Marvin Bergsrud

SPACE SOLAR POWER SATELLITE SYSTEMS, MODERN SMALL SATELLITES, AND SPACE RECTENNA

by

Corey Alexis Marvin Bergsrud
Bachelor of Science, University of North Dakota, 2009
Master of Science, University of North Dakota, 2012

A Dissertation

Submitted to the Graduate Faculty

of the

University of North Dakota

In partial fulfillment of the requirements

for the degree of

Doctor of Philosophy

Grand Forks, North Dakota
May
2016

This dissertation, submitted by Corey Alexis Marvin Bergsrud in partial fulfillment of the requirements for the Degree of Doctor of Philosophy from the University of North Dakota, has been read by the Faculty Advisory Committee under whom the work has been done and is hereby approved.

S. Noghanian
Name of Chairperson

Name of Chairperson

Yen Lee Loh
Name of Committee Member

Name of Committee Member

Name of Committee Member

Ronald Ferry
Name of Committee Member at Large

This dissertation is being submitted by the appointed advisory committee as having met all of the requirements of the School of Graduate Studies at the University of North Dakota and is hereby approved.

Wayne Swisher
Dean of the School of Graduate Studies

May 12, 2016
Date

PERMISSION

Title	Space Solar Power Satellite Systems, Modern Small Satellites, and Space Rectenna
Department	Electrical Engineering
Degree	Doctor of Philosophy

In presenting this dissertation in partial fulfillment of the requirements for a graduate degree from the University of North Dakota, I agree that the library of this University shall make it freely available for inspection. I further agree that permission for extensive copying for scholarly purposes may be granted by the professor who supervised my dissertation work or, in her absence, by the Chairperson of the department or the dean of the School of Graduate Studies. It is understood that any copying or publication or other use of this dissertation or part thereof for financial gain shall not be allowed without my written permission. It is also understood that due recognition shall be given to me and to the University of North Dakota in any scholarly use which may be made of any material in my dissertation.

Corey Alexis Marvin Bergsrud

4/29/2016

TABLE OF CONTENTS

LIST OF FIGURES

LIST OF TABLES

ACKNOWLEDGMENTS

So many people have helped in the making of this work. My longtime academic advisor (Dr. Sima Noghanian) for my MS and PhD work is acknowledged first for setting the stage with opportunity into the exciting field of electromagnetics. This work really began back in spring semester of 2007 when I was a math major and took a circuits class with lab. The lab class required a class project. Since my interest is in energy I decided to pursue energy technologies. The idea I came up with was called "Multi-Combinational Renewable Energy Efficient Generator (MCREEG)". This concept was to integrate multiple sources of energy harvesters (wind, solar, water, etc.) onto a single platform. I later gathered a team composed of electrical and mechanical engineers to help build-up the concept. These folks are acknowledged: Jonathan Alme (EE), Armen Mkrtchyan (EE), Joshua Goldade (EE), Phillip Siemieniewski (ME), and another ME student whose name I cannot recall. This group worked together for one semester and presented our concept of MCREEG to the student body senate. At that time Tyrone Grandstrand was student president and is acknowledged for allowing us to speak to an audience about our new concept at a student senate meeting.

The MCREEG concept was furthered explored in the fall semester of 2009 when I took a political science course called environmental politics. Professor Robert Wood allowed me and a group of three to do a class project on MCREE. Those students; Erik Littleton, Nick Svobodny, and Joseph Lassonde and Professor Wood are acknowledged.

My research with space solar power satellites really began in the spring semester of 2010 when I took an Energy Law class. For the class it was required to do a research project. The research project I choose was space based solar power satellites. At that time the idea was to generate power on Earth using MCREEG and transmit the power to a satellite in space that redirects the energy back to Earth. Professor Joshua Fershee is acknowledged for allowing me to pursue this topic for my class project. Mojdeh Mardani is acknowledged for attending the presentation in support of my work.

Next came entering the PhD program in engineering at UND. My research topic was on space solar power satellites. Dr. Sima Noghanian is acknowledged for allowing me to pursue the topic of interest. In the spring of 2012 a group I put together a team at UND from three different departments to compete in the SunSat Design Competition. The competition that took place at the International Space Development Conference in Washington, D.C. These team members are acknowledged: Timothy Dito, Matthew Anderson, Matthew Clausing, Chase Freidig, Sima Noghanian, Hossein Salehfar, Isaac Chang, James Casler and Ron Fevig. Also Don Flournoy and Kyle Perkins at Ohio University are acknowledged as the main organizers of the SunSat Design Competition.

After the presentation I received an email from Paul Jaffe NCST Systems Integration Section Head at Naval Research Laboratory. In that email he asked for my slides and mentioned he is also working on SSP for his dissertation work. I was quite excited to be emailed from Paul. Since then Paul has been a contact for me and actually ended up being a part of my dissertation committee. Paul has also became a friend. Paul Jaffe is acknowledged for his many contributions to SSP work as well as providing me mentoring throughout my work.

During the ISDC-2012 conference I also meet Darel Preble. Darel then passed my name to Christopher Valenta at Georgia Tech. Both Darel and Chris have been in contact since this time and both are acknowledged for their contributions into SSP and wireless power. Darel is the current director of the space solar power institute and has provided opportunities for students to continue to grow SSP concepts. I have reached out to Chris a number of times as well over the years for his knowledge and expertise in wireless harvesting circuits. I greatly appreciate both of you for these opportunities and sharing experience to help answer difficult questions.

The summer of 2012 Sima Noghanian presented an opportunity for a NASA travel grant. I was responsible for finding and reaching out for a contact as well as writing the short proposal for why this travel grant should be supported. The travel award was awarded and Geoffrey Landis at NASA Glenn research center is acknowledged for accepting the invitation and for his tour at NASA Glenn research center. Dr. Landis has since continued to be a contact of mine that I have reached out to with questions related to my research. Sima Noghanian is again acknowledged for presenting me this opportunity.

The next opportunity came in the spring semester of 2014 when again I gathered a team composed of five different departments to compete in the SunSat Design Competition. Those team members are acknowledged: Robert Bernaciak, Ben Kading, John McClure, Jeremy Straub, Subin Shahukhal, Karl Williams, Elizabeth Becker, James Casler Jeremiah Neubert, Sima Noghanian, Hossein Salehfar, and David Whalen. Again Don Flournoy and Kyle Perkins at Ohio University are acknowledged as the main organizers of the SunSat Design Competition.

Then at the end of the fall semester of 2014 and until now I have worked with Sofiane Chaieb on advancing SSP concept work. He was my intern in the spring semester of 2015 and we worked together to come up with a new hybrid electrical power system for a spacecraft equipped with microwave power receiving hardware. During that short time Sofiane and I along with others submitted two journal papers.

Also, during the spring semester of 2015 I started to reach out to James McSpadden at Raytheon Space and Airborne System in regards to specific research questions. I meet James at an IEEE A&P Conference in the summer of 2014 held in Memphis, TN. He has provided me the greatest insight into rectenna design and I greatly appreciate his mentorship during the process.

I want to acknowledge Siby Plathottam as a great friend to me and for our political and intellectual conversations we have had. I also want to thank my first science mentor Dr. Alvason Li. I remember still the lessons you have taught me my friend. Finally, I would like to thank my first internship mentor, Dr. Qamar Shams for his continued support throughout my academic career.

To Kayla Rose Thompson and Zac Moen,

you are not forgotten.

To humanity,

let this work help guide you in the future.

To my mom and dad, family, and friends thank you for the

values you have taught me.

ABSTRACT

Space solar power satellite (SSPS) systems is the concept of placing large satellite into geostationary Earth orbit (GEO) to harvest and convert massive amounts of solar energy into microwave energy, and to transmit the microwaves to a rectifying antenna (rectenna) array on Earth. The rectenna array captures and converts the microwave power into usable power that is injected into the terrestrial electric grid for use. This work approached the microwave power beam as an additional source of power (with solar) for lower orbiting satellites. Assuming the concept of retrodirectivity, a GEO-SSPS antenna array system tracks and delivers microwave power to lower orbiting satellites. The lower orbiting satellites are equipped with a stacked photovoltaic (PV)/rectenna array hybrid power generation unit (HPGU) in order to harvest solar and/or microwave energy for on-board use during orbit. The area, and mass of the PV array part of the HPGU was reduced at about 32% beginning-of-life power in order to achieve the spacecraft power requirements. The HPGU proved to offer a mass decrease in the PGU, and an increase in mission life due to longer living component life of the rectenna array. Moreover, greater mission flexibility is achieved through a track and power delivery concept.

To validate the potential advantages offered by a HPGU, a mission concept was presented that utilizes modern small satellites as technology demonstrators. During launch, a smaller power receiving “daughter” satellite sits inside a larger power transmitting “mother” satellite. Once separated from the launch vehicle the daughter

satellite is ejected away from the mother satellite, and each satellite deploys its respective power transmitting or power receiving hardware's for experimentation. The concept of close proximity mission operations between the satellites is considered.

To validate the technology of the space rectenna array part of the HPGU, six milestones were completed in the design. The first milestone considers thermal analysis for antennas, and the second milestone compares commercial off-the-shelve high frequency substrates for thermal, and outgassing characteristics. Since the design of the rectenna system is centralized around the diode component, a diode analysis was conducted for the third milestone. Next, to efficiently transfer power between the different parts of the rectenna system a coplanar stripline was consider for the fourth milestone. The fifth milestone is a balanced-to-unbalanced transition structure that is needed to properly feed and measure different systems of the rectenna. The last milestone proposes laboratory measurement setups. Each of these milestones is a separate research question that is answered in this dissertation. The results of these rectenna milestones can be integrated into a HPGU.

CHAPTER I

INTRODUCTION

Numerous studies [1-3] indicate that between the years 2050-2100, disruptive solutions need to be in place for population, energy, and environment sustainability. Although the term "sustainable" for population and energy maybe an oxymoron since population continues to grow but fossil fuel resources continue to decline. Therefore, it is practically impossible to sustain with fossil resources over a long time since the interrelation and dependency of one without the other cannot be held forever. So humanity should look to space as a solution to replenish our resources and to drive new innovations and economics. In particular, SSPS systems offer the opportunity to supply clean base load electrical power from space to Earth via microwaves almost indefinitely year round for millennia to come.

This dissertation begins by setting forth the motivation for this research endeavor in terms of population, energy and environment. Cheap and abundant fossil energy has driven accelerated growth in human population over the last century. During this exponential growth period fossil fuels, particularly coal, have been rapidly burned to supply the bulk of humanity's electrical energy. Even though the rate of population growth is slowing down, the same is not true for the burning of coal as modernized comforts continue to expand throughout the World. Because of the burning of coal for this length in time and at this rate the side effect is Global Warming prompting Global

Climate Changes. As humanity enters the coming time period 2050-2100 solutions to the over-arching problems of population, energy, and the environment need to be in motion as the motivation section will show.

Immediately following Chapter II Motivation comes Chapter III Problem Statement and Scope. The question that this dissertation work evolves from, is whether lower orbiting satellites can benefit from the available microwave energy sent from a possible future GEO-SSPS? The results of that analysis showed promise in a stacked hybrid solar PV/rectenna array power generation unit (HPGU). In order to practically realize the analytical findings of this HPGU a second hypothesis was proposed where the dissertation work pursues the idea of using modern small satellites as technology demonstrators to validate the proposed HPGU.

Chapter IV covers a literature review and is broken into four subsections. Subsection 4.1 begins by providing a brief historical background on microwave wireless power and relevant SSPS system developments and applications. Subsection 4.2 provides literature work focused on space-to-space microwave wireless power transmission experiments. Subsection 4.3 provides three rectenna element designs that were used as a guide in this dissertation. Subsection 4.4 provides a brief literature review on hybrid power generation systems that utilizes RF and solar.

This document then proceeds into the Chapter V Methods. To begin to study the first problem statement the term “power beam medium” is introduced in Section 5.1. Power beam medium is referred to as a volume of energy sent from the GEO-SSPS to Earth in a static case or from a GEO-SSPS to lower orbiting satellites in a dynamic case. The power beam medium was analyzed based on previous reference systems [4, 5] in

order to calculate power density and Airy disk. The analysis of the power beam medium provides a calculated understanding of the environment within the power beam medium in order to predict what amount of power is available within an area for various orbits within the power beam medium.

Section 5.2.1 investigates a possible beneficial opportunity for lower orbiting spacecraft to take advantage of this now additional available source of energy in orbit for use on-board. In order to harvest the microwave energy a technology called a rectifying antenna (rectenna) array is needed. The idea of equipping a rectenna array on a satellite for harvesting of RF energy coming from the GEO-SSPS as the satellite orbits through the beam in a static case or the beam is directed at the satellite in the case of a dynamic beam.

Three types of PGUs were compared, i.e., solar PV array, rectenna array, and a hybrid solar PV/rectenna array, in this analysis based on efficiency, mass, area, and component life. It was found that a HPGU with a dynamic power beam medium scenario offers perspective benefits in terms of reducing the mass of the PGU or reallocation of the mass to other sub-systems, increased mission life because of reduced dependency on solar PV arrays, and greater mission flexibility because an additional source of power would be available. The concept of a dynamic power beam medium scenario is that a GEO-SSPS can track and deliver power to other spacecraft via a pilot signal.

In order to practically realize the analytical findings of the HPGU with a dynamic power beam medium scenario, Section 5.3 provides the answer to the following hypothesis: “modern small satellites can be used as technology demonstrators for the proposed stacked hybrid PV/rectenna array PGU.” Modern small satellites offer much

lower cost than conventional satellites [6]. Modern small satellites also offer much reduced time of development and launch compared to conventional large satellite [6]. Therefore, their use as a technology demonstrator seems a logical path.

Thus, a novel mission utilizing two modern small satellites was designed where a smaller power receiving daughter satellite sits inside a larger power transmitting mother satellite during launch. Once in orbit and separated from the launch vehicle the daughter satellite is ejected from the mother satellite and both satellites deploy their respective power receiving or power transmitting hardware. The two satellites would utilize the concept of close proximity operations in order to maintain relative distance to each other for the lifetime of the mission. The mission would consider a Sun-synchronous circular orbit with an altitude of 500 km, an inclination of 97.4°, Sun angle of 0°, and a 94.4 minute orbit (35.9 minutes in eclipse + 58.5 minutes in daylight). A detailed experimental mission design is provided including orbital parameters, aperture-to-aperture efficiency, and the design of an electrical power system (EPS).

Section 5.3.3 and 5.3.4 investigates the design of an EPS for both the mother and daughter satellites, respectively. An EPS generates, stores, manages, and distributes electrical power for the satellite. Therefore, an EPS is composed of a PGU, PSU, and a PMADU. To best address both hypotheses, the EPS design for the daughter satellite was explored in greater detail compared to the mother satellite because it is proposed to be equipped with the payload of interest, i.e., a HPGU. A 3U (termed 3 unit) Cube satellite (CubeSat) was selected as the form factor for the daughter satellite design. The role of the PV array part of the HPGU is to harvest enough solar energy during the daylight part of the daughter satellite's orbit to ensure continued operations. The rectenna array part of

the HPGU is an experimental payload designed to harvest microwave energy transmitted from the mother satellite during the eclipse part of orbit.

As the rectenna array part of the HPGU is the payload of interest, it is explored in greater detail in Section 5.4. A rectenna is an electrical system that consist of various parts including an antenna – to capture the microwave energy, filter + matching circuit – to match the real impedance of the diode to the real impedance of the antenna and to filter out higher order harmonics coming from the diode, and a rectifier (diode + capacitor) – converts microwaves-to-direct current (DC) power.

A novel approach is taken in the study and design of rectenna by incorporating conditions of space. Therefore, the first milestone is thermal analysis for antennas, and the second milestone is a material analysis considering thermal and outgassing characteristics. Since the design of the rectenna system is centralized around the diode component a diode analysis was conducted for the third milestone. To efficiently transfer power between the different parts of the rectenna system a coplanar stripline was consider for the fourth milestone. The fifth milestone is a balanced-to-unbalanced transition structure that is needed to properly feed and measure the different systems of the rectenna. The last milestone proposes laboratory measurement setups. Each of these milestones set up a research question that is answered in this dissertation. The pieces of rectenna that were designed in this work can be integrated into a HPGU.

To capture the RF power an antenna is needed. Logically, the first question to address is what type of antenna option is best for the rectenna part of the HPGU equipped on a modern small satellite? A printed circuit board microstrip antenna design seems a logical fit for the application because of its low profile and low mass. Several printed

antenna designs were considered in Section 5.4.1 including an aperture coupled fed antenna. The aperture coupled fed antenna was designed and simulated using Computer Simulation Technology-Microwave Studio (CST-MWS) software. Part of that study incorporated change in dielectric constant due to a change in temperature. The multiple layers of the aperture coupled antenna are quite complex, and leads to greater fed losses. Therefore a shift in antenna design was decided

Coplanar stripline (CPS) fed antennas offers many benefits in the printed antenna design such as efficiency in transferring power between circuit components, and easier to realize high impedance, compared to other structures. Various CPS fed antenna architectures were studied in the literature. A dual rhombic loop antenna (DRLA) was selected as the antenna of choice because of its high gain, circular polarization capability, and ease of array design. The DRLA was designed using ANSYS Ansoft HFSS. However, to properly measure the antenna a filter must be integrated with the antenna. Filter study was not performed, and so the design of the antenna plus filter was never reached.

Section 5.4.2 studied five different Rogers Corporation substrate materials in order to determine the best fit material for the printed rectenna for space application. Two specifications were considered in the analysis, out-gassing and thermal stability. RT/duroid 6002 material had the best performance for space applications due to its thermal stability over a large temperature fluctuation. Moreover, material for bonding and constructing prototypes were studied. Rogers 2929 bondply was selected as the layer bonding material as it had the same dielectric constant as the RT/duroid 6002, as well as good temperature stability property. For constructing the prototypes, 71HERO foam

material from Evonik Foams, Inc. was selected because of its strength, low mass, low dielectric constant value, and thermal properties. All these materials were selected based on analysis (performance data) and discussions with the companies to ensure the best material for the application of in-space power reception experiments.

The next order of rectenna array development was diode analysis covered in Section 5.4.4. The diode is the first component in the rectenna system to be analyzed, because all other parts of the rectenna system are designed around the diode component's characteristics. Closed-form equations were used in order to conduct diode analysis and to predict the input power level and RF-to-DC conversion efficiency. These equations have proven to be accurate in numerous rectenna measured designs. The assumption is that the remaining parts of the system are matched/placed appropriately.

In order to understand the effects of the key diode parameters nine diodes were selected for comparison. The deciding factor in the selection of the diode component is the highest RF-to-DC conversion efficiency. Yokowo Co., Ltd. Diode showed the highest RF-to-DC conversion efficiency. This diode was selected to design the rectenna system. Moreover, the Yokowo diode allows much greater input power compared to the other options and has a high low-power RF-to-DC conversion ability as well. From the diode analysis an important result that was generated was the diodes real and imaginary impedance values as a function of load resistance. The reason why this is so important will be touched on next. The GaAs material of the diode makes it suitable for space. However, more research and experimentation needs to be conducted both in space and on Earth to determine its reliability in the conditions of space.

Section 5.4.5 covers the CPS structure part of the rectenna system. The CPS structure was the technique chosen to transfer power efficiently between the different components of the rectifier part (diode, capacitor, and load resistor) of the rectenna. The CPS technique was chosen over other techniques as it offers benefits to efficiently transfer power between rectenna components, and it is easier to achieve high impedance values compared to the other techniques.

Since the CPS structure cannot be measured directly, it was modeled in ANSYS Ansoft HFSS electromagnetic software in order to extract its characteristic impedance ($Z_{o,CPS}$). The CPS model in ANSYS Ansoft HFSS was studied in terms of dielectric constants (i.e. different substrate materials), substrate thickness, conducting metal thickness, and total attenuation losses. The conclusion was that higher $Z_{o,CPS}$ can be achieved with a lower dielectric constant, thinner substrate material, and thinner conducting metal thickness. It was also found that the greater the separation gap between the two striplines of the CPS the lower the total attenuation and the higher the impedance of the structure. All these CPS studies are important design parameters because they help in the design process in achieving the highest RF-to-DC conversion efficiency objective.

Now that the diodes real and imaginary impedance values, and $Z_{o,CPS}$ are known we set the diodes real impedance equal to $Z_{o,CPS}$ in order to determine the load resistance value. With this information the RF-to-DC rectification efficiency can now be calculated with a high degree of accuracy to the realized rectenna element as numerous works [7-9] have proven. This is an important step in the analysis as the diode and load resistor information was used to compare the nine different diodes on their RF-to-DC conversion efficiencies.

Section 5.4.6-5.4.19 pursued the design of a balanced-to-unbalanced (Balun) transition structure. This structure is a tool that allows all other parts of the rectenna element system (rectifier, antenna + filter, and rectenna) to be fed and measured properly for the CPS architecture. A novel Klopfenstein tapered step impedance technique was used to match the 50-Ω fed to $Z_{o,CPS}$. Then a CPS-to-Klopfenstein taper back-to-back transition was designed and measured in order to ensure the frequency of interest was passed through the circuit with low loss. This goal was achieved.

Section 5.4.10 maps out various setups to measure the different parts of the rectenna in the laboratory. A number of figures with block diagrams for experimental setups are provided. A novel experimental concept is proposed for testing the rectenna by imposing changes in temperature in order to measure the effects on the rectenna output. Most of the experimental equipment was obtained through grants and awards acquired through part of this research.

CHAPTER II

MOTIVATION: POPULATION, ENERGY, AND ENVIRONMENT

Abundant and cheap energy resources from fossil fuels have been rapidly extracted and burned by humanity over the last century, catalyzing human population growth. These two underlying correlations, energy and population growth, have impacted Earth's systems enough to cause global temperature rise leading to global climate changes. This chapter highlights population and how it correlates with energy, and the environment. This is a necessary chapter as it sets the stage for why humanity should invest in SSPS system endeavors. This chapter highlights the "big picture" motivation for this research which is to ultimately help advance the concepts of SSPS systems.

2.1 Population

Over the last 150 years or so the abundant, and cheap fossil energy resources has rapidly driven human population growth, as seen in Figure 1. However, "according to the limits-to-growth argument, the human population is outrunning the Earth's capacity to support it" – Judith A. Layzer [10]. Moreover, Bradshaw and Brooks [2] built deterministic population models to explore human population dynamics by comparing the "sensitivity of population trajectories to plausible and even unlikely social phenomena, and consider how these might influence long-term human demography." Their models demonstrated that the current momentum of the global human population cannot be fixed quickly in order to mitigate the problems to obtain global sustainability. Bradshaw and

Brooks mentioned that major solutions toward global sustainability should be underway by 2050 and ideally solved by 2100.

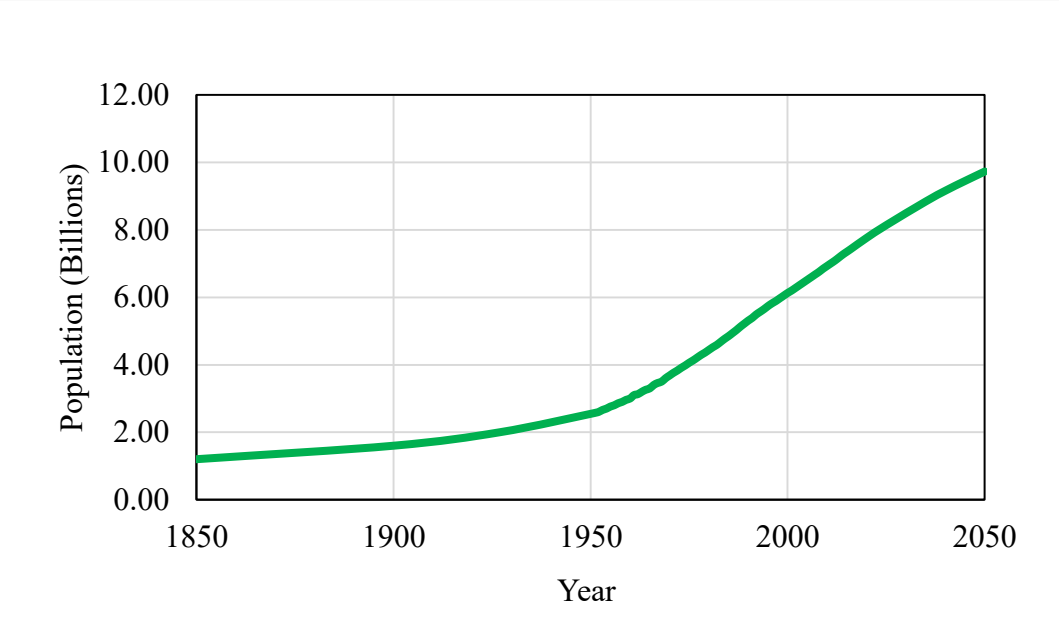

Figure 1. Population growth since 1850, and estimated up to 2050. Source: Worldometers (www.Worldometers.info)Elaboration of data by United Nations, Department of Economic and Social Affairs, Population Division. World Population Prospects: The 2015 Revision. (Medium-fertility variant).

2.2 Energy and the Environment

Even though global population growth rate is slowing down as indicated in Figure 2, the same is not true for energy consumption, as indicated in Figure 3. This is because the world's per capita energy demand has been steadily increasing over the last century, fueled by modern life styles. However, fossil fuels are finite resources, hence not sustainable over time, and according to the BP Statistical Review of World Energy 2015 the reserves-to-production (R/P) ratio indicates about five decades of global oil and natural gas remaining and about eleven decades of global coal remaining as indicated in Table 1. This ratio is used by companies and government agencies in forecasting the

future availability of a resource to determine whether more exploration must be undertaken to ensure continued supply of the resource. Although, the resource itself will become more expensive to extract.

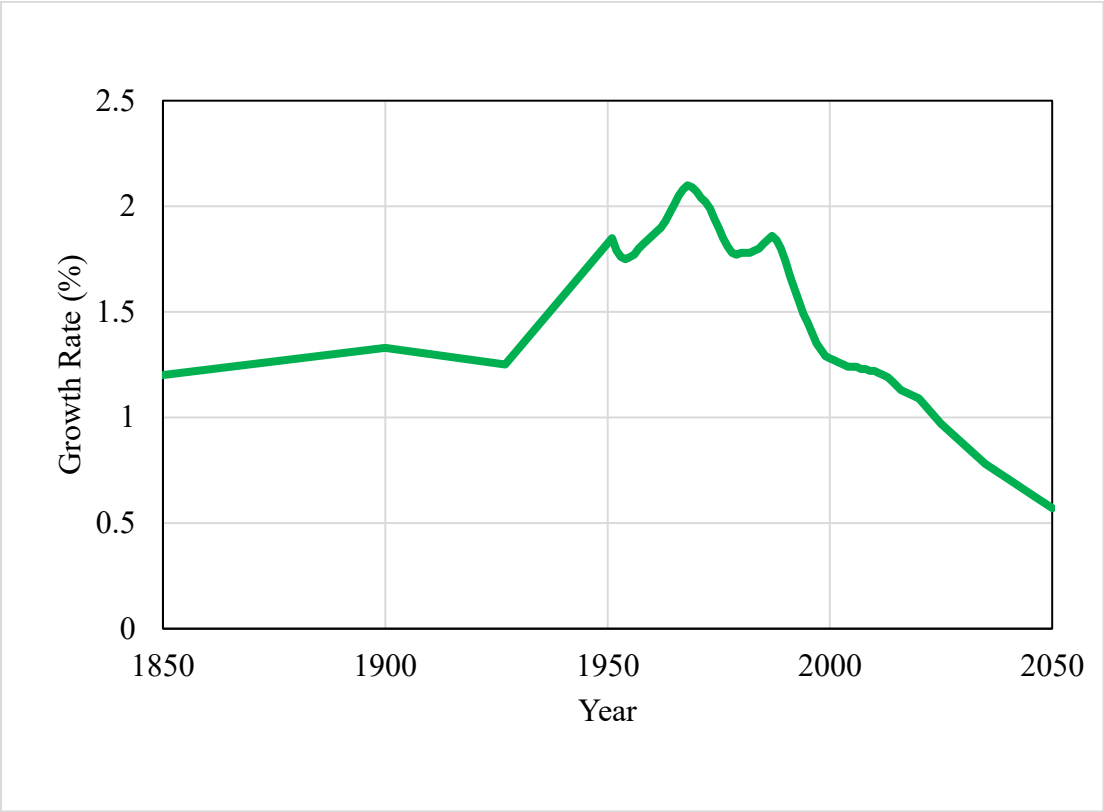

Figure 2. World population growth rate from 1850-2050 [11]. After 2015, projections are used.

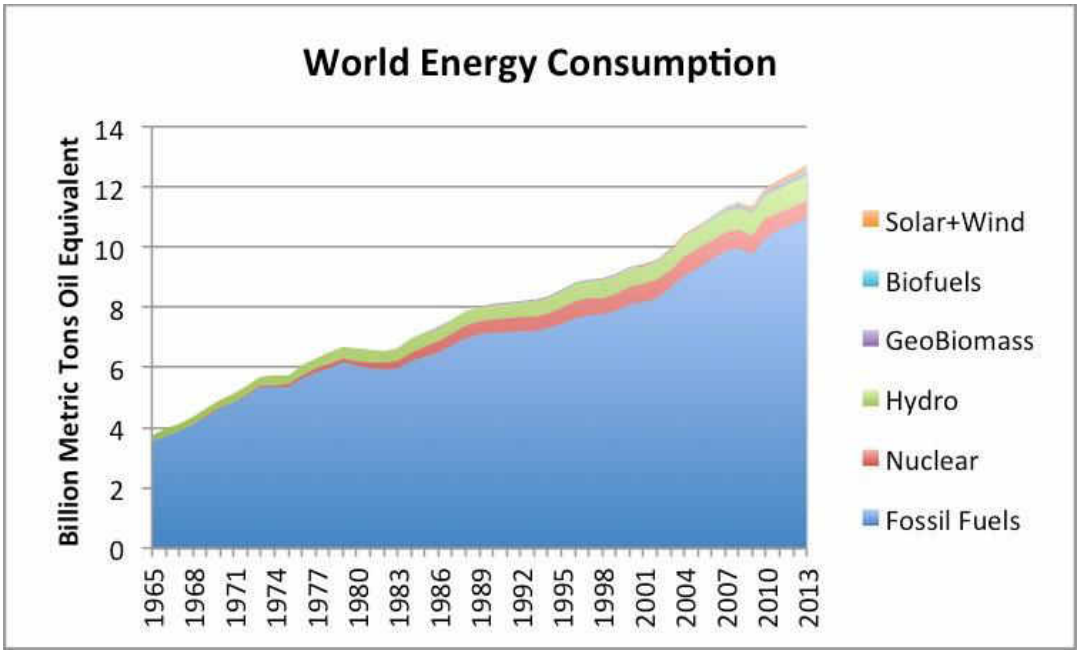

Figure 3. World energy consumption for various energy sources. Credit to Gail Tverberg for putting this graph together from data acquired from BP Statistical Review of World Energy – 2014 edition.

Table 1. Source of Energy and its World R/P ratio. Source: BP Statistical Review of World Energy – 2015.

Source	R/P Ratio (Years)
Coal	110
Natural Gas	54.1
Oil	52.5

The industrial scale burning of fossil fuels for energy has correlated with increasing concentration of Carbon Dioxide (CO_2) in the atmosphere as indicated in Figure 4. Today's CO_2 level is about 400 ppm or a 33% increase from what is possibly the Earth's normal peak CO_2 level (300 ppm) cycle [12], as shown in Figure 5. As

indicated in Figure 5, for 650,000 years the CO_2 levels in the atmosphere has never been above 300 ppm. This change or shift in CO_2 levels has been identified as one of the primary contributors to global warming by a majority of the world's scientists. What this means is that humanity cannot continue to burn fossil fuels at the same rate it has been burnt over the last century in order to quench its burgeoning energy needs. The bottom line is that fossil fuels are not a sustainable energy resource for future generations and there is need for disruptive energy technologies to replace them.

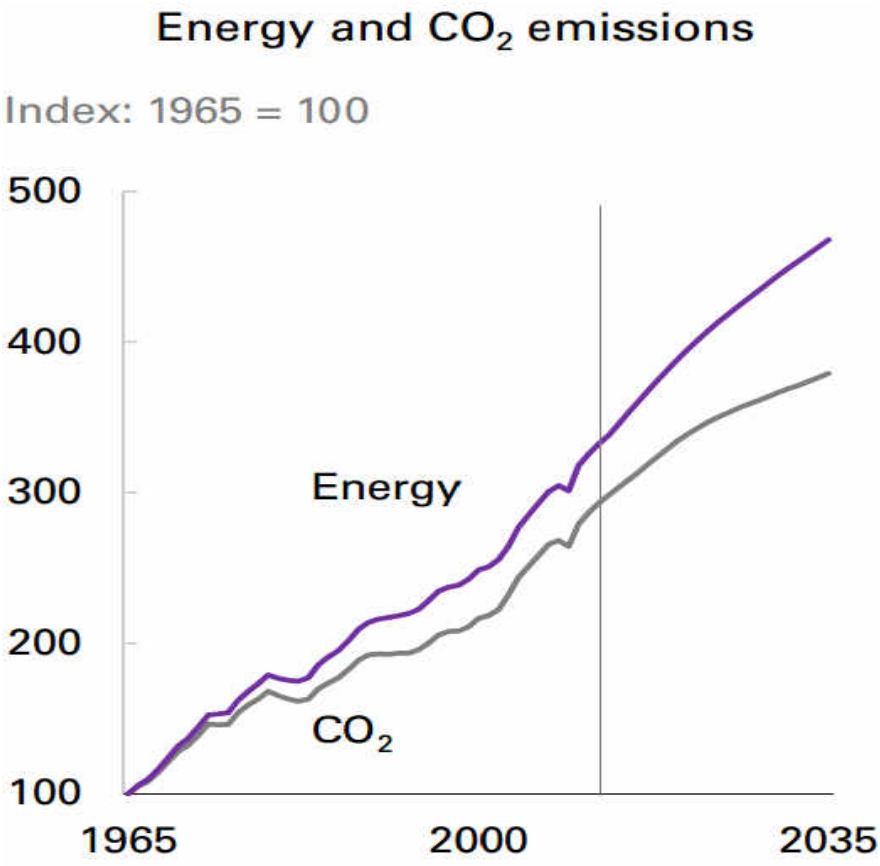

Figure 4. Energy and CO_2 emissions. Source: BP Energy Outlook 2035.

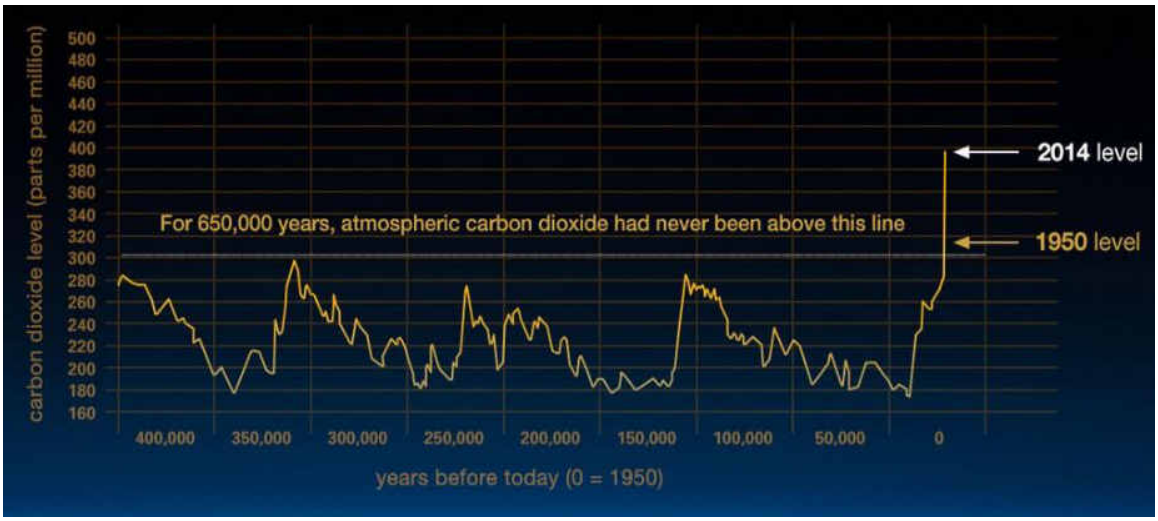

Figure 5. Atmospheric CO_2 levels as a function of time. Credit: Vostok ice core data/J.R. Petit et al., NOAA Mauna Loa CO_2 record.

2.3 Solution: Invest in Space Endeavors

In order to sustain humanity's energy future, and to reduce atmospheric CO_2 over time, it makes sense to build a machine that continually harvest solar energy from our sun. In fact, our star has unlimited energy. A SSPS is a machine to do just that. Since many researchers have focused on the GEO-SSPS, as well as the ground rectenna array, this work looked at the microwave beam space environment stretching from a GEO-SSPS to Earth or to lower orbiting satellites.

This research viewed the microwave beam from a GEO-SSPS as an additional source of power for satellites. The question then was if this new source of power can play a meaningful role for future satellites. To address this question the space environment with a microwave beam was studied first. The results indicated that a stacked HPGU offers prospective benefits in-terms of PGU mass reduction, increased mission longevity, and greater mission flexibility. In order to practically realize the analytical findings of the study the proposed HPGU needs to be built and flown. Therefore, the next question asked

was how we do this. The decision was to use modern small satellites as technology demonstrators. A mission was designed that catered to validate the HPGU payload experiment. The next goal is to build the HPGU based on the mission specifications. The design for the EPS and rectenna part of HPGU for the microwave power receiving experimental spacecraft is presented in this dissertation.

CHAPTER III

PROBLEM STATEMENT AND SCOPE

One day SSPS positioned in GEO may transmit super high frequency microwaves to Earth as an electric utility provider to supply humanity with clean base load electrical power. Obviously, many challenges arise from this concept. One challenge is for future GEO-SSPS electric utility to co-exist with other space industries. Bottom line is that the microwave power beam should not interfere (i.e. electromagnetic interference (EMI)) with other industries. Instead of viewing the microwave beam as a source of EMI for orbiting satellites, the microwave beam is considered as an additional source of power available for satellites. The question then was whether this new source of power can play a meaningful role for future satellites. Based on this question the following hypothesis is proposed: "satellites orbiting below GEO equipped with a rectenna array to harvest RF energy transmitted from a GEO-SSPS offer benefits in terms of satellite mass reduction, increased mission longevity, and increased mission flexibility."

To address this question, the space environment with a microwave beam was studied first. A power beam medium environment was designed, and three different types of PGUs (i.e., rectenna, PV, and HPGU) for energy harvesting (solar and/or microwaves) were compared. The goal of the study was to determine the prospective benefits of such an environment. The results indicated that a stacked HPGU offers prospective benefits in-terms of PGU mass reduction, increased mission longevity, and greater mission

flexibility. This study led to a journal publication in the *Journal of Spacecraft and Rockets* [13].

In order to practically realize the analytical findings of the first hypothesis, a second hypothesis is pursued: "modern small satellites can be used as technology demonstrators for the proposed stacked hybrid PV/rectenna array PGU." To address this second hypothesis a space-to-space microwave wireless power experimental mission using a pair of modern small satellites, i.e. a power transmitting mother satellite and a power receiving daughter satellite. This mission design concept led to a journal publication in *Acta Astranatica* [14].

Over the course of the research, improvements have been made on the original mission design, catering more to the daughter satellites HPGU experimental payload aiming to validate the first hypothesis and use the second hypothesis as an avenue for realization. Therefore, the experimental mission was further refined and the design for an EPS and rectenna part of HPGU for a microwave power receiving spacecraft has begun. The modified mission, EPS, and rectenna studies have been submitted for publication in *IEEE Transactions On Aerospace and Electronic Systems*, and at the time of this dissertation is in its second review.

CHAPTER IV

LITERATURE REVIEW

The sun is the provider of unlimited energy. Thus it makes sense to optimize a system in which to continually harvest solar energy in order to supply electrical power to humanity for centuries or even millennium to come. The potential innovation that will allow for this continued supply of power to Earth is called SSPS systems.

The concept of SSPS systems seems to fit well with Nikola Tesla's prediction that some invention will tap into this so-called "circuit of nature"…"…Throughout space there is energy. Is this energy static or kinetic! If static our hopes are in vain; if kinetic – and this we know it is, for certain – then it is a mere question of time when [humans] will succeed in attaching their machinery to the very wheelwork of nature [15]." – Nikola Tesla.

The first recording of a concept to beam power from space to a planet appeared in 1941 in a science fiction short story titled "Reason." The author was science fiction writer Isaac Asimov and the idea written was that a space station transmits energy collected from the Sun to various planets via energy beams. "I know that our director sends out beams to some of these dots, always to the same ones – and also that these dots shift and that the beams shift with them." "Our beams feed these worlds energy drawn from one of those huge incandescent globes…."

The literature review section is broken up into six subsections. Subsection 4.1 provides a brief historical background on microwave wireless power and relevant SSPS system developments and applications. Subsection 4.2 provides literature work focused on space-to-space microwave wireless power transmission experiments. Subsection 4.3 provides three rectenna element designs that were used as a guide in this dissertation. Subsection 4.4 provides a brief literature review on hybrid power generation systems that utilizes radio frequencies and/or solar. The fifth subsection discusses energy storage technologies. The sixth and final subsection discusses propulsion system.

4.1 Microwave Wireless Power and Space Solar Power Satellite Systems

Wireless power is the transmission of electrical power by means of an electromagnetic wave. James Clerk Maxwell's equations in his "A Dynamical Theory of the Electromagnetic Field", published in 1865 [16], predicted that power could be transmitted from one point to another in free space by electromagnetic waves [17]. Maxwell's theory was realized from 1886-1889 by Heinrich Hertz through a series of engineering/scientific experiments [18]. Hertz used a spark gap to generate high frequency power and to detect it at the receiving end. Around 1900, Nikola Tesla pursued the transfer of electrical power via electromagnetic induction and through the principle of resonance from one point to another without wires. In the late 1930s, the Klystron tube and the microwave cavity magnetron were invented [19]. These devices were capable of generating high powered microwaves.

Starting in the 1950s William Brown of Raytheon became a pioneer of microwave wireless power transmission and reception technologies and applications. In 1959, the Department of Defense (DoD) was interested in developing a microwave powered high

altitude atmospheric platform for communication and surveillance purposes [17]. The microwave power would be used to drive DC motors attached to rotor blades so the platform could hover. During this time the only available use of microwaves for wireless power transfer (WPT) was to convert it into heat, which was used either directly or to run a heat engine [20]. An example of the microwave heat exchanger is shown in Figure 6. Since the greatest limitation in this method is to convert heat to mechanical work with at most 30% efficiency [20], it was decided that there were too many mechanical complications, and therefore this method was not adequate for the application.

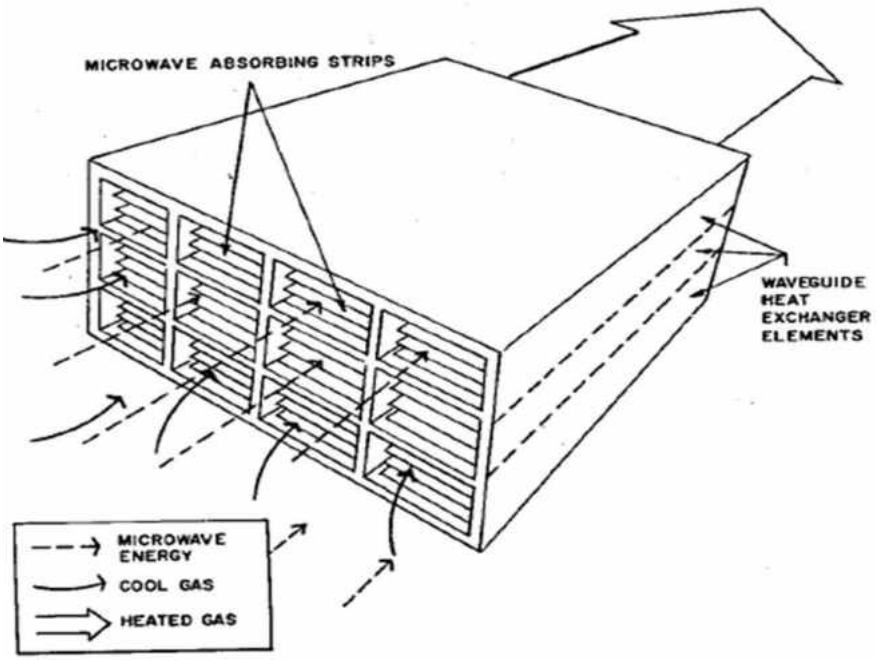

Figure 6. A microwave heat exchanger [21].

This was the first time it became widely recognized that there was no efficient means of converting the microwaves back into DC or low frequency electrical power at the receiving end of the system [21]. This led to the development of efficient electronic devices called rectifiers to convert the microwave energy directly into DC power and drive motors attached to rotor blades. In 1964, Brown demonstrated a beam-riding

microwave-powered helicopter [22]. The right side of Figure 7 shows Bill Brown with the constructed wireless power helicopter. The objective of this project was to have an aircraft flying at high altitudes for communication and surveillance functions and kept on station for months at a time by the weightless fuel of microwave power beamed to it from the surface of Earth. This helicopter was designed to "automatically position itself over the center of the microwave beam and control its roll, pitch, and yaw attitudes with sensors that derived phase, polarization, and amplitude information from the beam itself" [17]. The helicopter powered by microwaves would not be complete if it were not for the newly invented rectifying antenna (rectenna). The left side of Figure 7 shows the schematic drawing of the dipole rectenna with interconnections used on the wireless power helicopter. Brown, Roscoe George (Purdue University) and others patented the rectenna in 1969 [23]. This rectenna, believed to be the first, is seen in Figure 8.

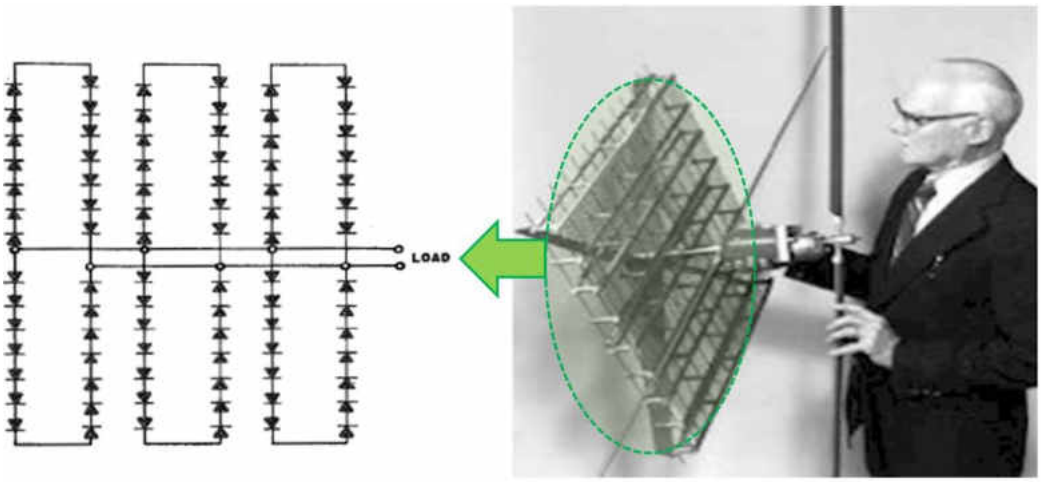

Figure 7. Figure on left shows schematic drawing of the arrangement of dipoles and interconnections within a diode module used in helicopter rectenna [24]. Figure on the right shows the special rectenna made for the first microwave-powered helicopter. Images courtesy of IEEE MTT Society.

Soon after the microwave wireless powered helicopter and rectenna milestones, Peter Glaser was granted a U.S. patent [25] in 1973 for his method of collecting and

converting solar radiation to microwaves and then transmitting that power to a rectenna array on Earth that converted the microwaves into usable electrical power for distribution. Glaser's concept later became known as Space Solar Power Satellite (SSPS) systems. A modern concept of SSPS is seen in Figure 15.

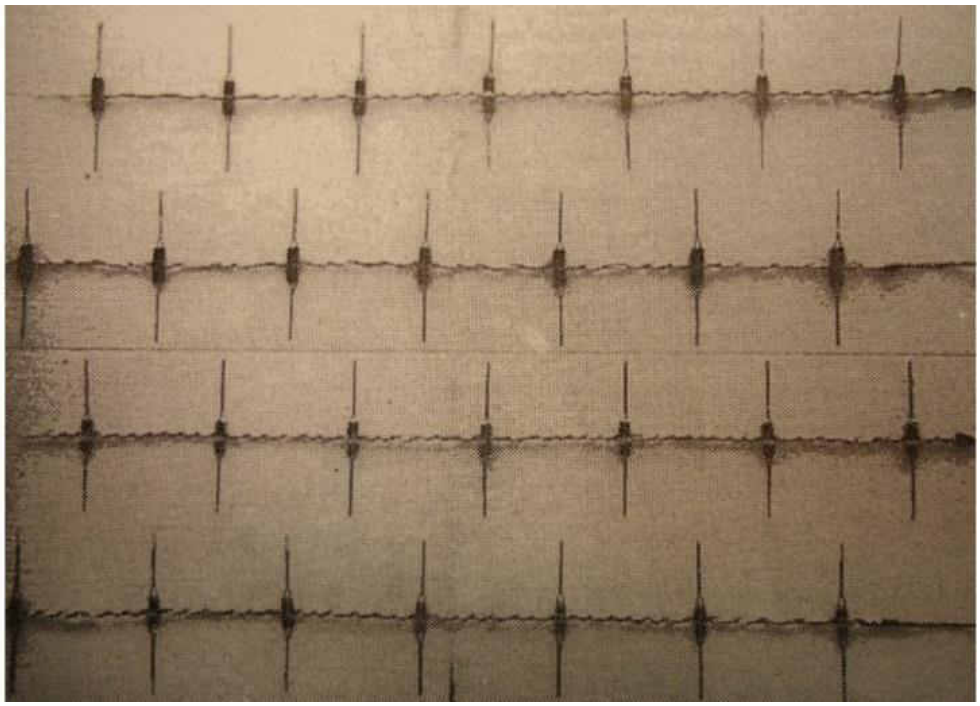

Figure 8. The first rectenna using half-wave dipole antennas as the receiving units and solid state diodes [17].

Building from Browns' beam-riding microwave-powered helicopter, microwave use was expanded to powering unmanned aircraft. In 1987, the Stationary High Altitude Relay Program (SHARP) put forth by Canada flew an unmanned aircraft on beamed microwave power [27]. In Japan, the Microwave Lifted Airplane eXperiment (MILAX) performed in 1992 also used microwave power to drive an aircraft [28]. Both SHARP and MILAX are shown in Figure 10.

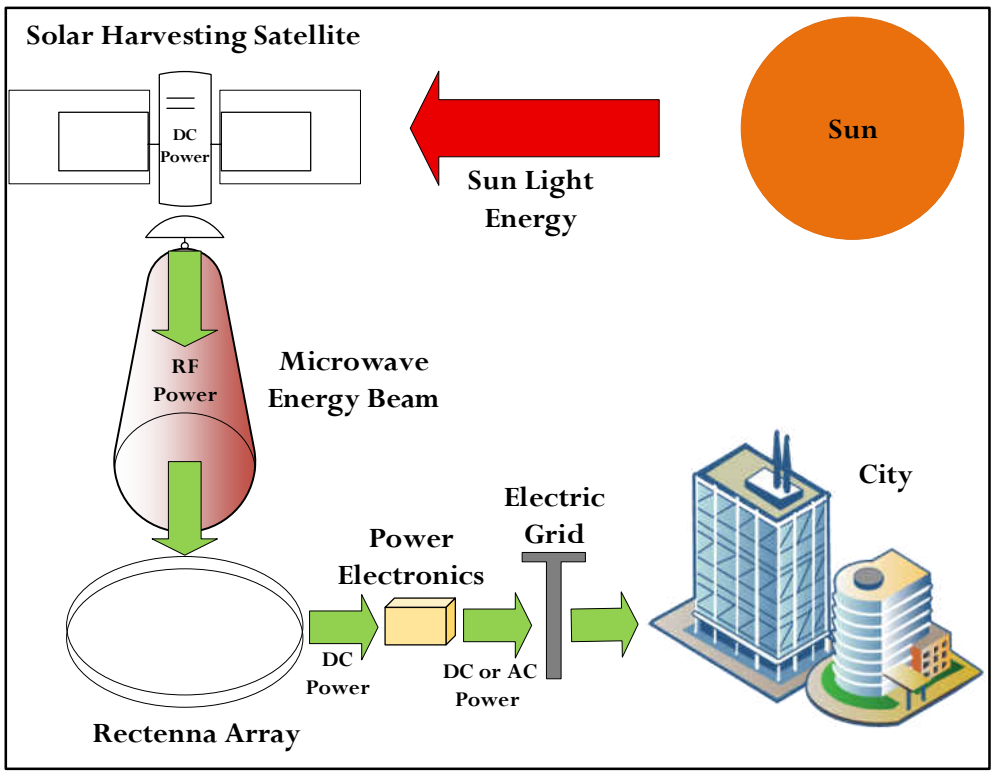

Figure 9. Modern concept for SSPS. Figure from Bergsrud et al. [26].

Figure 10. Model aircraft designed to utilize microwaves as their source of power. Figure on left is SHARP; and figure on right is MILAX.

4.2 Space-to-Space Microwave Wireless Power Transmission Experiments

To the author's knowledge, the Microwave Ionosphere Nonlinear Interaction Experiment (MINIX) was the first MWPT experiment in the space environment carried out on August 29, 1983 by the Japanese [29-31]. The objective of MINIX was to study possible impacts of a SSPS microwave power beam on the ionosphere such as the Ohmic heating and plasma wave excitation [29]. MINIX used a sounding rocket to get the experiment into space on a projectile. Once in space the sounding rocket separated into "mother" and "daughter" sections as shown in Figure 17. The mother section was equipped with a magnetron to generate microwave power (230 W/m^2 at 2.45-GHz frequency) and to transmit the power toward the daughter section where measurements were taken on the interaction of the microwaves with the ionosphere. The measurement of the electron temperature could not detect any Ohmic heating, and it was noted [29] that the rocket passed through the ionospheric plasma too quickly, and thus, the effective time of exposure of the microwave to the ionospheric plasma was too short compared with the characteristic time of the Ohmic heating. However, detections were sensed for the nonlinear excitation of the plasma waves, which discovered that the microwave beam interacting with the ionosphere causes nonlinear excitations of specific waves leading to nonlinear decay instabilities.

The MINIX work showed that a highly intense electric field from the microwave power beam causes modifications of the ionospheric medium. Thus the nature of the nonlinear plasma modifies the propagation path of the microwave power beam and thus results in mistransmission. This can be a serious problem because the power beam will miss the intended target, thus reducing power transfer efficiency. One solution to correct

for the mistransmission of the microwave power beam through the ionosphere is the active phased array antenna. The active phased array antenna for in-space testing was newly developed for the International Space Year for Microwave Energy Transmission in Space (ISY-METS) rocket experiment [32, 33] launched on February 18, 1993 by the Japanese's. ISY-METS.

In 1993, ISY-METS Rocket Experiment [32] used the first microwave wireless power (MWP) rectenna array system in the space environment. This experiment had a mother-daughter architecture in which the mother section was used as the microwave transmitter and the daughter section was equipped with two power receiving rectenna arrays as seen in Figure 17. One of the rectenna arrays consisted of two layers of rectenna elements, with each layer having a linear array of linear polarized elements, and the two layers were orthogonally polarized to each other as seen in the left side of Figure 18. The received power results of the WPT experiment are shown in the right side of Figure 18, where the solid line indicates concentrated power received by the dipole antennas at different distances from the transmitting antenna in a laboratory environment and the circles indicate the concentrated power received during flight. The mission concept of the ISY-METS rocket experiment was taken and a number of improvements were proposed by designing a mission concept utilizing modern small satellites, as will be presented.

In 1996, McSpadden, et al. [34] proposed an in-space wireless energy transmission experiment. Their concept proposed to use a transmitter on the Space Shuttle to beam power to a free flying satellite outfitted with a rectenna array as depicted in Figure 13. The use of an active retrodirective antenna array would be utilized and

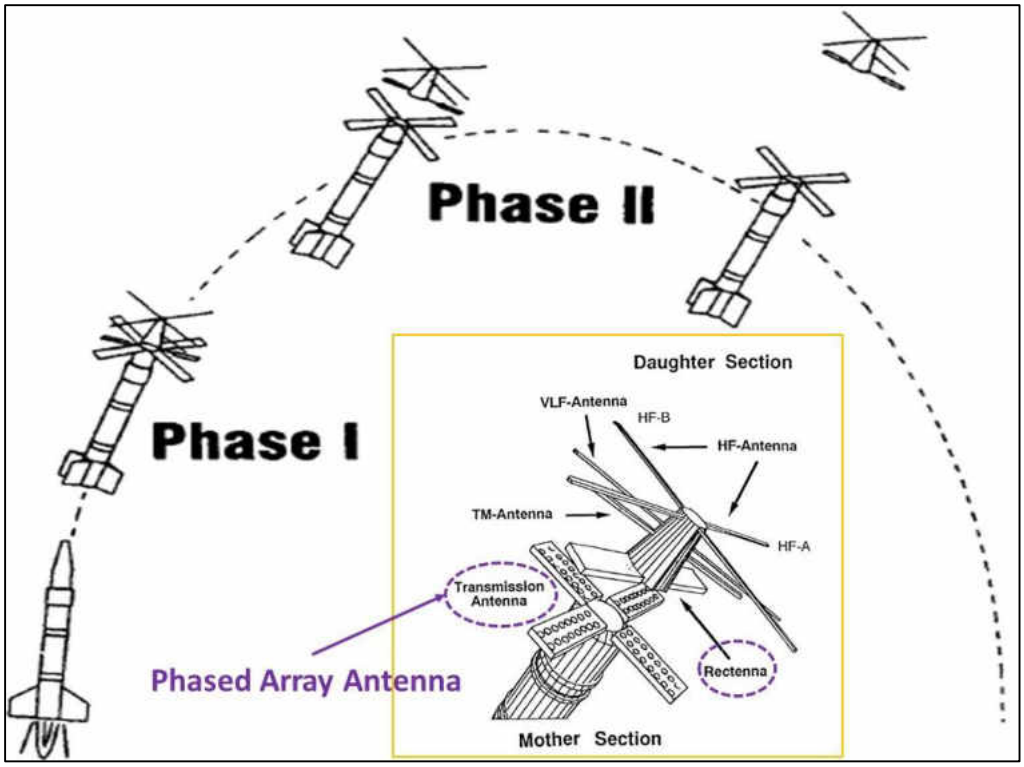

Figure 11. ISY-METS in-space power beaming experiment [32, 33].

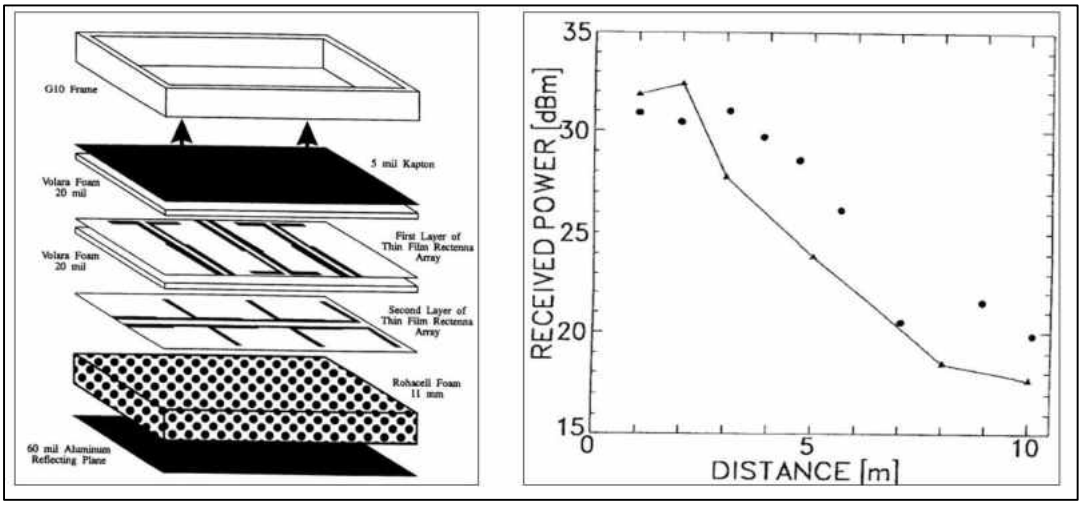

Figure 12. Figure on left shows the structure of the rectenna developed by ISU/Texas A&M University. Figure on right shows received power. Figures from [32].

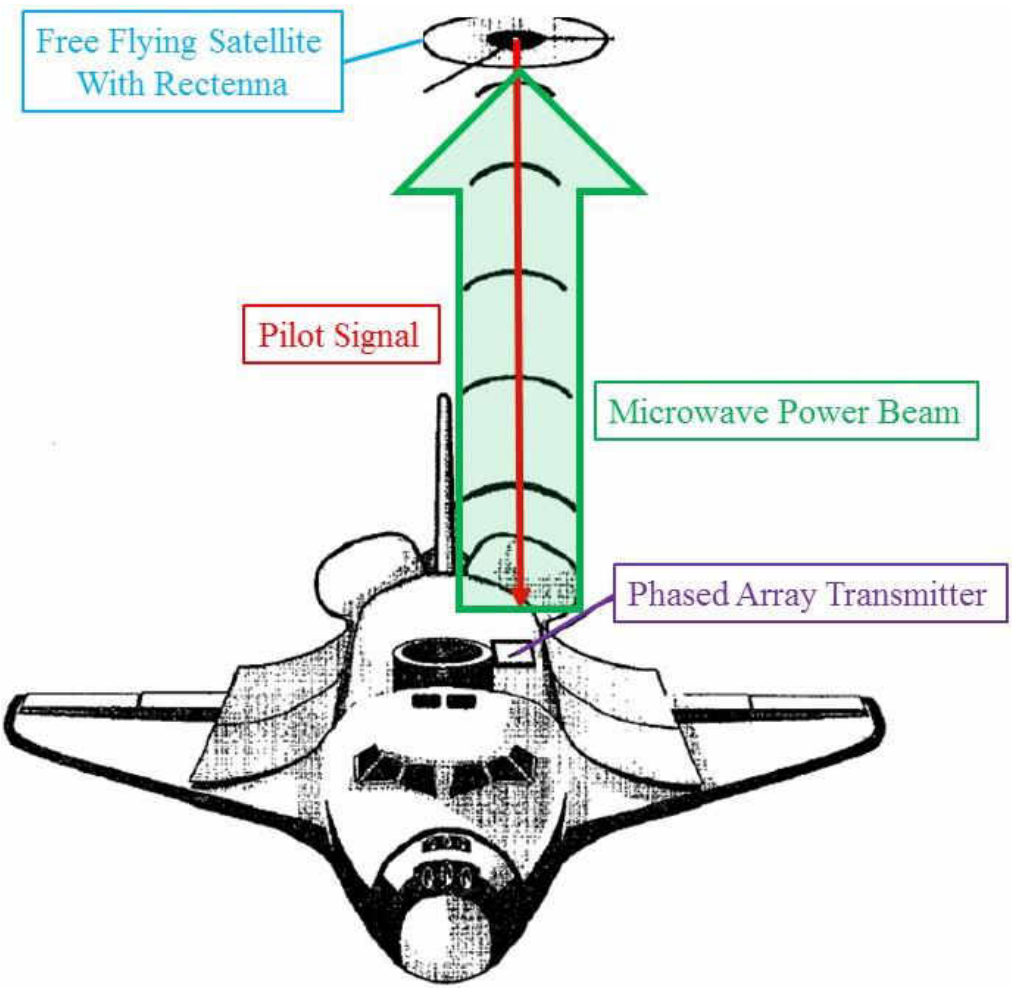

Figure 13. McSpadden's et al., [34] concept of a space shuttle beaming power to a free flying satellite.

Various experiments would be validated for power beaming in the space environment. For example, the experiment would demonstrate the capabilities of wireless power transmission system in space, monitor power transmission and reception efficiencies, and monitor the power beam. From collecting information form the power beaming in space experiments a data base can be generated, that may include information such as reliability, performances of components under severe thermal shocks, and effects on component degradation over time in space. This could then lead to comparing land and space experiments and allow for simulating the space environment on Earth for future

component and system testing. McSpadden's, et al. [34] suggestions on what could be tested in the space environment, and how the data could later be used, provides a reference sample for future space missions involving MWPT experiments.

This dissertation presents a novel mission concept of utilizing modern small satellites as MWP technology demonstrators which offers opportunity to incorporate/integrate McSpadden's, et al., list for MWP experiments just described into the modern small satellites as various modular experimental payloads. Moreover, batches of modern small satellites can be launched at the same time because of available technologies such as the P-POD and ESPA Ring which will be elaborated on in section 4.3. The point of this is that many of the questions that need to be answered in experiments can now be accomplished more rapidly and at reduced cost as will be presented.

One key technology advancement that evolved since McSpadden's proposed space-to-space power beaming concept is modern small satellites as is covered in Section 5.3. One idea emerged in 2014 from Barnhard [35, 36] who proposed using a Ka Band transmitter on the International Space Station (ISS) to transmit power to a swarm of CubeSats as seen in Figure 14. Barnhard proposed utilizing existing infrastructure (ISS and Ka Band TX), and modernized technology (CubeSats) to demonstrate MWP transmission experiments in the space environment in support of advancing SSPS concepts. Three limitations are attached to Barnhard's concept: (1) limited to a certain frequency band (Ka-Band), (2) limited power level (40 W), and (3) distance of the swarm of CubeSats must be greater than 200 m from center of mass (zone of exclusion). It must

be noted here that these limitations are subject to changes, however, this dissertation work presents a concept that offers greater flexibility in terms of mission design.

4.3 Developments in Rectenna Element

Many hundreds of rectenna designs can be found in the literature. A rectenna (Figure 15) is composed of an antenna, filter/matching network, and a rectifier (diode, and capacitor). For the application of modern small satellites there are certain rectenna design requirements that should be met for the proposed HPGU such as low profile, and low mass. This reduces the rectenna design options to a printed circuit board type of rectenna. Next the antenna part of the rectenna should have the following features: circular polarization, high gain, and array formation. All the aforementioned features are

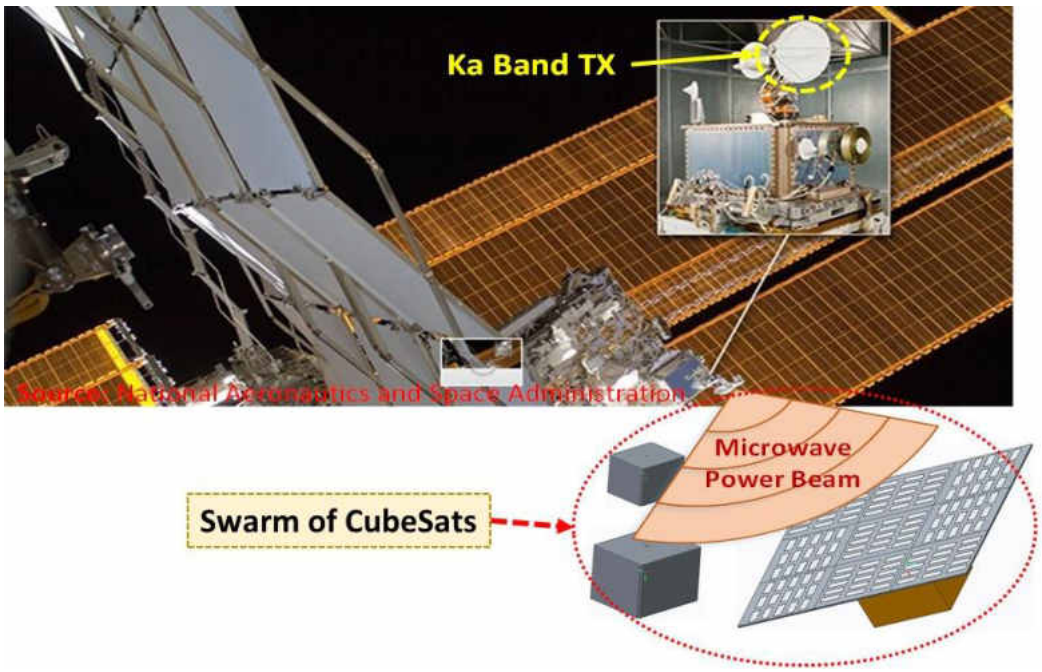

Figure 14. Concept of Barnhard's ISS Ka Band transmitter (TX) beaming microwave power to a swarm of CubeSats.

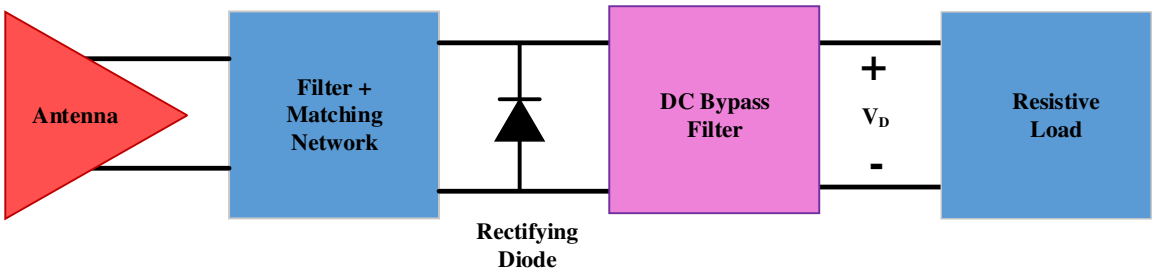

Figure 15. Block diagram of the components of a rectenna.

Key in the design toward a rectenna to be equipped on a satellite as will be presented in Section 5.2.1.3.

According to Strassner and Chang [37], the design of an efficient rectenna begins with the analysis of the diode component because the rest of the rectenna system is designed around diodes electrical behavior. In 1992, Yoo and Chang [8] developed and validated closed-form equations for the basic circuit structure of rectenna. Yoo and Chang discovered that three parameters of the diode: breakdown voltage, junction capacitance, and the series resistance determined the power conversion efficiency of the rectenna. Then in 1998, McSpadden, et al. [7] expanded the diodes closed-form equations from Yoo and Chang to account for varying input power levels. The closed form equations that calculate the diodes electrical behaviors accurately predict the RF-to-DC conversion efficiency of the rectenna, and has been numerously shown [7, 8, 38]. This dissertation work used these equations for the analysis of various diodes and for designing toward the rectenna as is presented in Section 5.4.4.

Starting from 1998, McSpadden, et al., [7], were the first group of researchers recorded to design a rectenna element using a full-wave electromagnetic simulator. Prior to their work, rectennas have been designed using transmission-line models [8, 39, 40]. The full-wave simulator allows the rectenna's antenna and passive circuit to be analyzed

together. McSpadden's, et al., rectenna used a coplanar stripline (CPS) half-wave printed dipole antenna designed for 5.8 GHz, as seen in Figure 22 and Figure 23. This design used a low pass filter by means of capacitive strips on the reverse side of the substrate from the antenna. The low pass filters' purpose is to match the impedance of the dipole antenna to the input impedance of the diode and to pass the 5.8 GHz signal while reflect the higher order harmonics produced by the diode. Their rectenna element RF-to-DC conversion efficiency reached >80%.

In 2002, Strassner and Chang [9] designed a CPS dual rhombic loop antenna (DRLA) with circular polarization (CP) capability and high gain as seen in Figure 18. Their design used a CPS band-reject filter (Figure 19) with λ/4 stubs to pass 5.8 GHz

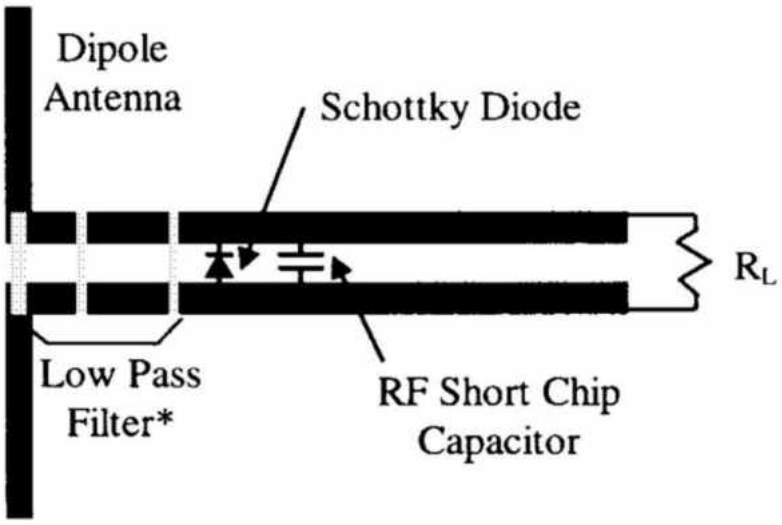

Figure 16. Rectenna element from [7].

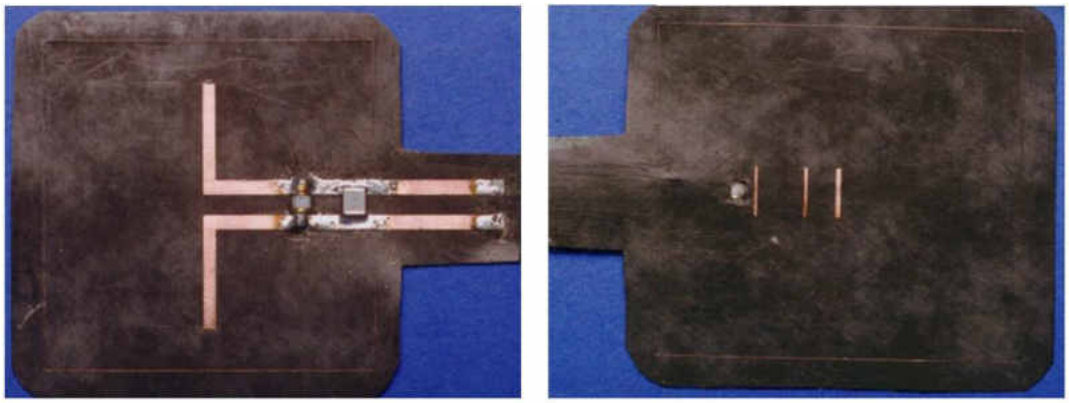

Figure 17. Realized rectenna element from Figure 22 with permissions use from Dr. James McSpadden.

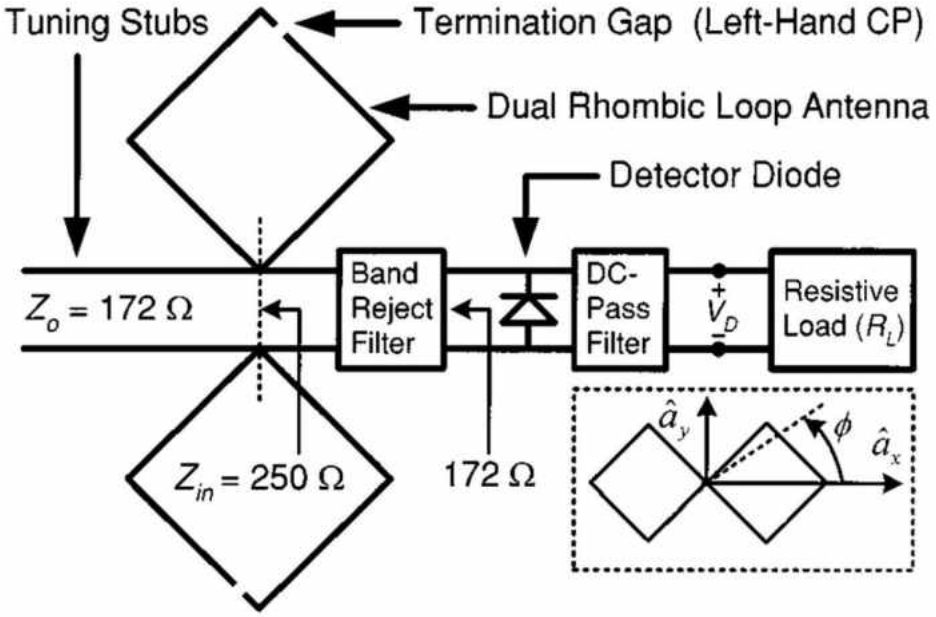

Figure 18. Block diagram of rectenna from [9].

Figure 19. Band reject filter from [9].

Signal from the antenna to the diode and to block the second order harmonic and match the DRLA to the resistance of the diode. They were able to achieve ~80% conversion efficiency.

In 2006, Ren and Chang [41] designed a CP CPS fed truncated patch rectenna, as shown in Figure 20. Their design used a CPS band pass filter to suppress harmonics. Tuning stubs were used to match the antenna to the diodes resistance. The unique feature of their design was the dual diode configuration. Their dual diode design configuration achieved ~76% efficiency with at least twice as much output voltage compared to a single-shunt diode rectenna for the same layout dimensions.

The designs from McSpadden, et al. [7], Strassner and Chang [9], and Ren and Chang [41], are used as reference guides toward the design of this dissertation's rectenna. The reason is because, to the author's knowledge, these pieces of work present a design format that helps to fully understand the stages of a rectenna system design using a CPS structure architecture. Other antenna designs were studied as is discussed next, however, none could compete with the elegancy of the aforementioned designs.

Sun, et al., [42] designed a high-efficiency 2.45 GHz rectenna with a CPS architecture that had the capability to harvest low input RF power (1.95 μW) effectively (~80% efficiency). However, the antenna designed by Sun, et al., as shown in Figure 27, has a major drawback as it is not designed for array configuration as is indicated by the double stub tuner matching. Also, this antenna does not have CP capability.

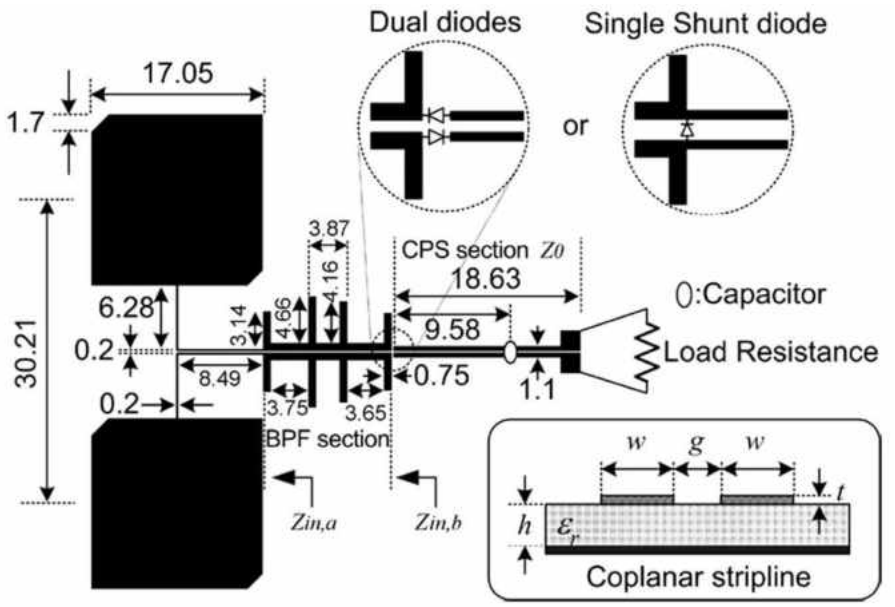

Figure 20. Layout of the rectenna from [41]. All dimensions in mm.

Another antenna design from Sun, et al., [43] was a bow-tie loop printed antenna with high gain and broad beam width at 5.8 GHz. Their design did offer a broad beam width feature that can avoid the precise main beam alignment typical of rectennas, however, their antenna design does not have CP capability. Another CPS fed antenna that was looked at came from Sun, et al., [44]. Their printed dual-loop antenna fed by CPS also offered high gain, low cross-polarization, and broad beam features. This design also did not offer CP capability.

An extremely important tool to properly feed and measure the CPS architecture designs (rectifier, antenna + filter, and rectenna) is called a balun or balanced-to-unbalanced transition. The CPS itself cannot be measured directly [42], therefore, a balun transition is used to realize efficient transition between the CPS and the microstrip lines. To design a transition, a field matching and an impedance matching are required [45]. Since the electric field in the microstrip line is perpendicular to the substrate and the

electric field in the CPS is parallel to the substrate, an electric-field rotation of 90° is needed.

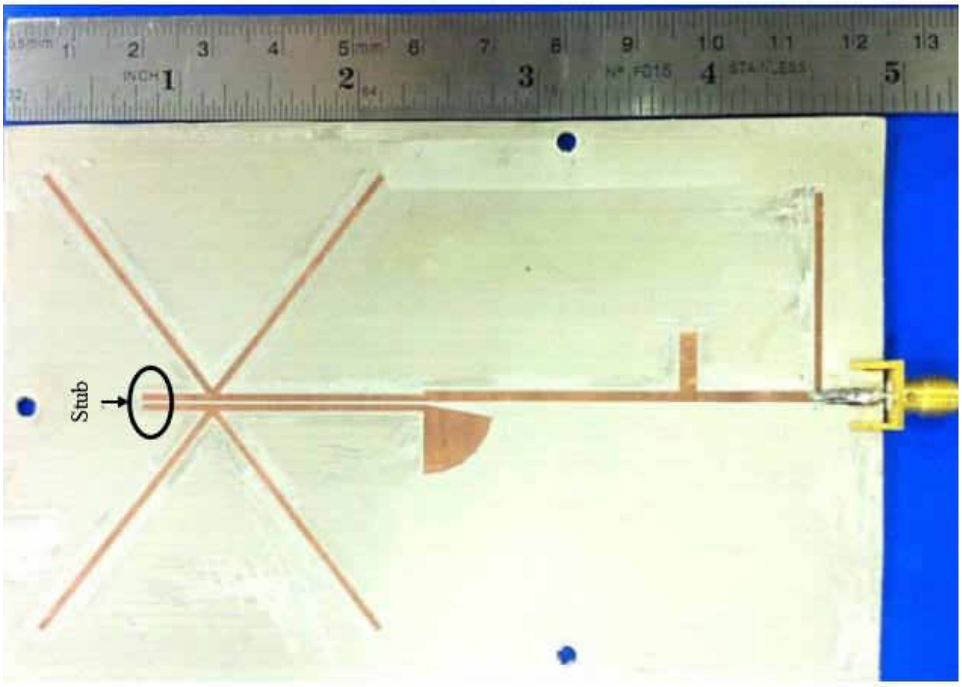

Figure 21. Fabricated antenna with transition and matching circuit [42].

Simons, et al., [46] designed two CPS-to-microstrip transitions in a back-to-back configuration as seen in Figure 22. These authors used radial stubs to rotate the electric field from being parallel to the substrate and across the CPS to being normal to the substrate when traveling along the microstrip line, as Figure 23 describes. The dielectric used was RT/duroid 6010 with a dielectric constant of 10.2 and 1/2 oz. copper (Cu) cladding (metal thickness = 17.78 microns). The high permittivity (ε_r) substrate is suitable for circuit design, and not for antenna design, and such transitions to feed antennas degrades the antenna performance.

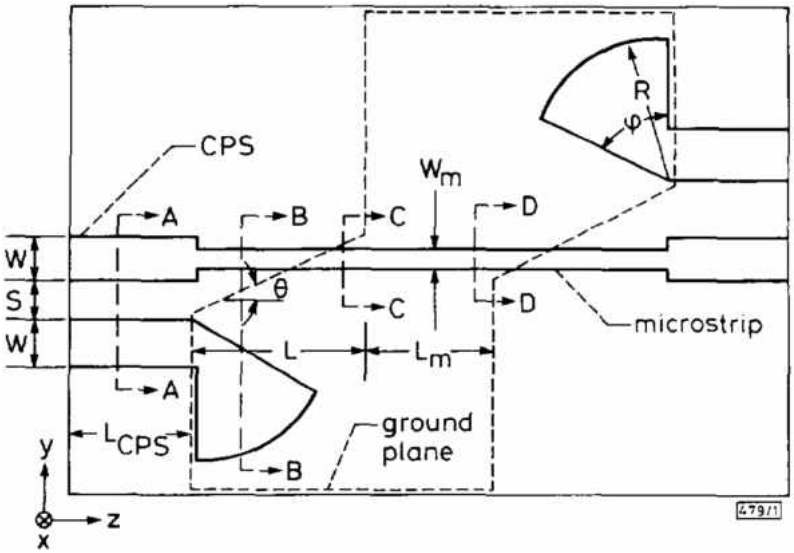

Figure 22. Schematic diagram of two back-to-back CPS to microstrip transitions [46].

Suh and Chang [47] designed a wideband CPS-to-microstrip line using lower ε_r material. Their design, as seen in Figure 30, used RT/Duroid 5870 substrate material with a dielectric constant of 2.33. Their design had a long smooth tapered ground plane. Their design had the following results: From 1.5 GHz-6 GHz (1:4) less than a 10dB return loss and less than a 0.5 dB insertion loss was achieved.

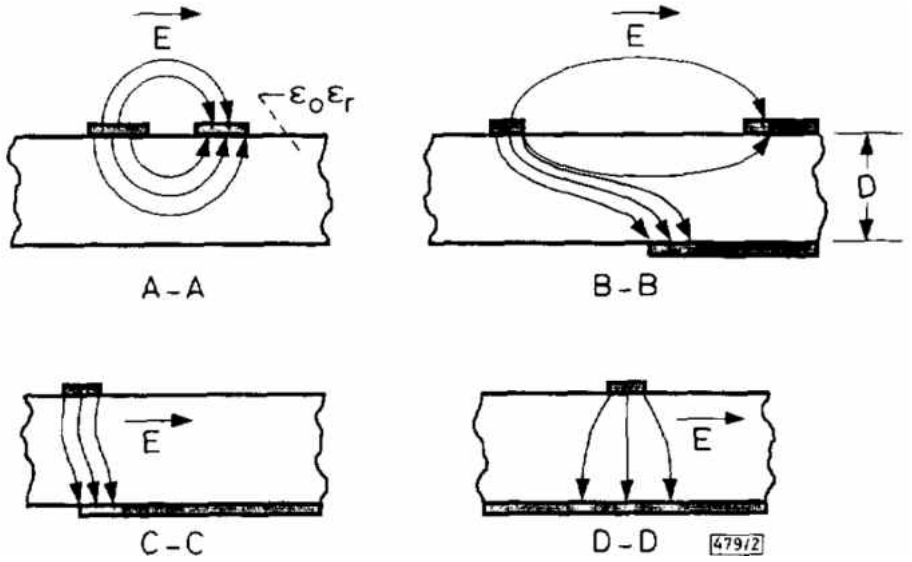

Figure 23. Electric field lines at various cross-sections along transitions [46].

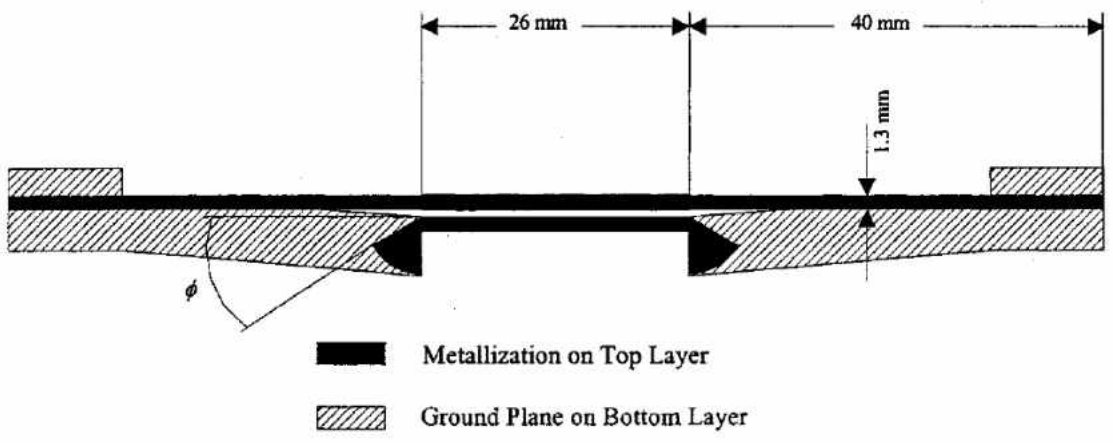

Figure 24. CPS-to-microstrip back-to-back transition structure [47].

The paper by Simons, *et al.,* [46] used a high dielectric constant material not ideal for antenna application and a complicated measuring technique was required. The paper by Suh and Chang [47] used a smooth tapered ground plane to match the high characteristic impedance of CPS to the 50 Ω microstrip line and to obtain good field matching. The challenges with this is accurate double-sided etching and alignment fabrication as well as no easy design equations are available or obtainable for the long tapered lines or taper ground plane, thus the design of these transitions can only rely on full-wave optimization. Moreover, the taper ground causes more power loss that introduces crosstalk, which is undesired in high-density circuits [45].

To overcome these disadvantages Tu and Chang [45] designed and experimented with two microstrip-to-CPS transitions as seen in Figure 25 and Figure 32. Field rotation is shown in Figure 27. Both designs used a Chebyshev transformer to match the CPS characteristic impedance to the 50 Ω microstrip line. Two techniques were explored to rotate the electric field: (1) a quarter-wavelength rectangular open stub and (2) a radial stub. It was found that the two transitions have a similar response at the center frequency

band, while the major difference is near the upper bound of the bandwidth. The work also showed that the transition with the radial stub provides a wider bandwidth.

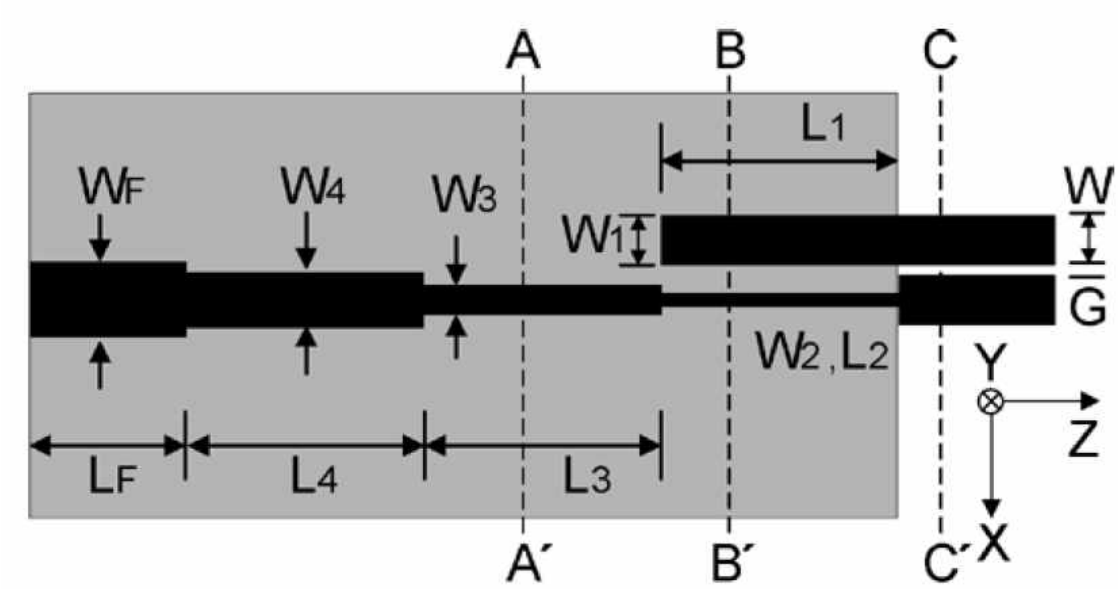

Figure 25. Configuration of the microstrip-to-CPS transition using a rectangular open stub [45].

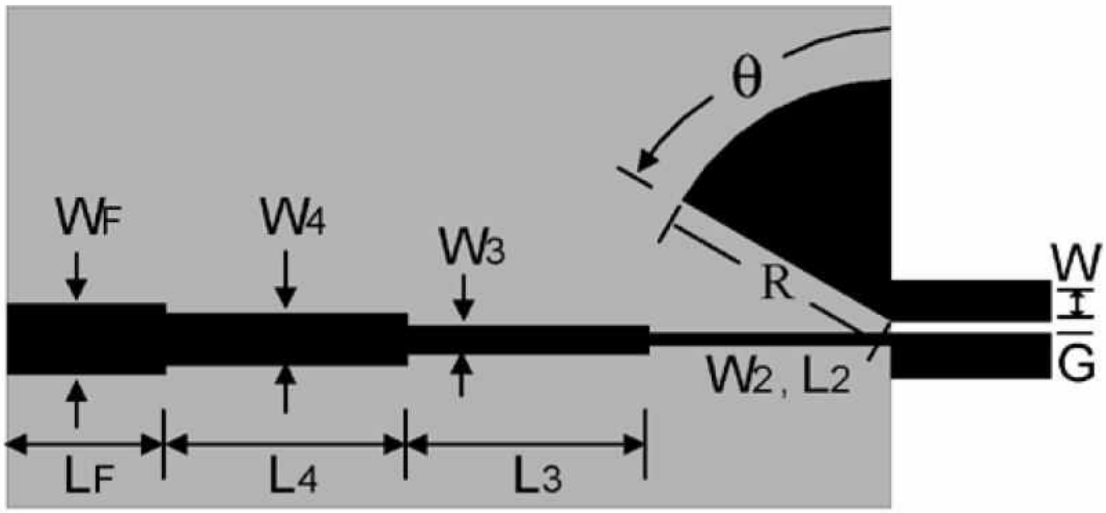

Figure 26. Configuration of the microstrip-to-CPS transition using a radial stub [45].

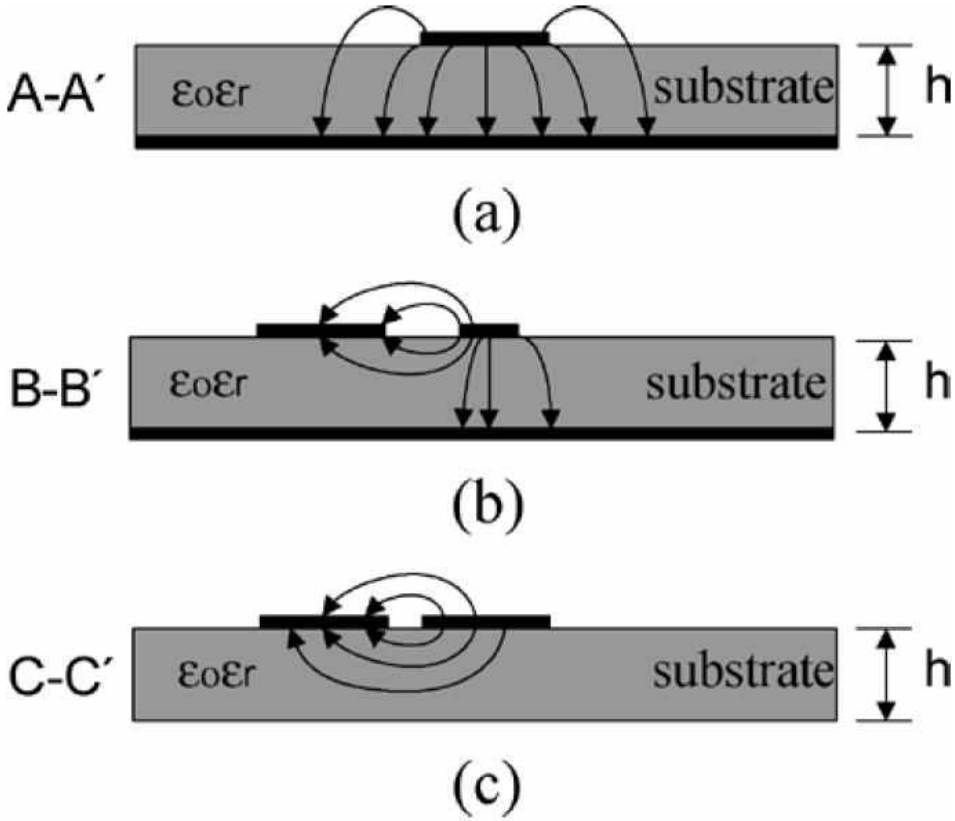

Figure 27. Cross-sectional view of the electric distributions [45]: (a) microstrip line, (b) coupled microstrip line, and (c) CPS.

4.4 Radio Frequency and Solar Energy Harvesting Technologies

Since a HPGU is proposed and analyzed some background literature on the topic is necessary. In 1995, Tanaka, et al. [48] developed a microstrip antenna at 2.225 GHz frequency with solar cells on its surface for microsatellties. The measured return loss and radiation patterns for the microstrip antenna with and without solar cells were nearly equal. This means that the addition of the solar cells with conducting lines had no effect on radiation. This was also a result given by Niotaki, et al. [49]. Vise versa Tanaka's, et al., research found that the antenna radiation did not influence the power generation of the solar cells. However, one fault from Tanaka, et al., work is that they did not vary the conditions of the two energy sources.

In 2014, the work of Niotaki, et al. [49] did study varying conditions of the two energy sources. They found that when both solar and RF energies are present, higher values of DC can be obtained. Breaking this down further, they found that when combining the DC values from the two sources (RF and solar) better efficiency can be obtained for when higher values of solar energy is present and no RF energy. Their work indicated that the hybrid PGU should operate in both modes (RF and solar) only when there is not enough light and there is a demand of DC power. If there is enough light, they showed it is more efficient to only operate in the solar harvester mode. This dissertation work presents a novel idea of two power paths for the HPGU. Power path 1 goes from the solar PV arrays to the batteries and power path 2 goes from the rectenna to the supercapacitors.

In 2000, Zawadzki and Huang [50] developed and demonstrated an integrated RF antenna with solar array for spacecraft applications. They found that combining these apertures reduces spacecraft mass, launch stowage volume, cost, and deployed surface area, without significantly affecting the performance of either the antenna or solar array. They mentioned that the mass savings comes from a reduction of one support structure which also reduces the launch stowage volume. Their work indicated that integrating RF and solar sources together is feasible. These promising results make a strong argument in support of this dissertation's work for a HPGU with stacked solar PV/rectenna array.

Suh and Chang [47] designed a wideband CPS-to-microstrip line using lower ε_r material. Their design, as seen in Figure 30, used RT/Duroid 5870 substrate material with a dielectric constant of 2.33. Their design had a long smooth tapered ground plane. Their

design had the following results: From 1.5 GHz-6 GHz (1:4) less than a 10dB return loss and less than a 0.5 dB insertion loss was achieved.

CHAPTER V

METHOD

5.1 Power Beam Medium

One day an SSPS positioned in GEO may transmit microwaves to Earth as an electric utility to supply humanity with clean base load electrical power. Obviously, many questions arise from this concept. One of the challenges is with a microwave beam coming from a GEO-SSPS to Earth and causing EMI with other satellite services. This dissertation work approaches the EMI problem not as a source of interference but as an additional source (with solar) of power in space. Section 5.1 addresses the first hypothesis: "Satellites orbiting below GEO equipped with a rectenna array to harvest RF energy transmitted from a GEO-SSPS offer benefits in terms of satellite mass reduction, increased mission longevity, and increased mission flexibility."

Note here that the design of the power beam medium for both a static and a dynamic scenario only considers a satellites altitude, and velocity. The static and dynamic scenarios assumes that lower orbiting satellites simply orbit through the diameter of the beam (defined by an Airy diffraction disk) for different altitudes in the static case, or lower orbiting satellites are locked-on for power beaming for an estimated GEO-SSPS field of view for a dynamic case. The assumption for both static and dynamic power beam medium scenarios is that the rectenna array on the satellite is always pointed toward zenith (gravity-gradient stabilized).

5.1.1 Power Density and Spot Diameter Calculation

A Department of Energy (DOE) and National Aeronautics and Space Administration (NASA) collaboration in 1977-1981 generated a Reference System Concept for Solar Power Satellites (SPS) [4]. The 2.45 GHz Reference System involved placing an SPS into GEO orbit with a 1 km transmitting antenna array diameter capable of delivering 5 GW of power to Earth's utility grid or 6.72 GW of transmitted power from the transmitting array. The peak power density at the center-of-beam was proposed to be 23 mW/cm^2 at the rectenna array located on Earth. Later, in 1999 [5] NASA conducted a Space Solar Power (SSP) Exploratory Research and Technology (SERT) Program. Assuring environmental health and safety, the SERT Program suggested the power irradiance level at the center-of-beam be 10-20 mW/cm^2 at the rectenna array located on Earth.

The next set of calculations uses the aforementioned reference systems in order to map out the power irradiance levels and beam diameter for different orbits that both current and future satellites may travel through. Three power irradiance levels, as defined at the rectenna array on Earth, were used; 23 mW/cm^2 (1981 Reference System), 20 mW/cm^2 (SERT High), and 10 mW/cm^2 (SERT Low). The diameters of the transmitters used in the analysis of these irradiance levels are 342 m, 319 m, and 226 m, respectively. The antenna array transmits 6.72 GW at 5.8 GHz. The frequency of 5.8 GHz was used as opposed to 2.45 GHz, because many researchers in the SSP community suggest that 5.8 GHz is a good balance between performance and cost.

Before delving into the calculations, the reader is referred to Figure 28 for a clear picture of the different orbits. Figure 30 and Figure 31 show power irradiance as a

function of distance for LEO and MEO orbits, respectively. Power irradiance is defined as [51]

$$p_d = A_t P_t / \lambda^2 D^2 \quad (1)$$

where A_t is the total area of the transmitting antenna, P_t is the total radiated power (6.72 GW) from the transmitter, λ is the wavelength, and D is the separation distance between the apertures.

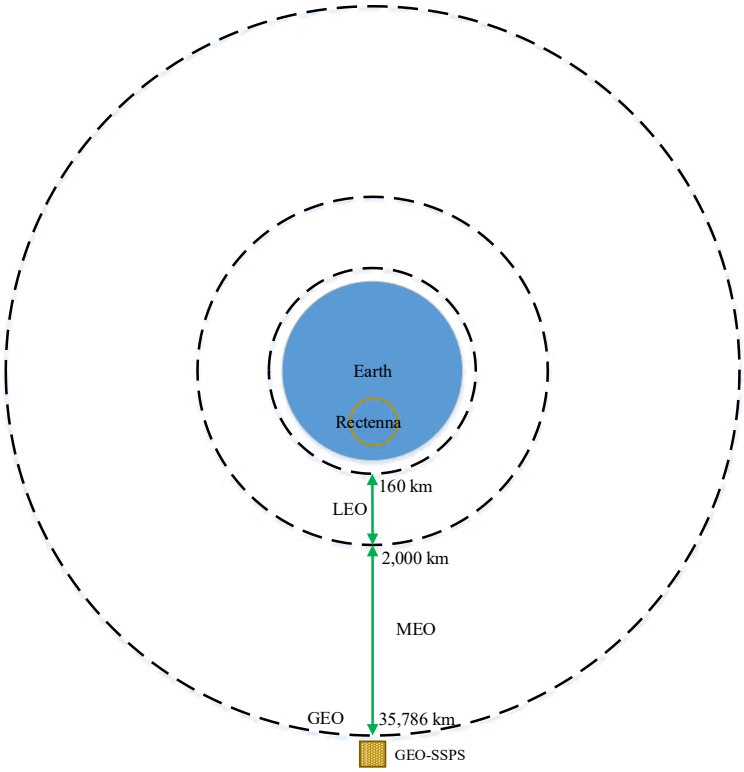

Figure 28. LEO, MEO, and GEO altitudes from the Earth.

In order to calculate the area for the microwave beam at different orbits, knowledge of spot diameter is essential. The minimum spot diameter of any transmitted electromagnetic beam is set by the diffraction limit [52]. The Airy diffraction disk is the diffraction pattern produced from a uniformly illuminated circular aperture whose area contains 84% of the beam energy [52] as seen in Figure 29.

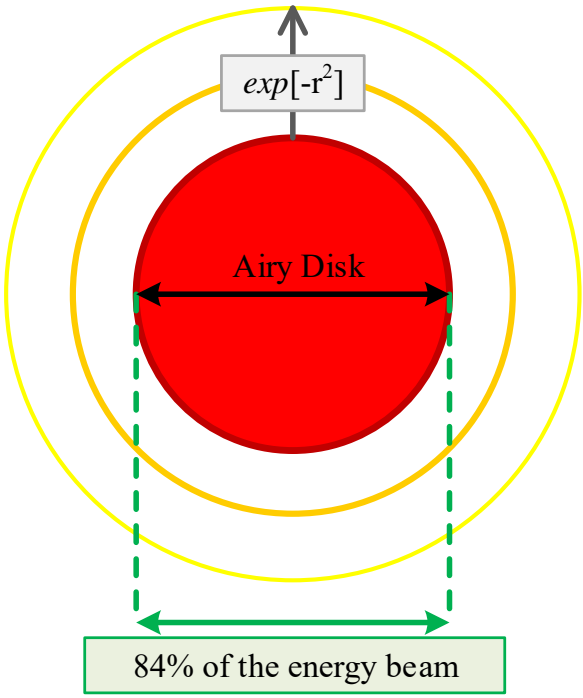

Figure 29. Airy diffraction disk [52].

In order for the calculation to make sense with the power beam medium scenario, we assume that at various orbits there is a uniformly illuminated circular aperture. The diameter of the Airy diffraction pattern is calculated from

$$d_{spot} = 2.44\lambda D / d_{transmit} \quad (2)$$

where $d_{transmit}$ is the diameter of the transmitting aperture. Outside this spot, the power falls off at approximately $exp[-r^2]$ where r is the distance from the edge of the spot diameter. Both equations (1) and (2) are far field calculations and are only valid at distances greater than $\left(2\times\left(d_{transmit}\right)^2/\lambda\right)$ from the transmitter [53]. Those respective distances for transmitter diameters of 342 m, 319 m, and 226 m are 4531 km, 3940 km, and 1970 km at 5.8 GHz.

Figure 32 and Figure 33 show the spot diameter as a function of distances for LEO and MEO orbits, respectively. Additionally, these figures show peak power values at the center of the beam. It would be useful in the future to recalculate the power beam medium using a tapered amplitude coming from the transmitter as the GEO-SSPS is proposed to utilize. This tapered amplitude would result in longer exposure time for the lower orbiting satellites through the power beam medium. Satellite velocity and exposure time are calculated next.

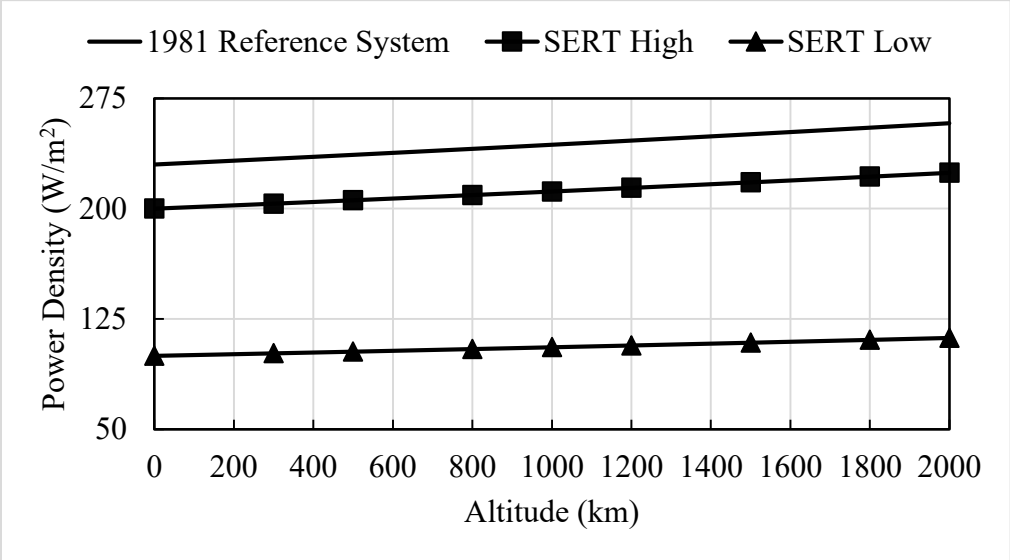

Figure 30. Power density as a function of altitude in LEO.

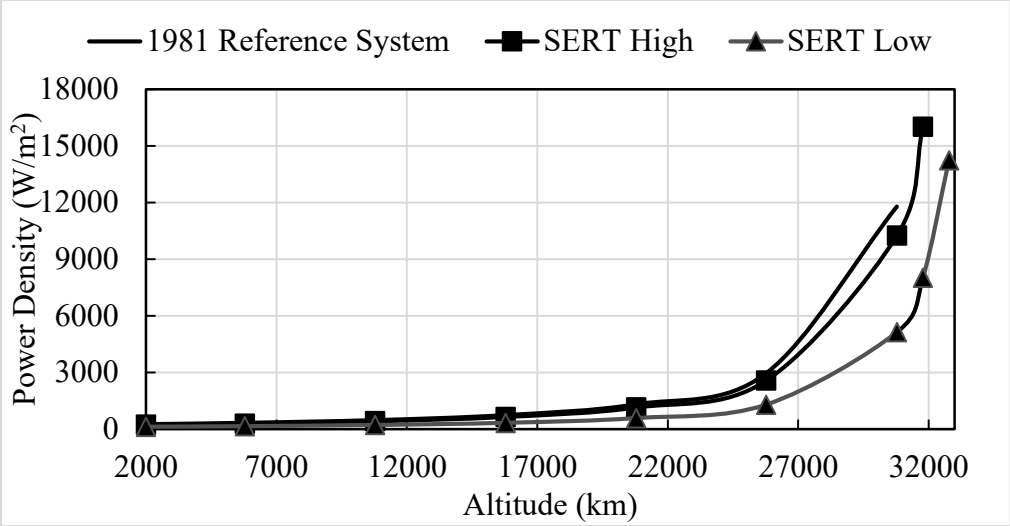

Figure 31. Power density as a function of altitude for MEO.

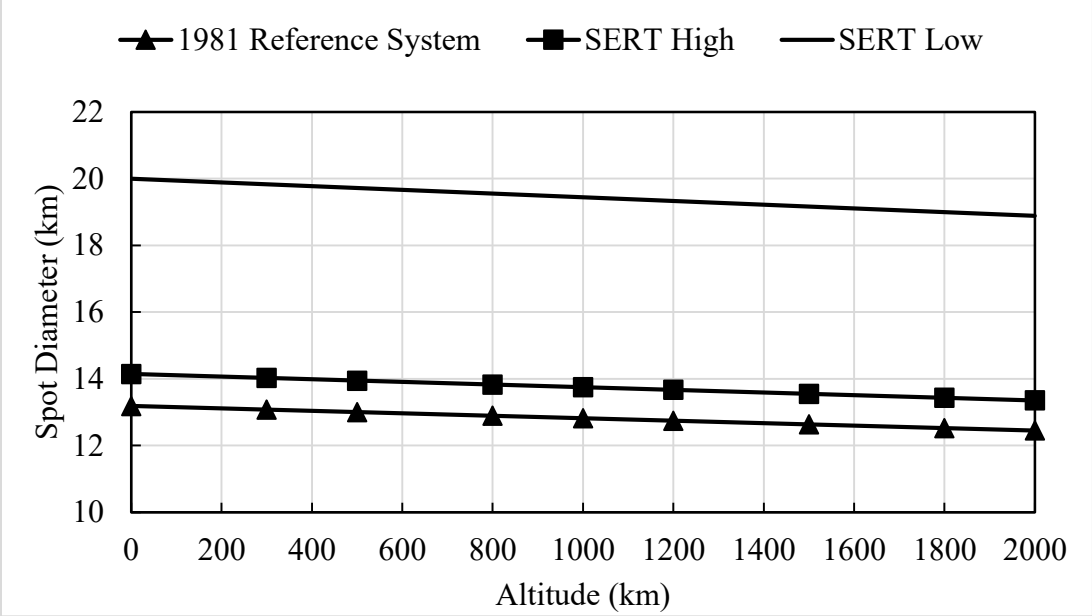

Figure 32. Spot diameter as a function of altitude in LEO.

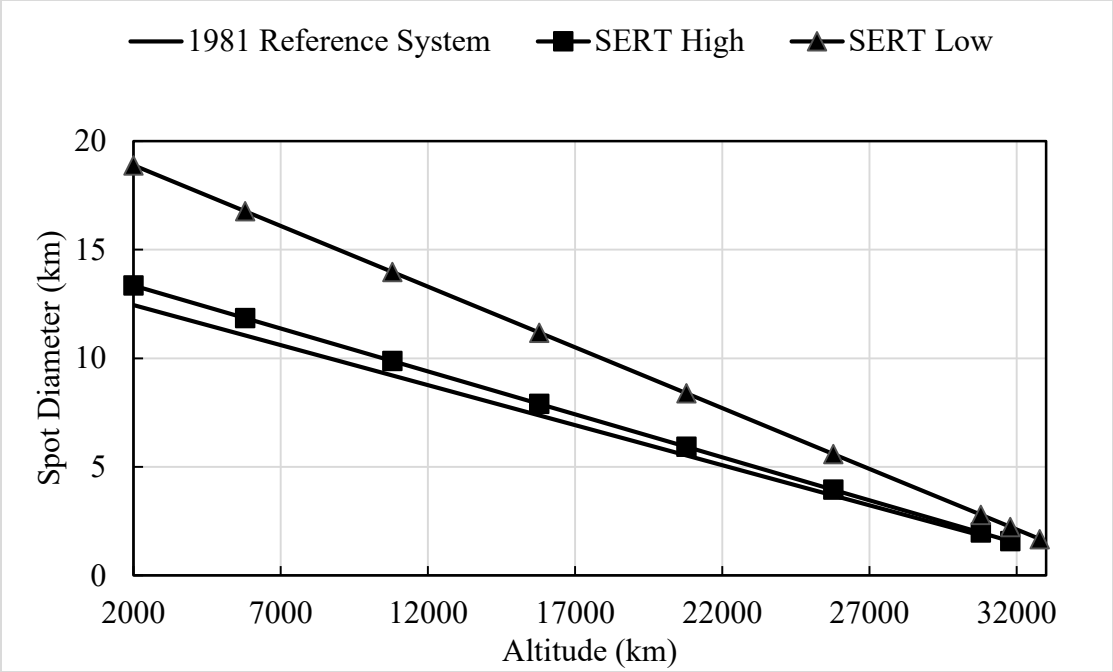

Figure 33. Spot diameter as a function of altitude for MEO.

5.1.2 Satellite Velocity and RF Exposure Time Calculations

The amount of exposure time experienced by a satellite for certain orbits must be calculated to predict total available energy (solar and/or RF) for on-board use. First, the velocity of the satellite must be known. Then, dividing the beam diameter by the velocity of the satellite will give the transit time. Treating LEO orbits as circular, the velocity of the satellite can be calculated easily from

$$V = \sqrt{\frac{\mu_{Earth}}{R}} \tag{3}$$

where μ_{Earth} is the gravitational constant ~398,600 km^3/s^2 and R is the mean radius of the Earth (6,371 km) plus the altitude of the orbit from Earth's surface in kilometers. For elliptical orbits, additional orbital parameters; such as the semi-major axis, are needed to determine the velocity of the satellite. For example, a Global Position System

(GPS) satellites have a semi-major axis (a) of about 26,838 km and a distance from the Earth of about 20,200 km [54, 55]. From this information, the average velocity of the satellite is calculated from

$$V = \sqrt{\mu_{Earth}\left((2/r)-(1/a)\right)} \tag{4}$$

where r is the distance from Earth's surface. Table 2 shows the velocity and time of exposure for satellites in various LEO altitudes and the case for the GPS in MEO. It also shows data for power irradiance and Airy disk (diameter).

Table 3 shows data for power irradiance and Airy disk (diameter) for MEOs. Notice that the time of microwave energy exposure (illumination) for satellites passing through the beam is very short for a single stationary beam from a GEO-SSPS. Assuming the satellites passing through the beam do so for the complete diameter, the higher the altitude the smaller the beam diameter, and therefore there is less exposure time of the satellite passing through the beam. Note that more MEO examples can be obtained, however, since they have elliptical orbits additional orbital knowledge is needed to obtain the velocity and therefore the time of exposure through the power beam medium.

The 1981 NASA/DOE reference system proposed 60 SPSs [56]. Using 60 SPSs and referring to SERT high power density levels - the average spot diameter, average velocity of satellite, and average time of exposure in LEO, respectively, are about 13.7 km, 7.3 km/s, and 2 s. Therefore, the total combination of spot diameters and time of exposure with 60 satellites, respectively, is about 822 km and 2 minutes in LEO. In order for the microwave scenario to be equivalent to covering the same diameter as the sunlight, about 2,000 SSPSs are needed. To alleviate this un-realistic scenario, the use of retrodirectivity is proposed and is covered in subsection 5.1.3.

Table 2. Distance, power density, Airy disk, satellite velocity, and time of RF exposure for a satellite in LEO and MEO (GPS) for SERT High.

Altitude (km)	Power Density (W/m^2)	Airy Disk (km)	Average Velocity of Satellite (km/s)	Maximum Time of Exposure (s)
0 (at Earth)	200	14.14	N/A	N/A
500	205	13.95	7.62	1.83
1000	211	13.75	7.35	1.87
1500	217	13.55	7.11	1.90
2000	224	13.35	6.90	1.94
20200 (GPS)	1054	6.16	4.96	1.24

Table 3 Distance, power density, and Airy disk for MEO for SERT high.

Altitude (km)	5786	10786	15786	20786	25786	30786
Power Density (W/m^2)	284	409	640	1,138	2,561	10,245
Airy Disk (km)	11.8	9.8	7.9	5.9	3.9	1.9

Clearly, from Table 2 and from the calculations in the previous paragraph, it is evident that a satellite equipped with a rectenna array could not benefit from this fixed power beam medium scenario. The “window of RF harvesting time” for the lower orbiting satellites through the diameter of the beam is simply too short and too little power is available for any significant impact. Thus, the concept of retrodirectivity

between the GEO-SSPS and lower orbiting satellites combined with a stacked hybrid PV/rectenna array equipped on the lower orbiting satellites offers a potentially viable solution to a modified power beam medium scenario. The next subsection will go into greater detail about the proposed dynamic power beam medium scenario using retrodirectivity.

5.1.3 Retrodirectivity

The concept of retrodirectivity can be utilized in a modified power beam medium scenario where the lower orbiting satellites transmit a pilot beam signal to the GEO-SSPS that, in turn, retransmits a phase conjugate power beam toward the source signal from a phased array antenna system. Retrodirectivity capability allows for tracking and delivering of RF power to lower orbiting satellites in a dynamic environment. Moreover, the phased array tracking and power beaming system could be used for supplying power for electric propulsion systems to assist with geocentric orbit transfers (GOTs) [57]. Figure 34 shows three potential customer opportunities with the proposed modified power beam medium scenario utilizing retrodirectivity.

Retrodirective capability equipped on the SSPS provides adaptability and inherent fail-safe properties. Adaptability comes from the changes in the SSPS structures that can degrade the performance of the phased array, such as temperature variations, surface irregularities, or mechanical misalignments between subarrays [58]. Basically, the integrated retrodirective system on the SSPS adapts to these changes so that they are unimpactful. The fail-safe property is mainly used for the base load power supplied to the rectenna array on Earth where the Earth rectenna array transmits a pilot beam signal from the center of its structure to the GEO-SSPS. If for some reason the pilot beam is not

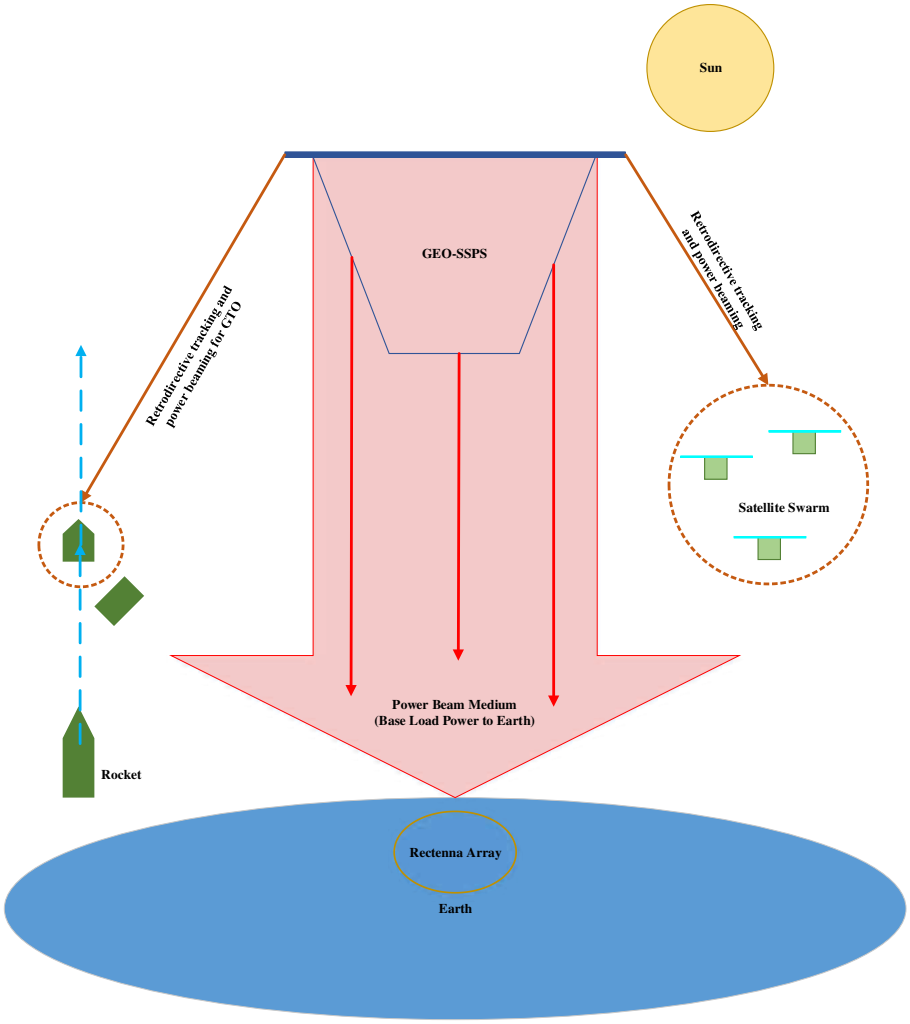

Figure 34. Customer opprotunities of a GEO-SSPS scenario: (1) Delivering base load power to Earth, (2) delivering power to spacecraft and (3) delivering power for GTO.

detected by the SSPS, the power beam is dephased, which causes the system to radiate power over a wider area, losing its directive properties [58].

The same fail safe mechanism can be applied to the dynamic power beam medium scenario but with modifications. First note that essentially the power beam is off-target from the rectenna array on Earth if it is tracking and delivering power to a moving satellite. Most of the radiation from the power beam is not collected by the lower orbiting satellite, but continues to transmit to Earth essentially sweeping the Earth's surface. To

ensure safety of radiation exposure from Earth one idea to prevent this is to only use a certain amount of subarrays from the GEO-SSPS to deliver power to the lower orbing satellites. The use of subarrays to track and deliver power will limit the power density level and area in any direction. Another idea is to incorporate a satellite servicing network where information on lower orbiting satellites is programed into the GEO-SSPS. The information can consist of expected angle of arrival, and time of arrival from a pilot signal coming from a customer satellite. Another piece of information that could be uploaded to the SSPS from the consumer satellite is time for charging.

To ensure that the pilot signal frequency is detected separate from the power beaming frequency, high RF isolation is needed. Two techniques have been proposed [58]: (1) Use separate frequencies between the pilot signal and the power beam, and (2) use the second harmonic of the pilot signal's frequency to operate the power beam (*i.e.* 2.9 GHz pilot beam signal to guide a 5.8 GHz transmit signal [59]). The latter offers advantages over the former in terms of being less complex while achieving high RF isolation.

A GEO satellite has a 17.4° coverage of Earth, as shown on the left side of Figure 35. The right side of Figure 35 shows a right triangle in order to calculate the "field of view" for the GEO-SSPS. Using trigonometry, we are able to calculate the tracking distance denoted as "Base" for the lower orbiting satellites. The hypotenuse of the right triangle is denoted as h, and the altitude is denoted as D. Table 4 contains the calculated results for this right triangle. Doubling the "Base" results, we get the "field of view" of the GEO-SSPS; 2 x Base = 11,000 km for a 300 km altitude, and 2 x Base = 10,400 km

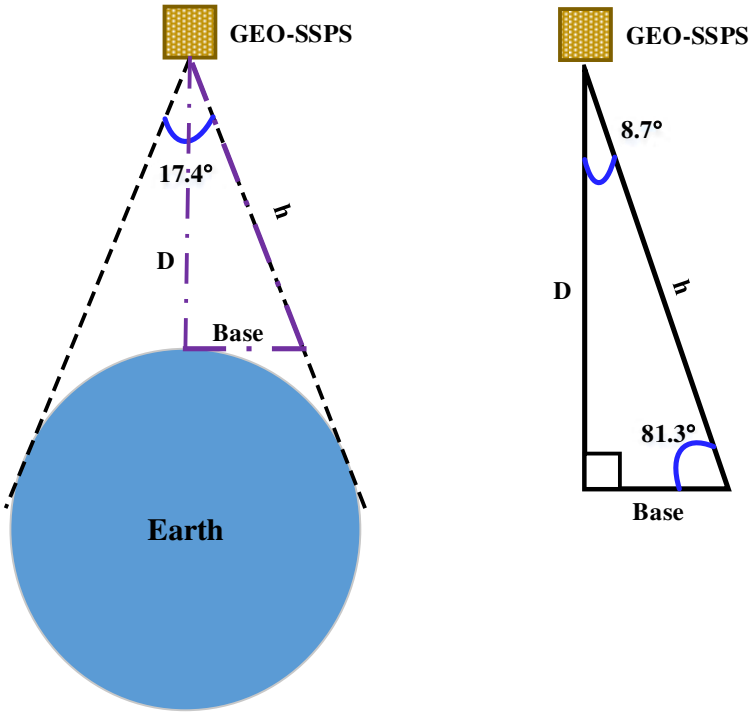

Figure 35. Earth viewed from a GEO satellite on the left side and a right triangle to calculate the "field of view" for the GEO-SSPS on the right side.

for a 2,000 km altitude. The potential "upper bounds" for RF time of exposure is about 24 minutes for the 300 km altitude case and about 25 minutes for the 2,000 km altitude case. This RF exposure time is about one-third the solar exposure time of 64 minutes for a LEO mission.

The modified power beam medium scenario with retrodirectivity offers the prospective benefit of providing RF power on demand over a greater duration of time to lower orbiting spacecraft compared to the fixed power beam medium scenario. Moreover, the modified power beam medium scenario with retrodirectivity compared to the fixed power beam scenario offers greater mission flexibility as lower orbiting satellites from a multitude of orbits can now take advantage of this option by sending a pilot signal to the

Table 4. Calculations for the right triangle of Figure 35.

Symbol	At altitude of 300 km	At altitude of 2000 km
D	35,486 km	33,786 km
$h = D/sin(81.3°)$	35,900 km	34,180 km
Base = $D/tan(81.3°)$	5,430 km	5,170 km

GEO-SSPS that, in turn, retransmits the power back to the signal sources. However, ultimately a balance needs to be made between SSPS infrastructure placed throughout the globe maintaining uninterrupted base load power supply to Earth while simultaneously delivering a useful supply of power to lower orbiting satellites. It would be beneficial for future research to analyze SSPS as an electrical service provider to potential customer satellites, their orbits, number of subarrays on the SSPSs, power density levels, and multiple SSPS sharing the power delivery task through their subarrays.

5.2 Electrical Power System

The electrical power system (EPS) generates, stores, manages, and distributes electrical power to all spacecraft subsystems. The basic components of an EPS are shown in Figure 36. The purpose of the EPS is to supply a regulated source of electrical power to spacecraft loads during a mission life. The EPS design is a key parameter for determining the spacecraft's lifetime and is directly impacted by (1) the life degradation of the solar arrays and (2) the battery capacity degeneration through the extended number of cycles [60]. The design lifetime is also indirectly impacted by the sizing of the power

controllers and regulators, as well as the harnesses and cabling that interconnect the spacecraft subsystems [60].

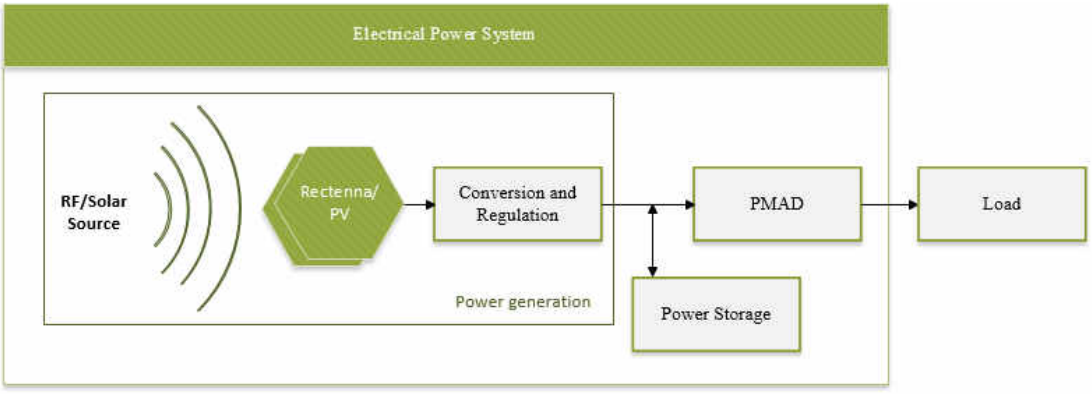

Figure 36. Functional breakdown for spacecraft power system.

Mass is one of the key design parameters for constructing a spacecraft. Mass consumed by an EPS can range between 20% to 75% of total spacecraft mass [61] while occupying a significant portion of the satellite volume [62]. According to Patel [63], "saving of even a few percent of the power system mass can result in appreciable savings at the spacecraft level." Moreover, a mass reduction in the solar array has multiple benefits at the satellite level, such as reduced drag (in lower orbits), inertia, and propellant needed for orbit transfer [63]. This work explores a possible solution to reduce mass (in the EPS) through the installation of a hybrid PV/rectenna array power generation unit.

The EPS has also been found to be the leader in spacecraft failures. Kim, et al., [64] analyzed 1584 Earth-orbiting spacecraft and showed that the EPS spacecraft failures account for more than a quarter of all total failures of spacecraft in orbit. The many components of an EPS increase the chances of failure and comprise the primary spacecraft reliability degrader. Out of 130 spacecraft analyzed by Tafazoli [65], almost

half of the power failures involved the solar array. The solar array is responsible for more failures than any other spacecraft component. Many solar array problems are due to panel deployment mechanism failures and insufficient power generation [65]. Next in line is battery failure, with slightly less than a quarter of failures.

This work investigates a hybrid stacked PV/rectenna array equipped on spacecraft as a possible solution to reduce power generation failures in terms of insufficient power generation. This section analyzes three power generation systems - solar PV array, rectenna array, and stacked hybrid solar PV/rectenna array. This comparison leads to an optimal system which benefits from the dynamic power beam medium scenario. Energy storage and Power Management and Distribution (PMAD) systems are also discussed. The seemingly only difference between a traditional EPS system with a PV array and the proposed new EPS system with a rectenna array or hybrid PV/rectenna array is the power generation function. The energy storage and PMAD functions remain identical. This section ends with EPS mass and cost estimations for the proposed rectenna system.

5.2.1 Power Generation

Electrical power generation systems on spacecraft are a major factor in determining the overall ability of the spacecraft to accomplish its mission. This subsection is broken up into four parts: (1) solar PV array, (2) rectenna array, (3) discussion of the two array, and (4) stacked hybrid solar PV/array. Each system will be analyzed and compared in order to find a viable power generation solution for the dynamic power beam medium environment.

5.2.1.1 Solar PV Array

PV solar arrays are the preferred primary power source for Earth orbiting spacecraft. Satellites in some LEO missions experience about 15 eclipse periods per day [66] (depending on the orbital parameters), which degrades the performance of the solar cells because temperature and incidence angles with respect to the sun are constantly changing throughout an orbit and from solar radiation damage. In some other cases, LEO spacecraft in sunsynchronous orbits can be exposed to continuous sunlight and the extended solar radiation can damage the cells. Moreover, the life degradation L_d of the solar array occurs from micrometeoroid strikes, plume impingement from thrusters, material properties, and outgassing [66]. For missions lasting longer than 10 years, the power generated by the PV cells/arrays becomes poor because of natural degradation in the solar array [66]. Life degradation is a function of the design lifetime and can be estimated as:

$$L_d = (1 - D)^L \tag{5}$$

where D is the degradation per year and L is the satellite lifetime in years.

Multi-Junction (MJ) Gallium Arsenide (GaAs) solar cells have become the standard for most space applications due to their high efficiency and radiation resistance, although these attributes come at a high cost [66]. Thus, this thesis will reference the MJ GaAs cell in its analysis. For an ultra MJ GaAs solar array, the degradation is about 0.5% per year. Table 5 shows necessary power at beginning of life (BOL) as a function of design lifetime for various end of life (EOL) power goals. The EOL power goal range is reasonable as micro satellites in the 10-100 kg mass range have a 26-120 W array [67], mini satellites in the 100-200 kg mass range reach into the 70-200 W power supply

capability [68], and small satellites in the 200-500 kg mass range will reach levels greater than 500 W [68]. Higher power levels (1000W and 2000W) are also considered for potential power level increase.

The solar array area A_{sa} required to produce the P_{BOL} is approximated [60] as

$$A_{sa} \cong P_{BOL} / (I_s \times \eta) \quad (6)$$

where I_s is the solar intensity at 1 astronomical unit (1368 W/m^2) and η is the solar cell's energy conversion efficiency (28% for Ultra Triple Junction [UTJ]) times array inherent degradation (0.64). Inherent degradation accounts for the inefficiencies of an assembled solar array such as cell design inefficiencies, shadowing, and temperature variations. Solar array area as a function of P_{BOL} is shown in Table 5. We then multiple 2.8 kg/m^2 (approximate) of the solar array [66] by A_{sa} to give the approximate mass of the solar array M_{sa} as seen in Table 5.

From Table 5 the range of values in the second column come from an assumed 3-15 year mission life for each P_{EOL} goal. The longer the mission life, the larger the area the solar PV array needs to be in order to collect the respective power for the duration of its mission. It must be noted here that other factors that would impact the calculations of PV array area and mass include accounting for the power needed in eclipse period, as well as a peak power tracking regulation efficiency. These calculations assumed continuous, optimal illumination.

5.2.1.2 Rectenna Array

A second power generation unit considered in this analysis is a stand-alone rectenna array. According to Brown and Eves [51], an 85-92% microwave power reception-to-DC

power efficiency can be reached at 2.45-GHz. However, the calculations in this work uses a 5.8 GHz operating frequency, where Valenta and Durgin [69] have put together a historical timeline of RF-to-DC conversion efficiencies for this frequency. Based on this history the next set of calculations we assumed an 84% microwave power reception-to-DC power conversion efficiency [17].

Table 5. Estimated solar array area and mass.

P_{EOL} (W)	P_{BOL} (W) Respectively for (3-15) year missions	A_{sa} (m^2)	M_{sa} (kg)
50	50.8-53.9	0.21-0.22	0.58-0.62
150	152.3-161.7	0.62-0.66	1.74-1.85
500	507.6-539.0	2.07-2.19	5.79-6.16
1000	1015.2-1078.1	4.14-4.39	11.59-12.31
2000	2030.3-2156.2	8.28-8.79	23.19-24.63

Table 6 shows the estimated rectenna array area A_{ra} and mass M_{ra} needed to produce the required power to the satellite. The rectenna area calculation was obtained by dividing the SERT high power irradiance (for a range of LEOs) by the power needed on the satellite, factoring in a 19% area increase to make up for the conversion efficiency loss. When comparing solar array area from Table 5 and rectenna array area from Table 6, we see that the rectenna array area is larger than the solar array area to collect a similar amount of power. Even though the efficiency of the RF-to-DC power conversion is nearly three times greater than solar-to-DC power conversion, the power irradiance of the

microwave beam in LEO is much less than the power irradiance from solar energy is. However, the rectenna array has essentially an infinite lifetime compared to that of the solar array.

Table 6. Estimated rectenna array area and mass.

Power (W)	A_{ra} (m^2) [300 km-2000 km]	M_{ra} (kg) [300 km-2000 km]
50	0.29-0.27	0.18-0.17
150	0.88-0.80	0.54-0.50
500	2.93-2.65	1.80-1.62
1000	5.85-5.30	3.60-3.25
2000	11.70-10.61	7.18-6.51

To calculate the mass of a rectenna array, this dissertation considers Roger Corporations RT/duroid 6002 [70] as the material to etch out the planar rectenna array design. This material was chosen because it offers qualities favorable for space-based applications [71, 72] in terms of out-gassing and temperature tolerances as will be elaborated on in Chapter VIII. Some initial assumptions about the specifics of the analysis are now made. Assume the material has a copper cladding of 1 oz/ft^2 (0.305152 kg/m^2), substrate thickness of 0.508 mm (20-mil or 0.000508 m), and a dielectric density of 2.1 mg/cm^3 (2.1 kg/m^3). Let Cu cladding be represented by c, substrate thickness by t, and dielectric density by d. The equation to calculate the mass of the rectenna is then given by

$$M_{ra} = A_{ra}\left(2c + td\right) \tag{7}$$

The factor of 2 in the equation accounts for two layers of copper in the rectenna topology, as shown in Figure 37. On one side of the substrate, the copper plate is for the etched rectenna design, and the other copper plate is placed a distance ~λ/4 (λ is the wavelength) behind the substrate to be used as a reflector. For this mass estimation, we assumed two solid copper plates with no etching or circuit components or coating material or bonding material, etc. The estimated rectenna array is shown in Table 6. It must be noted that the calculations for A_{ra} and M_{ra} assumed continuous, optimal illumination as the satellite with rectenna array travels through the power beam medium of the GEO-SSPS. When comparing the estimated mass of the solar array in Table 5 to the estimated mass of the rectenna in Table 6, we see a mass reduction in generation systems based on the assumptions used to estimate the masses.

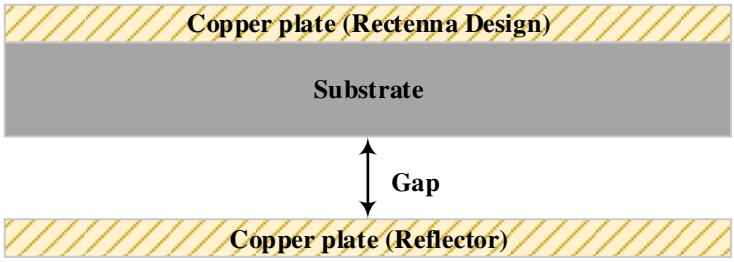

Figure 37. Substrate considered in the analysis.

5.2.1.3 Discussion of the Two Arrays

An interesting discussion arises on how does the conversion efficiency of PV and rectenna arrays compare for factors such as variations in incident power density, wave incidence angle, and polarization. This discussion, as well as a discussion comparing component life between the two arrays, is now presented.

Since the power density in LEO is relatively consistent for solar energy, the potential effects from a change in power density flux would come from the power beam medium. In the power beam medium, the power density is strongest in the center of the beam and weaker moving away from the center of the beam. As the power density increases, the efficiency of rectenna RF-to-DC conversion will also increase. Thus, it seems that at lower power density locations in the power beam medium the efficiency will be lower and as the satellite approaches the center of the power beam medium the efficiency will increase. Several studies indicate that the higher the input power the greater the efficiency [7, 9].

Typically, rectifier circuits for wireless reception applications are designed to operate for specific input power levels and loads. Deviation in power density from the nominal operation of the rectenna, i.e., through change in flux density, will decrease the system performance. The decrease in system performance, i.e., RF-to-DC conversion efficiency, happens because of the nonlinear behavior of the diode component in the rectifier circuit. That is, as the satellite travels through the power beam medium the power density levels change, thus the impedance of the diode changes (non-linearity), and this change in diode impedance is different than the design impedance of the circuit. Consequently, this deviation decreases the rectenna's RF-to-DC conversion efficiency. To help alleviate this problem, resistance compression networks (RCNs), as proposed by Han, et al., [73], may help as matching networks placed before the rectifier circuit(s) with the promise of reduction in the load sensitivity.

McSpadden, et al., [7], found that the rectenna efficiency proves to be very non-directional and that, when placed on a moving target, the rectenna will receive power

efficiently at various angles of incidences. The typical rectenna array pattern can be modeled as a $\cos^x \theta$ rolloff loss where x represents an exponent to model impedance mismatch over angles of incidence. The assumption is that each antenna element feeds a single diode. For a PV array, the equation to account for cosine loss is $\cos\theta$. The incident angle θ is measured between the vector normal to the surface of the PV array/rectenna array and the sun line/RF line. Assuming a LEO mission and $x = 1.3$ (assumption of a linearly polarized array of horizontal dipole antennas, each antenna terminated in a rectifying diode [74]), the cosine loss angle comparison between Solar PV array and Rectenna array is provided in Figure 38. Because of the effects of mutual coupling between the radiating elements, the radiation impedance of an element varies with beam steering and is also a function of the element location [75, 76].

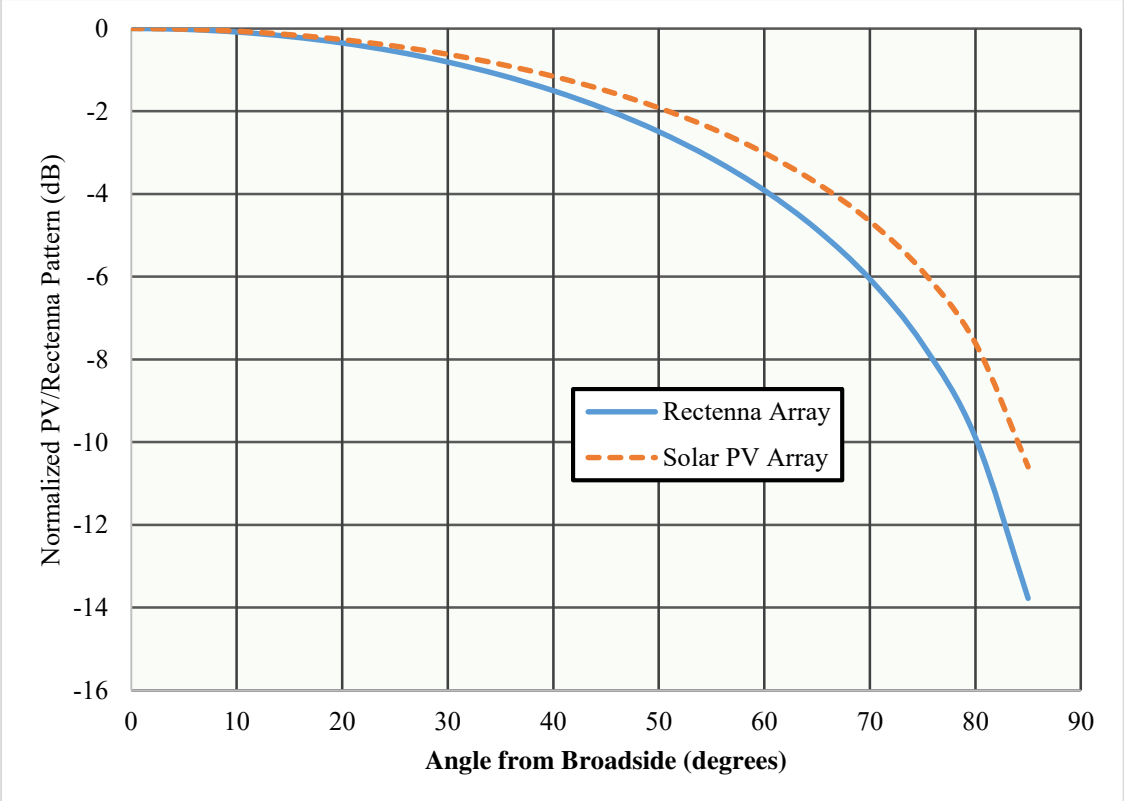

Figure 38. Normalized PV/rectenna losses as a function of theta angle.

Finally, polarization is not a major issue for PV as the PV process comes from the photoelectric effect and the orientation of the electric or magnetic field plays little or no role. However, it is an important question on how polarization would affect the efficiency of the rectenna array. Provided that both transmit and receive antennas are designed to transmit and receive the same CP wave with low axial ratio and low mismatch loss, then minimal loss would occur [56]. Moreover, CP is less sensitive to the rotation of the receiver or transmitter antennas and has less effect on the level of output voltage [9, 37]. However, as the receive antenna is rotated from broadside of the transmit antenna a polarization loss factor $PLF = \left|\cos\psi_p\right|^2$, needs to be accounted for. Multiplying the PLF by the pattern loss we obtain an estimated angular losses as the receiving antennas rotates away from broadside.

One last discussion in the comparison of the two arrays is component life. GaAs Schottky diodes are very resilient to space radiation and single-event effects [77]. GaAs Schottky diodes on the rectenna array will outlive the solar cells as the diode components that convert RF-to-DC naturally live longer than cell components that convert solar-to-DC do. The solar cell component over time has a higher rate of depletion than does the diode component because of the nature of the former's function in the space environment. We also know that microstrip antennas can be designed to handle hundreds of watts [78]. However, due to the multipacting breakdown effect [78], microstrip power handling in space is reduced with respect to the expected value of the Earth's atmosphere. Designs can be made to preclude the onset of multipaction breakdown [78]. Microstrip antennas in space also last a very long time and methods employed to protect the antennas can be

found in [78]. The Phoenix Program from the Defense Advanced Research Projects Agency (DARPA) studied existing communications spacecraft. The program found that, while most spacecraft components would have 25 year lifespans, the communications antenna's useful lifespan could be as high as 100 years [79].

Section 5.2.1.4 combines the analysis from 5.2.1.1, 5.2.1.2, and 5.2.1.3 in order to present a possibly viable option for lower orbing spacecraft to benefit from a dynamic power beam medium scenario with a hybrid power generation unit.

5.2.1.4 Stacked Hybrid Solar PV/Rectenna Array

A third system considered is a hybrid PV/rectenna array power generation unit [48-50]. The hybrid power generation unit would allow power to be generated from both solar and microwave sources, separately or simultaneously, while maintaining compactness by integrating the solar panels on top of the radiating structure used by the RF harvester [48, 49]. According to Zawadzki and Huang [50], combining these apertures will "reduce spacecraft mass, stowage volume, cost, and deployed surface area, without significantly affecting the performance of either the antenna or solar array." In fact, previous experiments implementing solar cells on the surface of microstrip antennas showed that antenna radiation did not influence the power generation process of the solar cells [48]. Similarly, experiments showed that solar cells did not affect RF radiation [48].

For the stacked hybrid solar PV/rectenna array system, let us first assume a case where the previously calculated solar PV array (3-15 year mission life) would be stacked on top of the previously calculated rectenna array (300 km – 2000 km) for continuous, optimal illumination. Table 7 shows the results of this calculation, which indicates that the area of the stacked hybrid system A_{hybrid} (equal to area of the rectenna array) does not

change, whereas the hybrid array mass M_{hybrid} is increased and the power level is doubled. The objective of this research is to show how the stacked hybrid area can be used as a design parameter to reduce a satellite's EPS mass while still obtaining the desired power level from a dynamic power beam medium environment.

Table 7. Area and mass estimations for the hybrid array. The previously calculated PV array was stacked on top of the previously calculated PV array.

Power (W)	Hybrid P_{BOL} (W)	A_{hybrid} (m^2)	M_{hybrid} (kg) [3 year mission, 300-2000 km]	M_{hybrid} (kg) [15 year mission, 300-2000 km]
50	100.8-103.9	0.29-0.27	0.76-0.75	0.80-0.79
150	302.3-311.7	0.88-0.80	2.29-2.24	2.39-2.35
500	1007.6-1039.0	2.93-2.65	7.59-7.41	7.96-7.78
1000	2015.2-2078.1	5.85-5.30	15.19-14.84	15.91-15.56
2000	4030.3-4156.2	11.70-10.61	30.37-29.70	30.49-31.14

Figure 39 combines information from Figure 38 with power density levels from both solar levels in LEO and RF levels from SERT High for 300 km and 2000 km altitude orbits. These calculations are based on continuous, non-optimal illumination, as the satellite orbits in the field of view for both solar energy from the sun and RF from the GEO-SSPS. Clearly, the hybrid system offers greater available power for harvesting compared to the two standalone systems. However, at angles greater than $\pm 45°$ - $\pm 50°$, the RF system experiences significant losses [80], assuming antennas halfpower beamwidth are less than 40°.

Factoring in the field of view coverage for GEO-SSPS where the lower orbiting spacecraft begins harvesting RF power at 45°, the "field of view" is reduced to 2×Base×*cos(45°)* ≅ 7,800 km for a 300 km altitude orbit, and ≅ 7,400 km for a 2,000 km altitude orbit. Figure 40 shows this modified scenario with the new base indicated in green. In terms of the two orbits, the "RF exposure time" for a continuous beam reduces to 16.8 minutes and 17.8 minutes, respectively.

Using the previously calculated "time of exposure" results for solar and RF sources in LEO and assuming continuous, optimal illumination during that time interval for a dynamic power beam medium scenario, we now show that the area of the hybrid array can be modified so that the mass of the hybrid array, and ultimately the mass of the EPS, can be reduced while maintaining required power level demands for the mission.

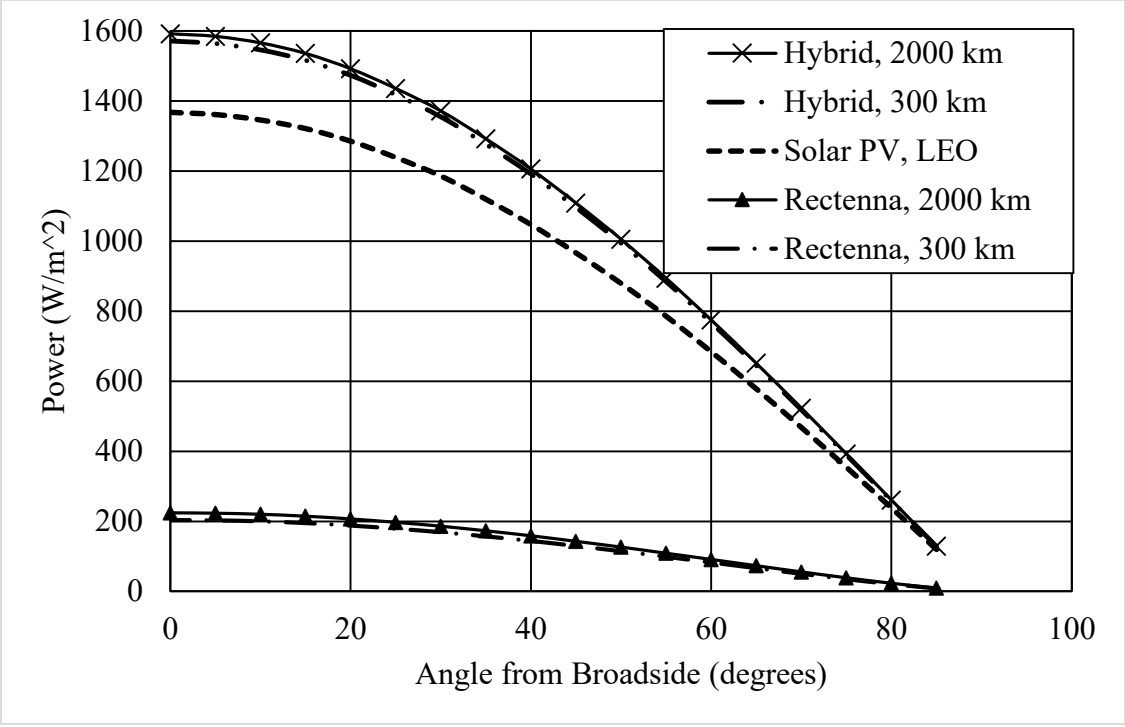

Figure 39. Power density losses for PV, rectenna and hybrid PV/rectenna arrays as a function of theta angle.

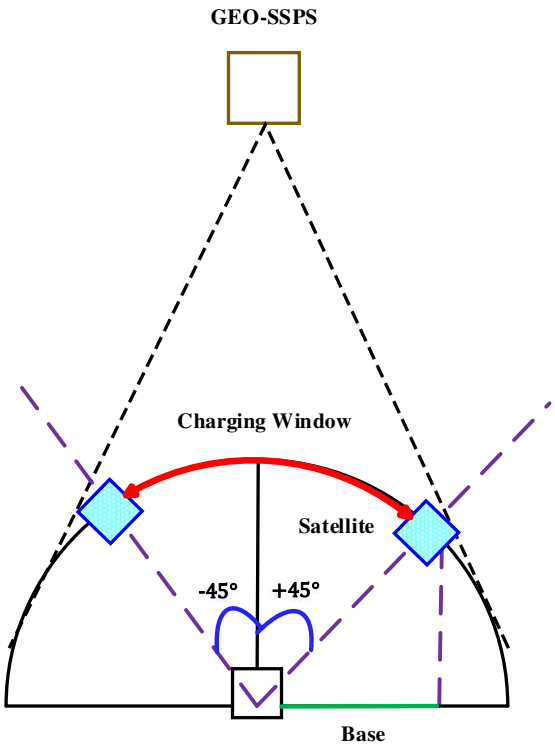

Figure 40. Charging window or the estimated time that the lower orbiting satellite can generate RF power from a GEO-SSPS.

To simplify the calculations, we used the average RF exposure time of 17.3 minutes, or about 0.29 hours in LEO and multiplied that by power (i.e., 50, 150, 500, 1000, and 2000 W) to get the power generated per time per orbit as shown in Table 8. The average of P_{BOL} from the solar array calculations found in Table 5 are multiplied by the daylight period of the satellite orbit in LEO (64 minutes, or 1.06 hours) to get the power generated per time. These results are also found in Table 8. As can be seen from these calculations there is excess power available per orbit from the hybrid system. From these results we could alter the size of the area as a parameter from the stacked arrays in order to acquire the necessary power level demand for the proposed mission life of 3-15 years while simultaneously reducing the power generating unit mass.

Table 8. Averages of power per time per orbit for rectenna, PV, and hybrid array systems.

Power (W)	Average Rectenna Array Power · Time (Whr)	Average (3-15 year mission) P_{BOL} (W)	Average (3-15 year mission) PV Array Power - Time (Whr)	Total Average Power of Hybrid System for P_{BOL} (Whr)
50	14.5	52.4	55.5	70.0
150	43.5	157.0	166.4	209.9
500	145.0	523.3	554.7	699.7
1000	290.0	1046.7	1109.5	1399.5
2000	580.0	2093.3	2218.9	2798.9

In order to set a premise, let the area and mass of the rectenna array as previously presented in Table 6 be fixed. It was previously calculated that M_{ra} is less than M_{sa}. Also, the previous analysis indicated that the rectenna array will have a much longer life than that of the solar PV array. Because $M_{ra} < M_{sa}$, and considering the fact that the component life of the rectenna array is longer than the component life of the solar array, the P_{BOL} parameter is varied to reduce A_{sa} and M_{sa}. About 32% reduction in the PV arrays P_{BOL} gives us the power generation units P_{BOL} goal for the hybrid system, as seen in Table 9. The reduction in A_{sa} part of the hybrid array corresponds to slight mass savings in the power generation unit, as seen in Table 10.

From these calculations, we can see that the areas of the hybrid array can be used as a parameter to decrease the mass of the power generation unit, thus, ultimately decreasing the mass of the satellites' EPS. In the design process for a P_{EOL} goal the area

Table 9. Power per time calculations.

Power (W)	Average Rectenna Array Power - Time (Whr)	$P_{BOL,sa}$ (W)	Average (3-15 year mission) PV Array Power - Time (Whr)	Total Average Power of Hybrid System for P_{BOL} (Whr)
50	14.5	35.6	357.8	52.3
150	43.5	106.8	113.2	156.7
500	145	355.8	377.2	522.2
1000	290	711.8	754.5	1044.5
2000	580	1423.4	1508.9	2088.9

Table 10. EPS mass reduction calculations.

Power (W)	Average A_{sa} (m^2)	Average A_{sa} (m^2) 32% P_{BOL} Reduction	Average M_{sa} (kg)	Average M_{hybrid} (kg)	Average M_{hybrid} (kg) 32% P_{BOL} Reduction
50	0.2	0.15	0.6	0.77	0.58
150	0.5	0.44	1.8	2.32	1.73
500	2.1	1.45	5.9	7.71	5.83
1000	4.3	2.90	11.9	15.38	11.47
2000	8.5	5.81	23.9	30.76	22.94

of the solar array can be decreased in order to decrease EPS mass, yet the area of the rectenna array can be increased in order to accommodate for the power degradation losses over time from the solar PV array. Clearly, the areas of the hybrid power generation unit as a satellite design parameter seem to offer the projected benefits of reducing EPS mass, as well as allowing longer mission durations and greater flexibility in the missions. With the rectenna array outliving the solar array and if various SSPS are one day being operational, then orbiting satellites could take advantage of the various "fueling stations" placed throughout the globe. Of course, an extensive analysis is needed on placement of the GEO-SSPS throughout the globe, on satellite orbits, on sub-arrays, and on the delivery of power to lower orbiting spacecrafts in order to optimize and take full advantage of the dynamic power beam scenario.

5.2.2 Energy Storage

A spacecraft that uses PVs as a power generation method requires a system to store energy for eclipse periods and peak power demands [66] such as communication with ground systems. Similarly, a spacecraft that uses a stand-alone rectenna array as a power generation method needs to store energy for periods when it is outside the microwave beam and during peak-power demands. Clearly, the same logic applies for the hybrid PV/rectenna array. This section focuses on secondary power sources, such as batteries and super-capacitors as energy storage methods. Secondary power sources are recharged in sunlight for the PV systems and when inside the microwave beam for the rectenna systems. They discharge during eclipse or during spacecraft peak power demands. Eclipse for this thesis means that the satellite is neither in daylight nor the

microwave beam. This section also discusses a hybrid battery/super capacitor power storage unit to accommodate for the hybrid PV/rectenna array power generation method.

Satellites in LEO missions experience about 15 eclipse periods per day (~5,000 cycles each year). However, the satellite equipped with rectenna array traveling through the microwave beam will experience shorter periods of charging compared to a satellite with PV charging through its daylight orbital period. This disparity exists because the satellite illumination time through a microwave beam is only a small fraction in comparison to a satellite illumination time through a daylight period for a fixed power beam medium scenario. However, in the case of a dynamic power beam medium, it was calculated that the RF exposure time is about one-third the solar exposure time for a LEO. During eclipse periods, the satellite is highly dependent on its pre-charged secondary power source. It currently appears that Lithium Ion (Li-Ion) will likely become the preferred rechargeable battery for most, if not all, spacecraft missions [66]. Therefore, emphasis will be given to Li-Ion batteries as a storage element.

An important characteristic for batteries is the Depth-of-Discharge (DOD), the percent of total battery capacity removed during a discharge period. For LEO, the battery's DOD is 20-40% for Li-Ion, in order not to overstress the batteries [66, 81]. High DOD levels (mainly during the eclipse phase) will shorten the battery lifetime and, thus, the mission-life. Options to help maintain a longer mission life include the following; (1) enlarge the battery capacity and/or utilize batteries with higher allowed DOD and/or higher power irradiance, (2) adapt the adequate/flexible mission profile(s), or (3) enlarge the solar array area and/or utilize more efficient cells. These options will now be discussed.

Increasing battery capacity through the installation of more or bigger batteries (or super capacitors) requires more mass. Because the rectenna array is lighter than the PV array is, the saved mass could be reallocated to increase energy storage. Additionally, using a hybrid storage pack, i.e., battery/super-capacitor, as suggested by Shimizu and Underwood [68], allows acquisition of the best properties of both technologies to support spacecraft operations and may allow for higher allowed DOD. Adding a super capacitor with the battery to make a hybrid storage pack would provide the system with the needed power during peak-power periods and make the satellite operate over a wider storage and temperature range [68]. Additionally, super capacitors show an excellent charge/discharge efficiency and a high power density due to their low internal resistance and the absence of chemical reactions for storing energy [68]. Additionally, charge and discharge can take place in relatively extreme temperatures where Li-Ion batteries could not operate [68]. This flexibility could make the satellite work in a wider range of missions and lead to a simpler thermal system and a mass savings.

A possible option to explore would be to decrease the use of the batteries when the temperature inside the satellite is too low or too high and give priority to the super capacitor pack to charge and discharge. Also, the energy stored in the super capacitors can be used for peak power demands, thus reducing the demand on the batteries. Inversely, if the satellite experiences average temperatures and a low power demand from the load, the batteries would have priority in the charging and discharging process. Finally, the super capacitors would benefit a satellite with a rectenna array by allowing for only a short time of charging as it travels through the microwave beam. The rectenna array part of the stacked hybrid power generation unit could be used solely to send

energy to a super capacitor bank to store that energy for peak times, which would reduce the demand on the batteries and, therefore, increase the battery performance lifetime.

Enlarging a PV area and utilizing more efficient cells usually indicates acquiring greater costs and mass. The stacked hybrid PV/rectenna array system may help to alleviate this issue by decreasing the EPS mass through reducing A_{sa} while simultaneously increasing the collection area through A_{ra} and still acquiring a reduced EPS mass.

Continuing with energy storage, the battery energy capacity (C) is defined from [66] as

$$C = P_e T_e N n / DOD \ (Wh) \tag{8}$$

where P_e is the average eclipse load, T_e is the length of eclipse duration, N is the number of batteries, and n is the battery-to-load transmission efficiency. The objective in the next set of calculations is to acquire an estimated mass of the spacecraft batteries for the power levels, *i.e.*, 50, 150, 500, 1000, and 2000 W. This mass will be used later in the EPS Cost Estimation subsection. To perform the battery mass estimation, reference Figure 21-6 in [66] and assume that the energy storage mass is 15% higher than the mass of the power source (PV array). Table 11 shows the battery mass estimation based on a 15% mass increase from the solar array found in Table 5. For this work, we only consider the mass of batteries calculation provided in Table 11 for the three power generation units analyzed.

Table 11. Mass estimations for batteries.

P_e (W)	C (W-Hr)	Mass of Batteries (kg) (15% greater than M_{sa})
50	67.5	0.67-0.71
150	202.5	1.99-2.12
500	675	6.67-7.08
1000	1350	13.33-14.16
2000	2700	26.67-28.32

5.2.3 Power Management and Distribution

Power management pertains to power conditioning and to charge and discharge control. Electrical power generated from the primary sources**,** i.e.**,** solar and microwaves**,** must be controlled to prevent the storage elements from overcharging**,** as well as reducing or preventing any undesired spacecraft heating [66]. For this part, we will focus on the common charging methods for PV systems and propose a method for rectenna systems. Methods employed include directive energy transfer (DET) or peak power tracker (PPT).

In the DET system, power is sent from the PV panels directly to the loads without control units. In a DET system the solar array must operate at the same voltage as the rest of the bus. PPT system is similar to the DET system with addition of a PPT regulator between the PV panels and the load. In a PPT system the solar array and bus can operate at different voltages. According to Patel [63], PPT architecture is generally advantageous for small satellites in low or irregular orbits having a power requirement of less than 500W. Therefore, PPT architecture is attractive for missions in LEO that have large

variations in solar flux, solar array temperature, and sun angle. The advantage of the PPT is that it makes the maximum use of the incident solar energy. The disadvantage of the PPT is that it requires more circuit design effort compared to DET, thus causing higher weight and cost [82], as well as more heat dissipation inside the spacecraft body [63].

To alleviate this power loss, a gimbal system, as seen in Figure 41, connected to the PV array can use mechanisms to rotate (Elevation and/or Azimuth) the PV array during orbit to point at the sun longer, thus capturing greater amounts of energy. However, in general, spacecraft designers try to avoid these methods (PPT and gimbal system) because they add complexity and expense. The advantages and disadvantages of each solar tracking mechanism are listed in Table 12.

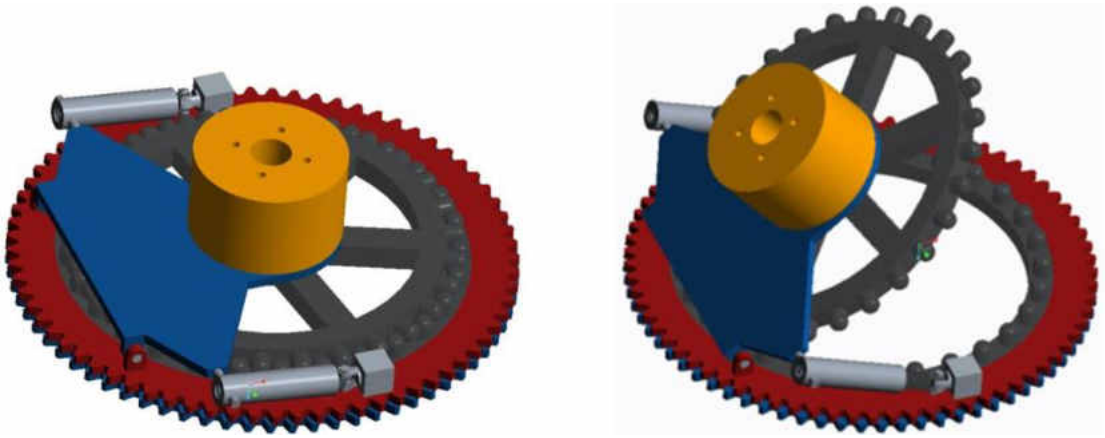

Figure 41. An example of a gimbal system [26].

In the case of the rectenna array equipped on spacecraft, a DET system can be utilized, but during an orbit the rectenna array may experience large ranges of voltage changes due to power density flux, as well as range changes. In this case, a regulating system may be inserted after the rectenna module in order to protect the EPS. Also, orienting the spacecraft equipped with a rectenna array toward the microwave power

Table 12. Pros and cons of different solar/RF tracking mechanisms [26].

System	Gimbal [83, 84]	Regulated DET [63, 66]	Un-regulated DET [63, 66]	PPT [63, 66]
Advantages	Continuous pointing at the sun for max energy collection through sunlight period	Well regulated input voltage to all loads. Simpler, lighter, more efficient load converters.	High power transfer efficiency from solar array and battery to load. Fewer EPS components.	Shunt regulator or battery charge regulator not required. Makes the max use of the incident solar energy.
Disadvantages	Additional: Weight Complexity Source of jitter. Hardware and software required.	Additional EPS converters. Series power loss between battery and load.	More complex load converters. Potential "lockup" problems. Larger solar array.	Additional: Weight Complexity Significant noise source Less efficient than DET at EOL in many cases. More heat dissipation inside spacecraft.
Best Application		Large solar array power/voltage variations	Small load variations. Small power source variation for most of sunlight period.	Large variations in solar array illumination throughout the mission.

beam may be simpler than orienting a satellite equipped with a solar array toward the sun [63]. If the former is always normal to the Earth, then changes in irradiation and temperatures inside the beam are minimal, thus no PPT or gimbal system is necessary to

optimize the power intake at the satellite. The use of only a rectenna array would further decrease the EPS mass, potential failures, and complexities of the system. A hybrid solar PV/rectenna array with retrodirectivity capability seems the most beneficial option as has been shown.

Power distribution is routed from the power conditioning unit and a charge and discharge control unit. This power path will remain the same for the rectenna array EPS as the one for the PV array EPS. The conditions of daylight, eclipse or peak demands determine what route the power comes, i.e., primary or secondary power source. The power is then distributed to the respective subsystems. The power conditioning unit for this EPS may contain a DC-to-DC regulator that provides a stable voltage regulation from the primary power source to the main power bus. A charge and discharge control unit will then regulate the voltage from the main bus in order to give a safe charge to the different components of the energy storage packs. The flow of voltage and current levels from the storage unit is also going to be monitored to track failures and keep the storage elements charge and discharge rate in the safe margins. In case of failure in one load or if the satellite does not have enough power for one subsystem, a control switch cuts off the power going to the selected load. All data will be sent to the EPS microcontroller. This microcontroller decides whether or not to cut the power over subsystems depending on the data available. The components and implementation of this process are shown in Figure 42 and Figure 43.

The switches in Figure 43 exist in case of a hard reboot for a serious malfunction that cannot be corrected by a soft reboot. The EPS MCU is the micro-controller that will

be responsible for doing this action, as well as for maintaining power to other subsystems during that period.

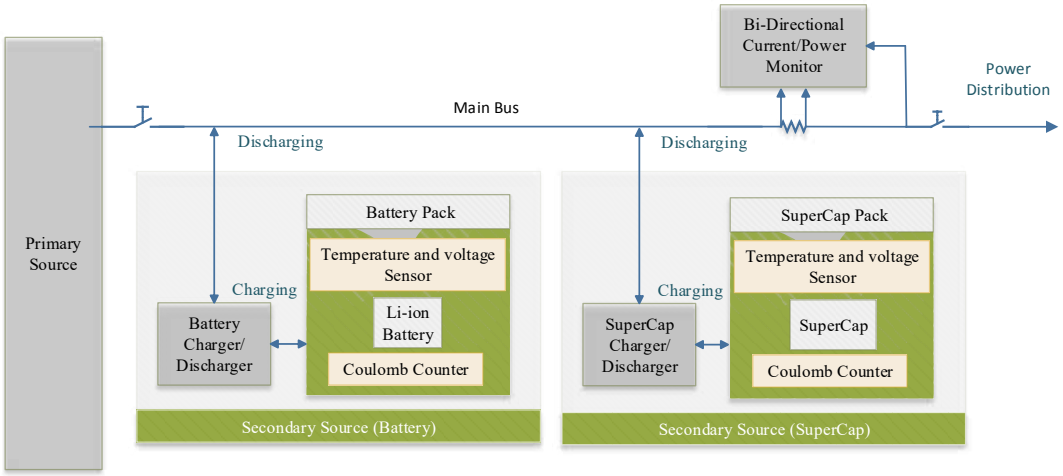

Figure 42. Power storage subsystem.

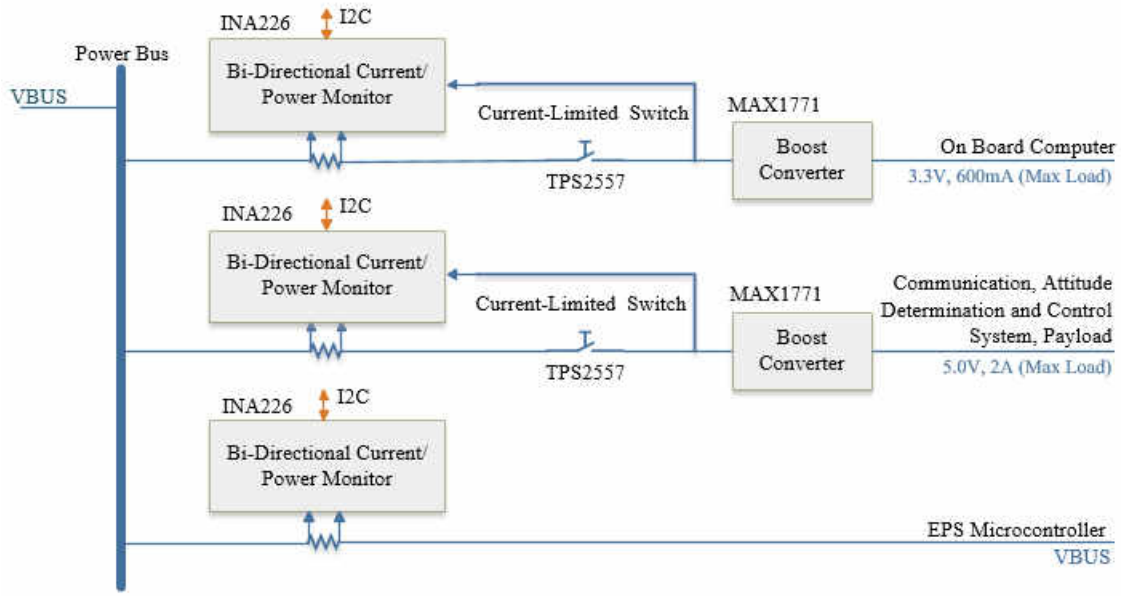

Figure 43. Power distribution block of the satellites EPS. I2C is the communication protocol used by the EPS Microcontroller.

5.2.4 EPS Mass Estimation

We have previously calculated the masses for each of the three power generation systems and for the energy storage system. Mass of the EPS (M_{EPS}) can be calculated using [60] as

$$M_{EPS} = M_{array} + M_{batteries} + M_{PCU} + M_{dist} \tag{9}$$

The mass of the power control unit (M_{PCU}) is provided in [60] as

$$M_{PCU} = 0.0045 \times P_{BOL}. \tag{10}$$

The mass of the power distribution system (M_{dist}) constitutes a large part of the EPS mass, roughly 10-20% [60] and is calculated as

$$M_{dist} = 0.15 \times M_{EPS} \tag{11}$$

Therefore equation (9) becomes

$$0.85 M_{EPS} = M_{array} + M_{batteries} + M_{PCU} \tag{12}$$

Table 13 shows the estimated mass of the EPS for solar PV array and rectenna array. These mass estimations considered a 7-year mission goal in the case of the solar PV array and a 300 km altitude orbit for the case of the rectenna array. The results of this example calculation show around 28% mass decrease in the rectenna array compared to the solar PV array. However, as we stated previously, the stand-alone rectenna array system in a fixed power beam medium scenario does not work. Therefore, a stacked hybrid PV/rectenna array system was proposed for a dynamic power beam scenario (i.e., retrodirectivity). The hybrid EPS mass $M_{EPS(hybrid)}$ calculation was with the assumption of a 7-year mission goal at a 300 km orbit. The results show that the EPS mass of the hybrid system is similar to the EPS mass for the stand alone PV solar array system. Note that the area parameters of the two arrays in a stacked configuration can be tuned to further decrease the EPS mass, although, the design parameter, A_{sa}, depends on available RF power throughout the satellites' orbit, which is a topic for future research.

Table 13. Mass calculations for the solar PV array, rectenna aray, batteries, PCU, and EPS.

Power (W)	P_{BOL} (7 yr)	M_{sa} (kg)	M_{ra} (kg)	M_{hybrid} (kg) 32% P_{BOL} Reduction	$M_{Batteries}$ (kg)	M_{PCU} (kg)	$M_{EPS\ (sa)}$ (kg)	$M_{EPS\ (ra)}$ (kg)	$M_{EPS\ (hybrid)}$ (kg)
50	51.8	0.6	0.2	0.6	0.7	0.2	1.8	1.3	1.8
150	155.4	1.8	0.5	1.7	2.0	0.7	5.3	3.8	5.2
500	517.9	5.9	1.8	5.8	6.8	2.3	17.7	12.8	17.5
1000	1035.7	11.8	3.6	11.5	13.6	4.7	35.4	25.8	35.0
2000	2071.4	23.7	7.2	22.9	27.2	9.3	70.8	51.4	69.8

5.2.5 EPS Cost Estimation

The cost estimating model, Small Spacecraft Cost Model, 10th edition, was used to estimate the cost for development and for the Theoretical First Unit (TFU) of the proposed EPS with rectenna array. Production of N number of EPS units will also be calculated. The cost driver for the cost estimating relationship (CER) is the beginning of life power (P_{BOL}). Table 14 shows the estimated cost (C_{Total}) in fiscal year (FY) 2014 dollars for development and TFU of the EPS for a satellite with deployable sun-pointing array, GaAs solar cells, and Ni-H2 battery for desired power levels of 50, 150, 500, 1000, and 2000 W. Note that the planned battery (Li-Ion) is more efficient. Consequently this estimate is expected to be conservative. Nonrecurring cost (C_{NRe}) and recurring cost (C_{Re}), i.e., TFU, are also provided.

The production units are calculated from equations (13)-(15):

$$B = 1 - \frac{\ln\left((100\%)/S\right)}{\ln 2} \tag{13}$$

$$L = N^{B} \tag{14}$$

$$\text{Production cost } = TFU \times L \tag{15}$$

Table 15 shows the estimated cost (C_{Total}) for development and TFU of the EPS for a satellite with deployable rectenna array and Ni-H2 battery for desired power levels of 50, 150, 500, 1000, and 2000 W. Since there is essentially no decay over time, the $P_{BOL} = P_{EOL}$. Comparing these two tables shows that the cost of the EPS with rectenna array equipped on a satellite is essentially the same as the cost of the EPS equipped with a PV array on a satellite.

Table 14. Cost estimation with deployable sun-pointing array, GaAs cells, and Ni-H2 battery for 3-15 year service life for FY14$.

P_{EOL} (W)	P_{BOL} (W) (3-15 years)	C_{NRe} (FY14$K)	C_{Re} (FY14$K)	C_{Total} (FY14$K)
50	50.8-53.9	1667-1702	2501-2553	4169-4255
150	152.3-161.7	2428-2478	3642-3718	6070-6196
500	507.6-539.0	3665-3741	5497-5611	9162-9352
1000	1015.2-1078.1	4645-4742	6968-7113	11613-11854
2000	2030.3-2156.2	5888-6010	8832-9015	14720-15025

The production units are calculated from equations (13)-(15):

$$B = 1 - \frac{\ln\left((100\%)/S\right)}{\ln 2} \tag{13}$$

$$L = N^B \tag{14}$$

$$\text{Production cost } = TFU \times L \tag{15}$$

Table 15. Cost estimation with deployable rectenna array, NiH2 battery, and 3-15 year service life for FY14$

$P_{EOL} = P_{BOL}$ (W)	C_{NRe} (FY14$K)	C_{Re} (FY14$K)	C_{Total} (FY14$K)
50	1658	2488	4147
150	2415	3623	6038
500	3646	5469	9115
1000	4621	6932	11553
2000	5858	8786	14644

The learning curve slope (*S*) of 95% gives a learning curve factor (*L*) of 0.926 where *N* is the number of units. At this learning curve factor value, the total production cost is very close to a straight line, particularly as the number of production units gets large. Figure 44 shows production cost estimation as a function of number of units for the proposed rectenna array system. Unfortunately, at this point insufficient cost history exists for the stacked hybrid array system to distinguish it from either the rectenna array or the PV array.

5.3 Space-to-Space Microwave Wireless Power Transmission Experiments and Modern Small Satellites

In order to practically realize the analytical findings of the stacked hybrid PV/rectenna array with a dynamic power beam medium scenario from the first hypothesis, a novel concept of utilizing a modern small satellite as a technology

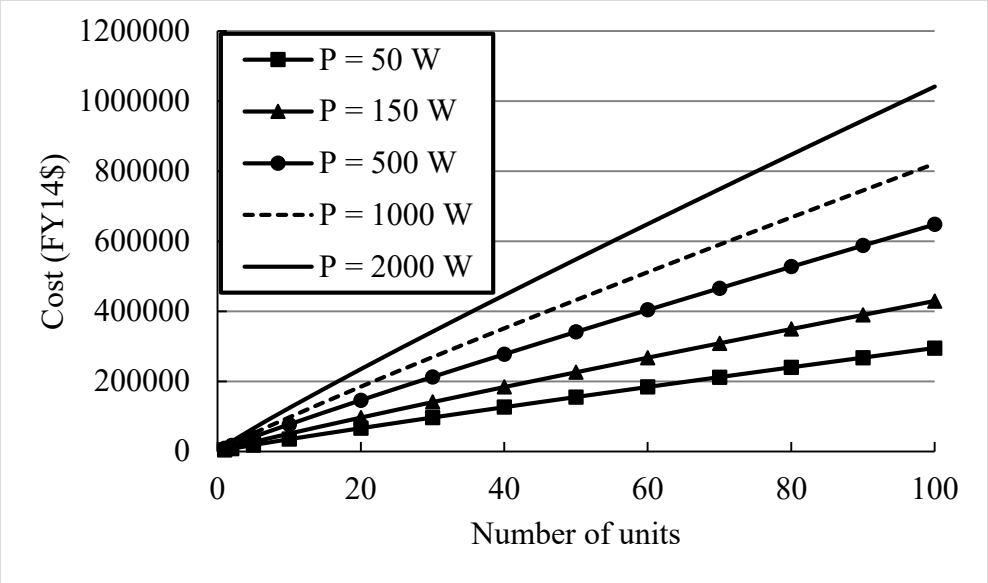

Figure 44. Production cost estimation as a function of number of units for proposed rectenna EPS system.

demonstrator for the proposed stacked hybrid PV/rectenna array PGU is proposed. The section begins with a brief background on the history and classification of modern small satellites. Then mission design phases that uses modern small satellites as a microwave wireless power transmission technology demonstrators is presented. Next design details toward the construction of a power transmitting "mother" satellite and a power receiving "daughter" satellite are presented. Emphasis will be on the daughter satellite as it is to be equipped with the proposed rectenna array.

5.3.1 History and Classification of Modern Small Satellites

According to Gao, et al. [6] modern small satellites include: mini, micro, nano, pico, and femto-satellites. Table 16 shows a comparison of different types of satellites in terms of mass, cost, and development time. As can be seen from Table 16, significant savings in mass, cost, and development time can be achieved by using modern small satellites compared to conventional large satellites. In fact, modern small satellites

Table 16. Classification of satellites by mass and cost [6]

Type	Mass (kg)	Cost (US $)	Time of Development from Proposal to Launch
Conventional large satellite	>1000	0.1-2 B	>5 years
Medium satellite	500-1000	50-100 M	4 years
Mini-satellite	100-500	10-50 M	3 years
Micro-satellite	10-100	2-10 M	~1 year
Nano-satellite	1-10	0.2-2 M	~1 year
Pico-satellite	<1	20-200 k	<1 year
Femto-satellite	<0.1	0.1-20 k	<1 year

operating in LEO are increasingly being used as a cost effective means to complete technology demonstration missions [6, 68].

Modern small satellites provide an opportunity to alleviate some of these challenges associated with a GEO-SSPS, as mentioned previously. According to Emrick [85]. “Low-cost access to space or riding to orbit by piggybacking CubeSats or [modern] small satellites as a secondary payload on a major launch vehicle is a disruptive innovation.” Cube satellites or CubeSats are considered a disruptive technology that standardizes the spacecraft’s form factor as well as its mass. A 1U CubeSat is defined as a cube-shaped 10x10x10 cm^3 volume satellite with a mass not exceeding 1.33 kg [86]. Another valuable feature of the CubeSat is its scalability. For example, depending on the mission to perform; 1.5U, 2U, 3U and 6U CubeSat configurations are scaled from the 1U

standard shape. These constraints provide a boundary for engineers and scientists within which to be innovative.

Moreover, the CubeSat design specifications is also made to fit inside a Poly-Picosatellite Orbital Deployer (P-POD). The P-POD has a standardized launch interface [87] that can carry a total size of three 1U CubeSats or a single 3U CubeSat. The P-POD allows separation of the development, integration and verification between the spacecraft and the launch vehicle, which in turn, reduces cost and schedule. The P-POD is flown as a secondary (or tertiary) payload on unmanned launch vehicles thus capitalizing on the excess capacity of a rocket carrying a larger, primary payload. New methods allow multiple CubeSat launches by carrying many P-PODS such as the Naval Post Graduate Schools CubeSat Launcher [88] or the U.S. Air Forces Evolved Expendable Launch Vehicle Secondary Payload Adapter (ESPA Ring) [89]. Technologies like P-PODS or ESPA Ring provide the option to launch batches of modern small satellites each equipped with various modular MWP experiments.

5.3.2 Design Phases of the Experimental Mission

In 2014, Bergsrud and Straub [14] proposed a space-to-space microwave wireless power beaming experiment using modern small satellites. This experimental mission proposed to utilize a micro-sized satellite as the power transmitting spacecraft and a nano-sized satellite as the power receiving spacecraft. The nano-sized daughter satellite would sit inside the micro-sized mother satellite for launch. Once in orbit and separated from the launch vehicle, the daughter satellite would be ejected from the mother satellite. The micro-sized satellite would deploy its solar PV array and the nano-sized satellite would deploy its rectenna array. Power beaming experiments would then commence. The

concept from Bergsrud and Straub is pictured in Figure 45. This proposed experiment advances the concept of the ISY-METS sounding rocket experiment by replacing the rockets mother and daughter sections with mother and daughter modern small satellites.

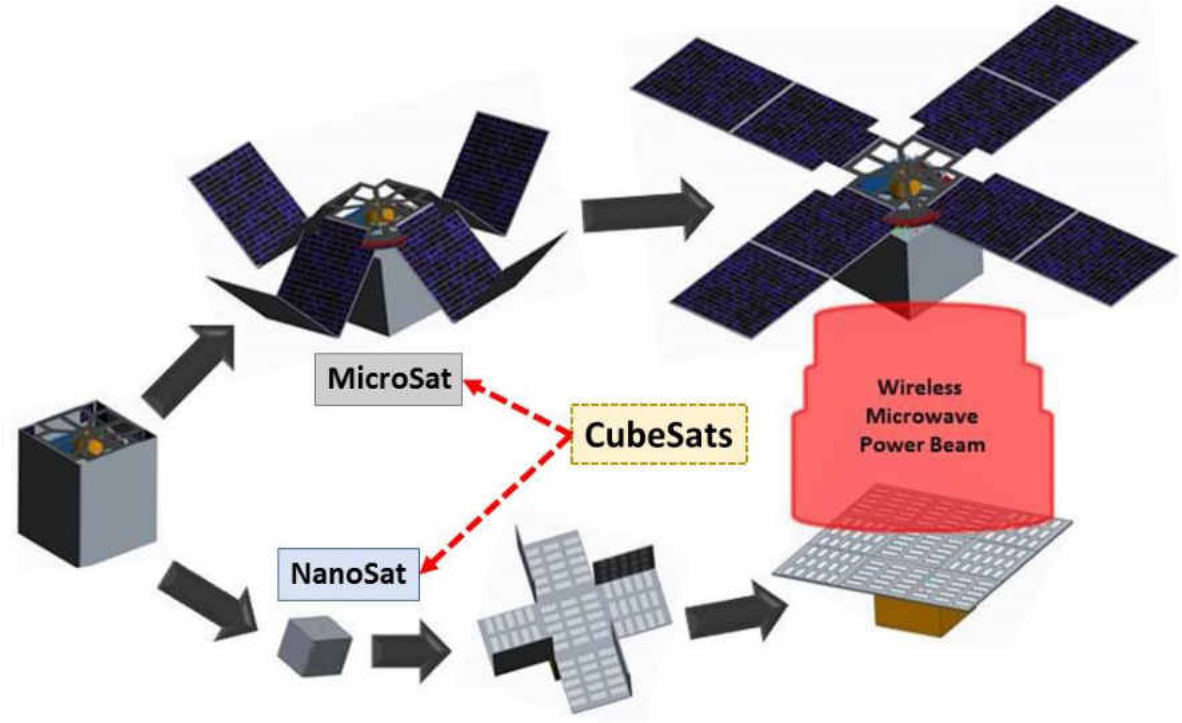

Figure 45. Concept for a space-to-space MWPT experiment using CubeSats [14].

Bergsrud and Straub [14], presented a useful calculation of aperture-to-aperture efficiency. They used equations presented from Brown and Eves [51] in order to understand the relationship between transmitting and receiving aperture areas, the distance between the two antennas, and the efficiency. Power density received at the center of the receiving location as defined by Brown and Eves [51] is

$$p_d = A_t P_t / \lambda^2 D^2 = \pi d^2 P_t / 4\lambda^4 D^2 \tag{16}$$

where p_d is the power density at the center of the receiving location, P_t is the total radiated power from the transmitter, A_t is the total area of the transmitting antenna, λ is the wavelength, D is the separation between the apertures, and d is the diameter of the

parabolic reflector, if it is circular. The mother satellite used a parabolic dish to transmit power and the daughter satellite had a rectangular area to receive the power. For example, let the transmitted power be 200 W and the frequency be 5.8 GHz. Varying both aperture areas, shows the resulting power density values. As both aperture areas increase, the power density decreases. This is because the same transmitted power is divided over a wider area, thus decreasing the amount per area.

Setting a desired value for the power density at the interface of the receiving array and from knowing the effective area (antenna aperture) (A_{reff}) of the receiver unit, the received power (assuming a uniform field) per element can be determined from

$$P_r = p_d \times A_{eff} \tag{17}$$

Table 17 Estimated diameter size of parabolic reflector and aperture size of rectenna array.

Diameter of parabolic reflector (m)	Aperture size of receiver (m^2)	Power Density (mW/cm^2)
0.1	0.09	347
0.2	0.12	260
0.4	0.15	208
0.8	0.2	156
1	0.25	125

Equation (17) can be used to estimate the power received per antenna element in a planar array assuming a uniform field distribution. Taking these calculations a step further, the aperture-to-aperture transmission efficiency can be estimated generally from Brown and Eves [51]

$$\tau = \sqrt{A_t A_r} \big/ \lambda D \tag{18}$$

in order to achieve optimum power density transfer based on a Gaussian profile scenario.

Figure 2 of Brown and Eves [51] is used to get a sense of the distance between the two spacecraft with the associated power density and transmission efficiency based on a Gaussian profile scenario. Using their figure, selecting τ to be a value of 2.5, i.e., 100% power density transfer efficiency, solving equation (18) for *D*, and using the aperture size estimations from Table 17, theoretical distances between the apertures to acquire 100% can be determined. Figure 46 fixes five cases of the receive apertures and varies the size of the transmitter area to provide the optimal distance required to achieve greatest power density transfer between the two apertures. These data help in setting the distance limits between the two spacecraft to supply enough power to the receiver to run its various subsystems. Similarly, Figure 47 and Figure 48 show results for 10 GHz and 220 GHz frequencies, respectively, holding all other values and procedures the same. Notice that the higher the frequency the greater the distance can be achieved for power density transfer as well as the option for smaller apertures. However, the disadvantage would be a decrease in component efficiency and for a LEO mission, since it is not complete vacuum, the higher frequency will also suffer from greater attenuation losses through the LEO medium.

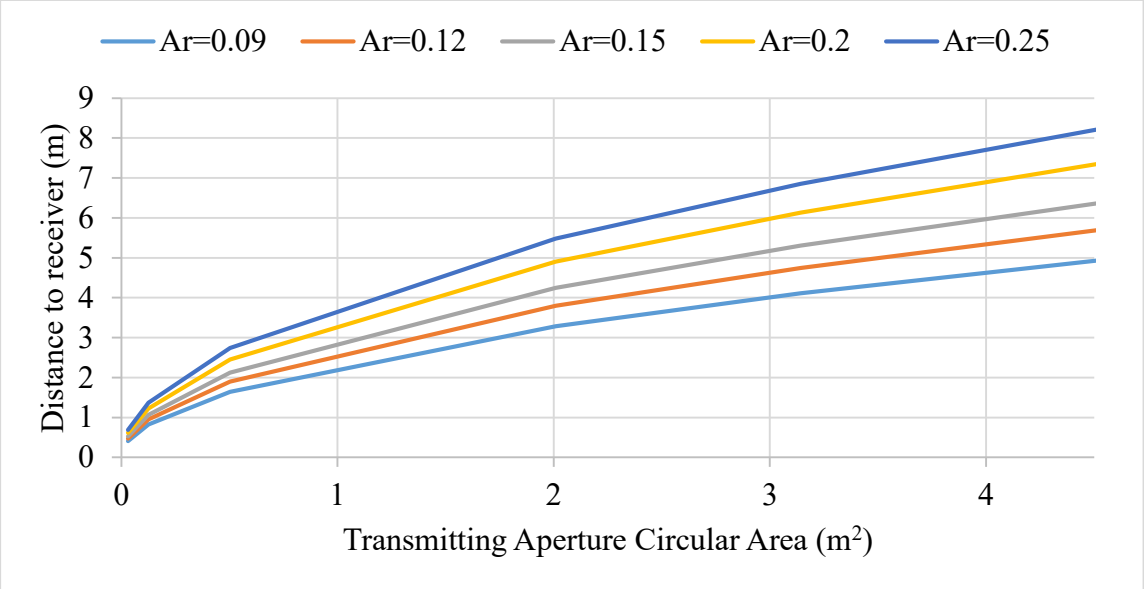

Figure 46. Shows the optimal distance required to achieve greatest power density transfer between the aperture antennas. The center frequency is 5.8 GHz.

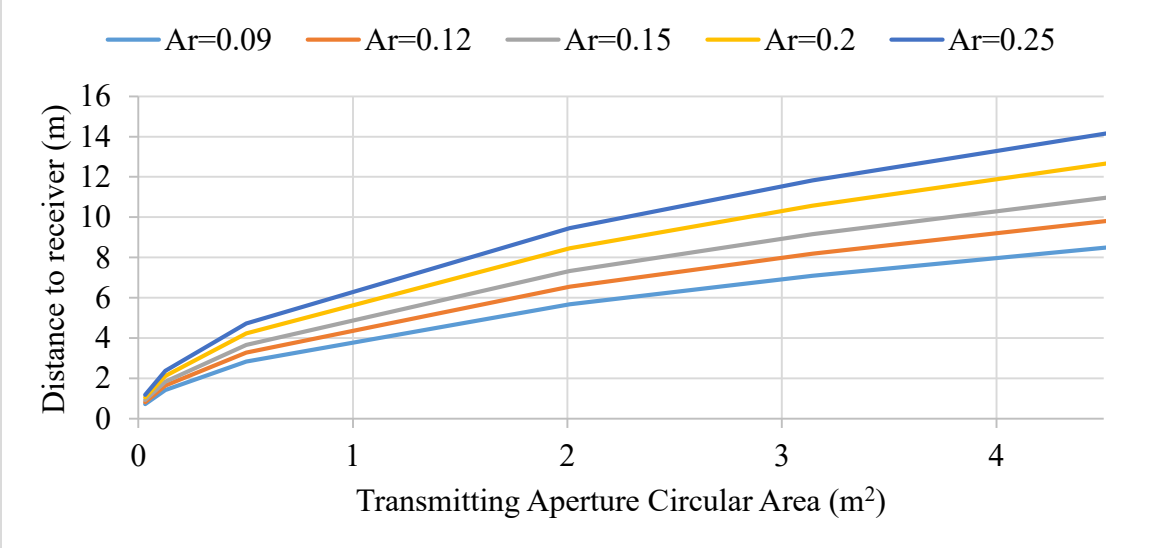

Figure 47. Shows the optimal distance required to achieve greatest power density transfer between the aperture antennas. The center frequency is 10 GHz.

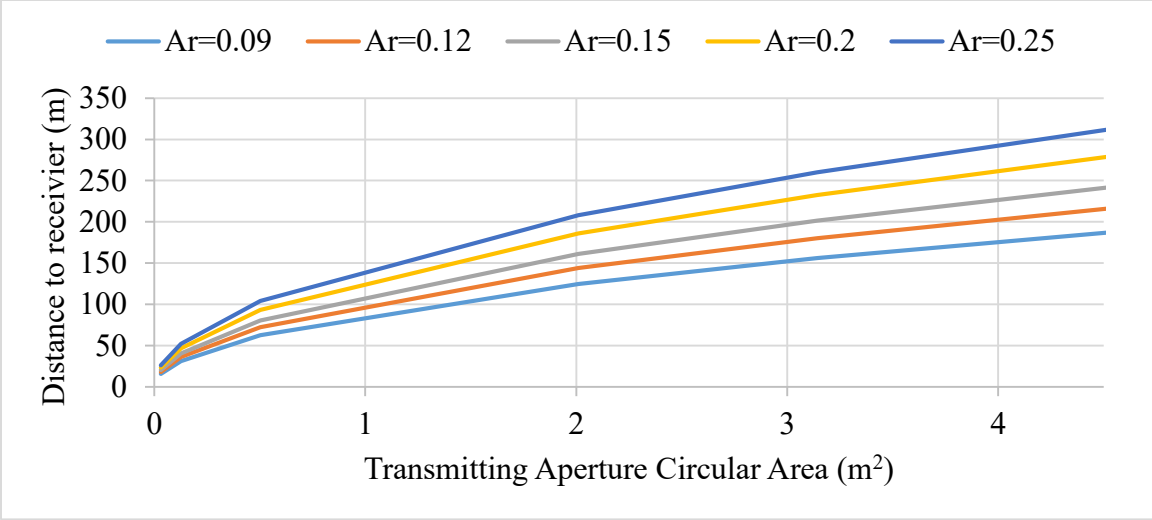

Figure 48. Shows the optimal distance required to achieve greatest power density transfer between the aperture antennas. The center frequency is 220 GHz.

However, just like the ISY-METS experiment this proposed experiment would be short-lived because there is no propulsion system nor was close proximity stabilization between the two satellites considered. Such a system requires control systems and thrusters, and the power-receiving spacecraft did not have a means to gain enough power from the microwave beam to maintain even the most basic of operations. The mission concept was improved to equip the two satellites with propulsion units, as well as take advantage of close proximity operations. Moreover, the daughter satellite would be equipped with a HPGU in order to collect enough power for operation. With these modifications much greater mission flexibility can be achieved.

The modified LEO mission concept proposed that the two satellites generate and store power during the daylight part of their orbits (Figure 55), and power beaming demonstrations are conducted in the eclipse part of their orbit (Figure 56). Greater mission details are presented in the Section 5.3.4.

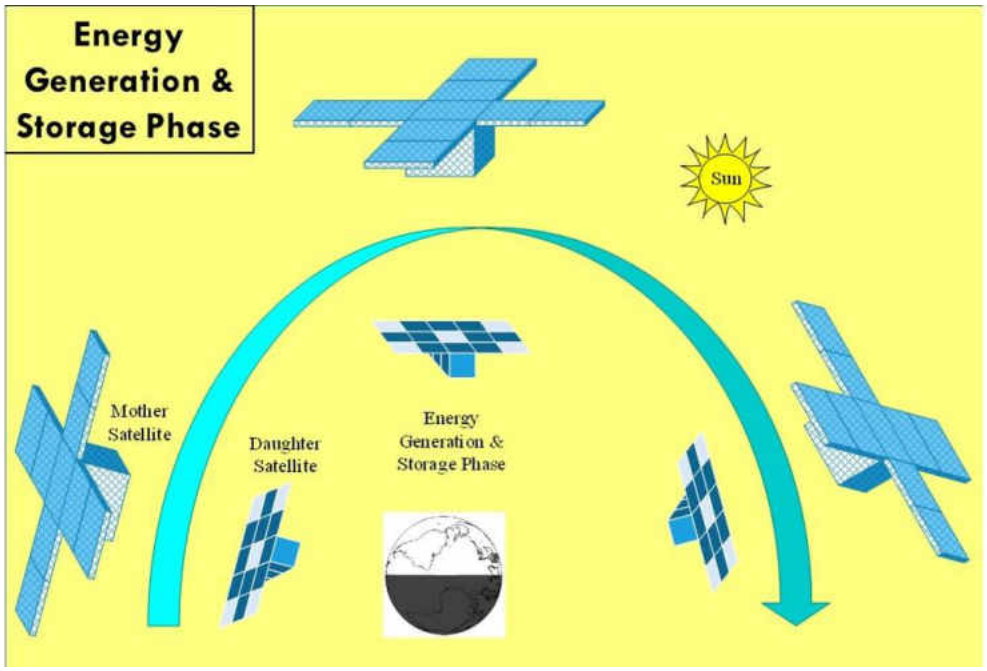

Figure 49. Energy generation and stroage phase of the mission [90].

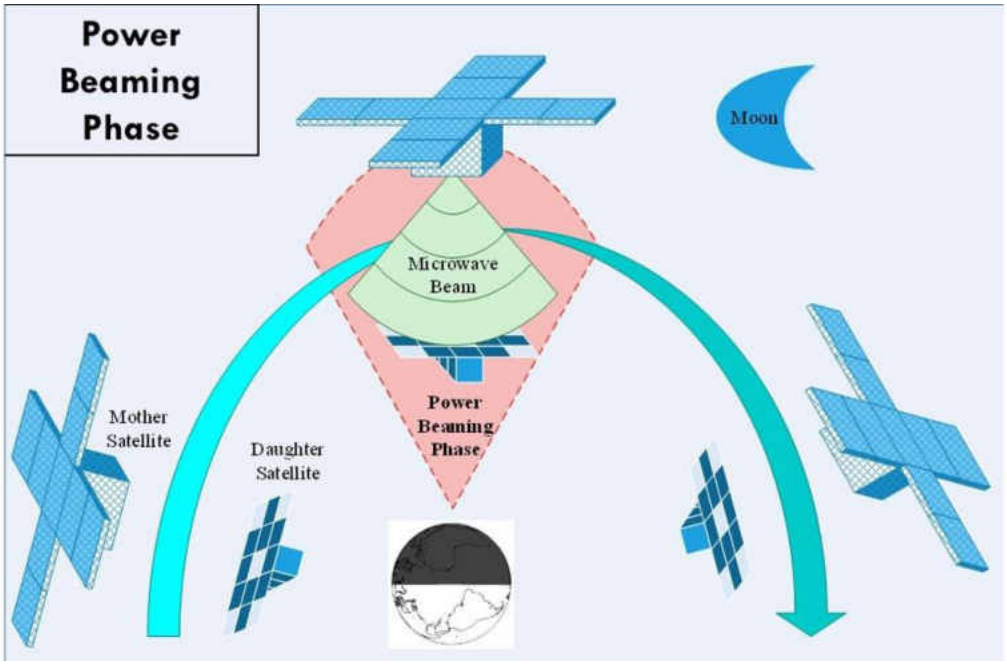

Figure 50. Power beaming phase of the mission [90].

5.3.3 Power Transmitting "Mother" Satellite

Bergsrud and Noghanian [91] investigated the design of a transmitting satellite or mother satellite from the previously proposed mission by Bergsrud and Straub [14]. To begin the power transmitting spacecraft design, the first pursuit was to map out a flow chart of necessary satellite systems as shown in Figure 51. Each block of the flow chart was then elaborated to some degree.

First, two solar array deployment mechanisms were presented as a possible design for the spacecraft as shown in Figure 58. The area, mass, and efficiency of the solar array are all key design parameters that ultimately determine the life of the satellite mission (given that all other subsystems are successfully operational). As was mentioned previously in Electrical Power Systems, Subsection Solar PV Array, it seems likely that

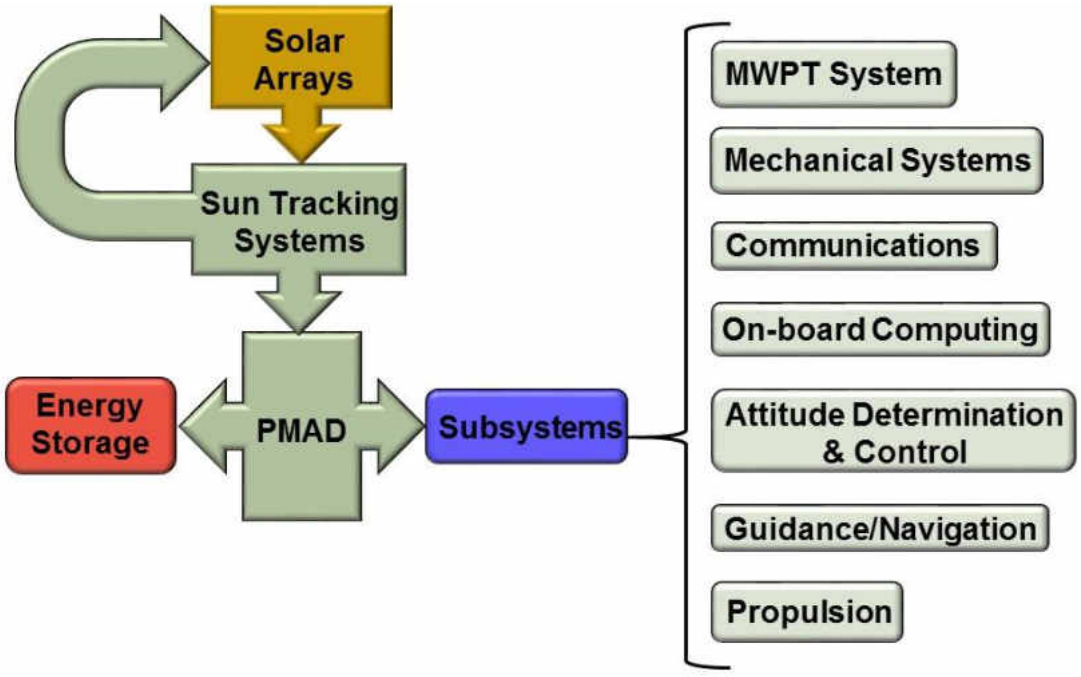

Figure 51. Conceptual flow chart for the proposed mother satellite [91].

MJ GaAs solar cells are the way to go for best performance. Three key phenomena affect solar cells: temperature, constant changing of incidence angles throughout an orbit, and

radiation which cases a constant slow decline in solar cell performance. Options to consider for optimization of solar cell degradation and mission life include DET, PPT, and gimbal systems. These techniques were mentioned previously in Electrical Power Systems, Subsection Energy Storage.

Additional thoughts to take away are that the secondary power source is needed for prelaunch operations, launch phase, eclipse periods, and emergency operations. During an eclipse period key functions that need to have power include attitude determination and control, guidance and navigation, computing, and communications.

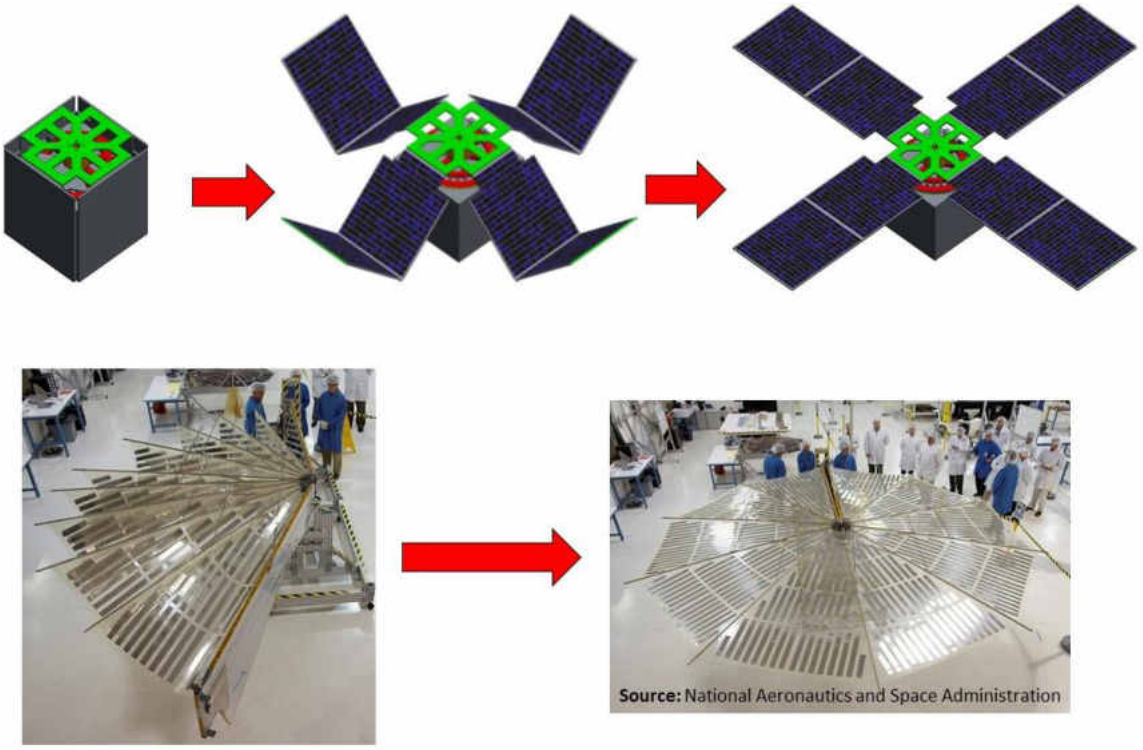

Figure 52. Solar array deployment mechanisms.

The next item in the flow chart is the MWPT subsystem. The MWPT subsystem is the novelty of the spacecraft design. The spacecraft EPS is essentially designed to support this system. Two categories of MWPT payloads were investigated as options to

equip on the spacecraft; vacuum electron devices, and transistor technologies. As shown in Figure 59, the transistor technology is a solid state power amplifier (SSPA), and the vacuum electron devices include the magnetron and traveling wave tube amplifier (TWTA). Each technology has its advantages and disadvantages. Transistor devices are used mostly at low-power and low-frequency, and vacuum devices predominate in high-power and high-frequency regions as seen in Figure 60. Comparisons between the two technologies are summarized in Table 18 and Table 19. Depending on the mission, these options are available.

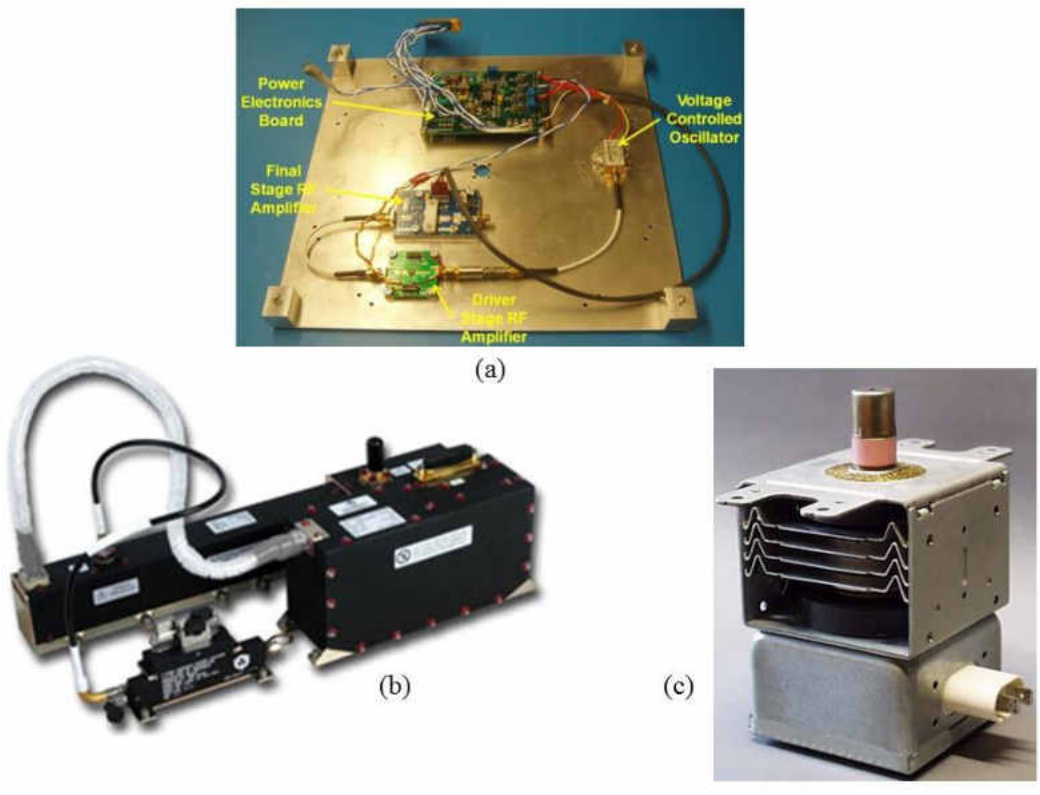

Figure 53. Transistor Technology: (a) solid state power amplifier [92]; Vacuum Technology: (b) traveling wave tube amplifier, and (c) magnetron.

Part of the MWPT system is the antenna that focuses and guides the electromagnetic wave to its target. One design idea, as shown in Figure 61 and Figure 62,

is to “crunch back” and “spring lock” a parabolic dish so to conserve volume. So there is a mechanism to release the Nano-sized satellite away from the mother satellite. In order for the “spring locked” concept to work, both the parabolic dish (reflector) and the arms that hold the sub-reflector need to be mechanically “crunched back” to conserve volume. Some lock mechanism on the back of the sub-reflector will help hold the daughter satellite in place. Once in orbit the spring will release and the antenna will be deploy while simultaneously releasing the daughter satellite away from the mother satellite, i.e., giving birth.

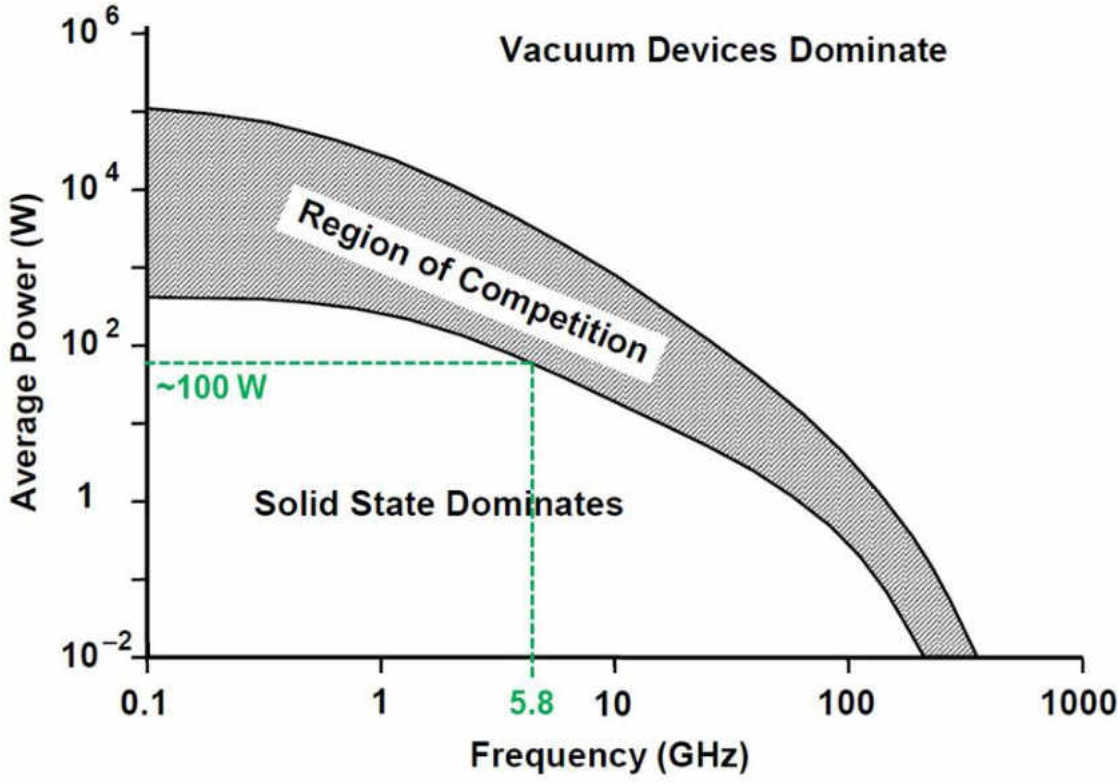

Figure 54. Ranges of application of microwave tubes and solid-state devices. Reproduced with permission from A.S. Gilmour, Jr., [*Klystrons, Traveling Wave Tubes, Magnetrons, Cross-Field Amplifiers, and Gyrotrons*], Norwood, MA: Artech House, Inc., 2011. © 2011 by A.S. Gilmour, Jr.

Table 18. Table shows advantages and disadvantages between Vacuum and Transistor devices. Source of information [93].

Function	Vacuum Electron Devices		Transistor Devices	
	Advantages	Disadvantages	Advantages	Disadvantages
Efficiency		High Voltage		High Current
Size/Weight	TWTA packages including power supplies are smaller and weigh less		Basic RF modules are smaller than TWTA but the power supply and required heat sinks make the overall packages larger than the TWTAs	
Reliability	Logged many years of reliable operation	Limited life 70,000-100,000 hours of continuous operation	No limited life	Power supply
Heat Dissipation	TWTA power distributed over relatively large area, making heat sinking a less challenging task.			Power FETs dissipate large amounts of power at a concentrated point. Heat dissipation is one of the most challenging problems in SSPA design.
Temperature Stability	Stable over temperature	Solid state driver amplifiers need to be temperature compensated		SSPA and driver amplifiers need to be temperature compensated.

Table 19. Table of potential models in the 2-10 GHz frequency range. Table generated by Dr. Paul Jaffe [92].

Method	GaN SSPA	Magnetron	TWT
Efficiency	43-70%	44-73%	66-70%
Mass (kg)	< 0.1	0.9-4.3	0.7-3.0
Power Output (W)	25-220	900-5,000	20-300
Input voltage (V)	28-50	4,000-20,500	5,000-20,000
Manufacturers	Cree, TriQuint	Toshiba, Hitachi	L3, Thales

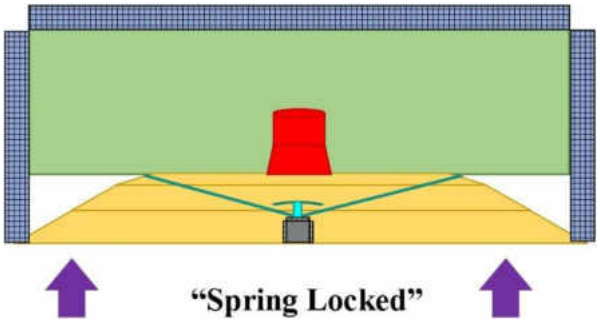

Figure 55. Satellites while in launch vehicle not deployed.

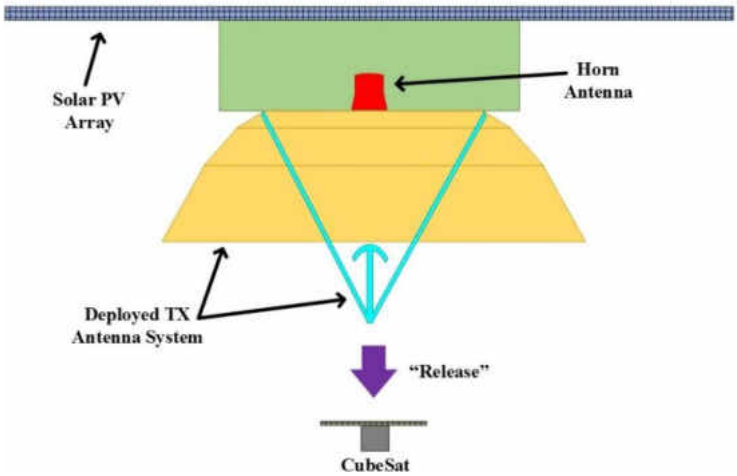

Figure 56. Satellites separated from launch vehicle deployed.

Another possible transmitter architecture is the sandwich module as pictured in Figure 63. Instead of the MWPT system being internal to the spacecraft body as Figure 61 and Figure 62 presented, the MWPT system would be sandwiched into a single module. It is worth noting here that in the future, a study for the different kinds of TX architectures for the proposed "mother satellite" need to be investigated and compared for pros and cons, and mission suitability.

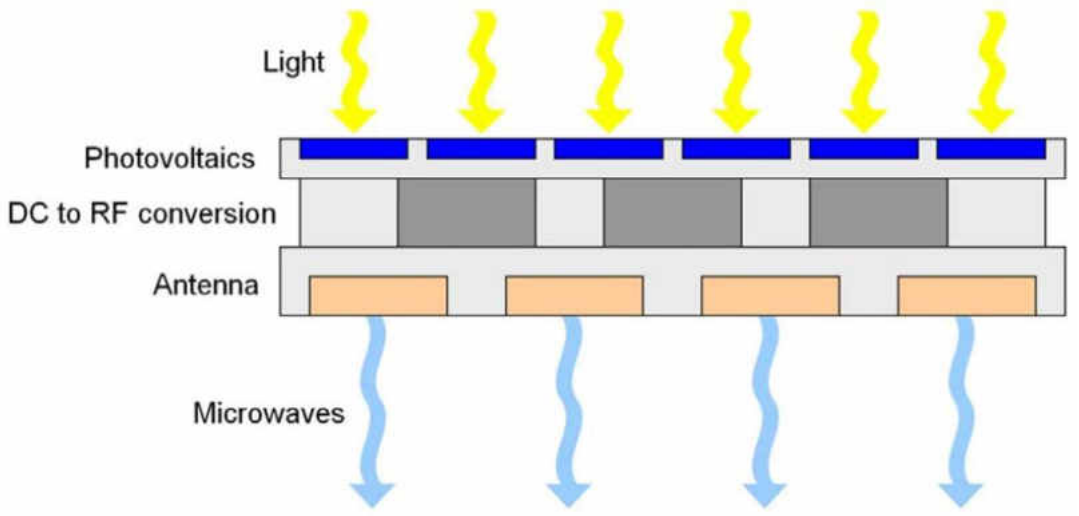

Figure 57. Example of transmitter antenna architecture called a sandwich module [92].

5.3.4 Power Receiving "Daughter" Satellite

5.3.4.1 Mission Design

A updated mission concept is presented that advances upon Bergsrud and Straub's previous mission concept [14]. The idea of a smaller daughter satellite secured inside a larger mother satellite during launch remains intact. The modified mission concept is that the mother and daughter satellites fly in close proximity to one another during their orbits. In order to do this, both satellites are now equipped with propulsion technology and advance control systems to maintain relative distances. Another mission modification is to equipped the daughter satellite with a stacked hybrid PV/rectenna array in order to

allow mission duration flexibility (compared to a purely equipped rectenna array as was previously presented by Bergsrud and Straub), and to address the first and second hypothesis. By equipping the daughter satellite with a PV array in addition to the rectenna array allows power to be generated for necessary spacecraft functions and power to be generated for experimental functions, respectively. The benefits of the stacked HPGU is the ability to adjust the areas of either the PV part and/or rectenna part to best accommodate mission objectives.

5.3.4.2 Orbit Selection

Based on an orbit, and the life of a mission, the design of satellite's EPS, and an experimental payload can be pursued. Different orbits serve different purposes with each orbit having its advantages and disadvantages. Ultimately, the CubeSat's orbital altitude and inclination usually depend on the launch service provider as the CubeSat is not a primary payload. None-the-less we proceed in the mission design.

For the proposed case of a microwave WPT experimental mission using a pair of modern small satellites a Sun-synchronous circular orbit seems a logical choice. The Sun-synchronous orbit has the characteristic of maintaining the satellites orbital plane at a fixed angle relative to the Sun year round. A typical Sun-synchronous orbit has a 98.7° inclination and 833 km mean orbit altitude [94]. In order to determine a specific mission inclination (i) and altitude for a Sun-synchronous circular orbit the following equation is used:

$$\Delta\Omega = -2\pi \frac{J_2}{\mu\rho^2}\frac{3}{2}\cos i \tag{19}$$

where

- $\mu = 398600$ (km^3/s^2), standard gravitational parameter of Earth.
- $\rho = a(1 - e^2)$, semi-latus rectum of the orbit.
- $J_2 = 1.7555\times10^{10}$ (km^5/s^2), Earth's oblateness effects.
- i = inclination of the orbit to the equator.

An orbit is Sun-synchronous when the precession rate, ρ, equals the mean motion of the Earth about the Sun which is 360°. Therefore we set $\Delta\Omega/P = \rho$ where P is the orbital period of a spacecraft defined by:

$$P = 2\pi a\sqrt{\frac{a}{\mu}} \tag{20}$$

Therefore,

$$\cos i \approx -\frac{\rho\sqrt{\mu}}{\frac{3}{2}J_2}a^{7/2} = -\left(a/12352\text{ km}\right)^{7/2} \tag{21}$$

Plugging semi-major axis (a) values into equation (21), we obtain

Figure 58 for Sun-synchronous inclination for low-altitude circular orbits. A special kind of Sun-synchronous orbit is called a dawn/dusk orbit. For a dawn/dusk orbit the satellite rides the terminator allowing the solar panels to always see the Sun, without being shadowed by the Earth. A full sun dawn-dusk orbit stretches from about 1389 km to 3334 km [95].

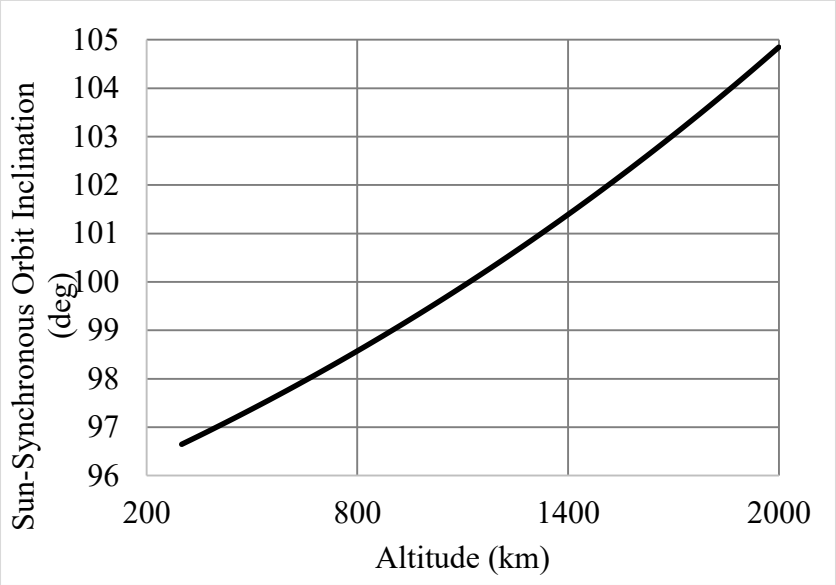

Figure 58. Sun-synchronous inclination for low-altitude circular orbits.

A full sun dawn-dusk orbit is a seemingly great choice for experiments for the power transmitting mother satellite because future GEO-SSPS will be in almost continuous sunlight year round as the full sun dawn-dusk orbit offers. But in order to avoid engineering a deorbiting mechanism for the daughter satellite a 500 km altitude (h) is selected. In fact, all launch providers at present require certifications of the de-orbit time for the CubeSat to be 25 years or less [96]. Since university CubeSats are typically designed for an operational life of one year or less, orbits less than 500 km generally do not require specific de-orbing systems [96]. Future work should consider: (1) possible use of the rectenna array part of the HPGU as a technique to increase orbital drag, and (2) propulsion unit where both are used as a de-orbing mechanism which in-turn can increase the mission altitude while satisfying de-orbit requirements.

According to Figure 64, in order to maintain a circular orbit for a satellite at a 500 km altitude the inclination must be $i \cong 97.4°$. At this altitude, the orbital velocity (v) of the satellite around the earth is calculated by:

$$v = \sqrt{\frac{\mu_{Earth}}{R}} \tag{22}$$

where μ_{Earth} is the gravitational constant (~398,600 km^3/s^2), and R = 6871 km is the mean radius of the Earth (6371 km plus the distance from Earth's surface (500 km)). Thus the orbital velocity of the CubeSat is $7.62\ km/s$.

The satellite travels around the entire circumference of the circle $(2\pi R)$ in period T. Thus the orbital velocity is equal to

$$v = \frac{2\pi R}{T} \tag{23}$$

and the period of the satellite is then calculated by:

$$T = \frac{2\pi R}{v}. \tag{24}$$

Plugging in R and v into equation (24) yields a 94.43 minute orbit. In order to calculate the time in sunlight (T_S) and the time in eclipse (T_E), we introduce the term β. The term β is the angle between the solar vector and the satellites orbital plane as seen in Figure 59. The angle β can vary between +90° and -90°, depending on the direction of the spacecraft. As β increases (or decreases) away from the solar vector, the satellites will experience sunlight for a longer period of the orbit due to decreasing eclipse time. At β = 90° (+Z axis), the satellite will be subject to a circular orbit with no eclipse as the orbital

plane is parallel to the terminator. The fraction of an orbit spent in sunlight and eclipse for h = 500 km as a function of angle β is plotted in Figure 66 using the eclipse fraction:

$$f_E = \frac{1}{\pi}\cos^{-1}\left[\frac{\sqrt{h^2+2Rh}}{(R+h)\cos\beta}\right] \tag{24}$$

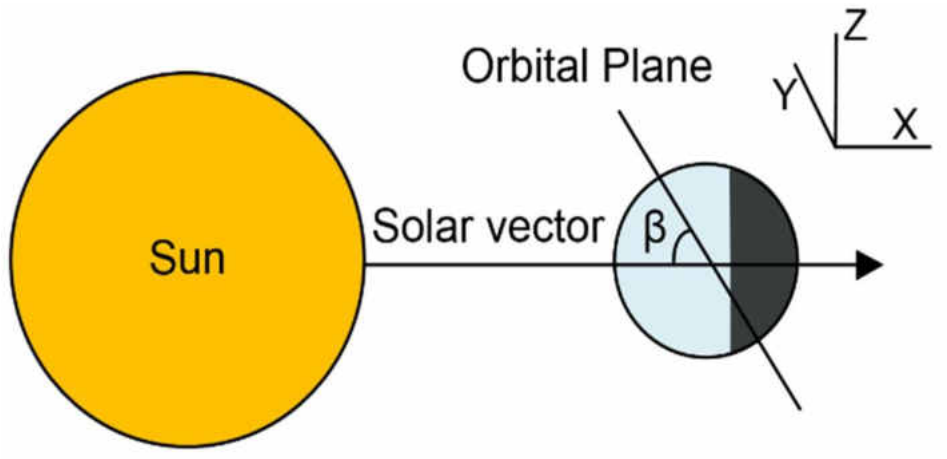

Figure 59. Pictorial representation of angle beta relative to the solar vector.

Figure 60 shows that at $\beta = 0°$ the most time is spent in eclipse. At this angle, the orbital plane is in the same direction as the solar vector with the longest eclipse time from shadowing by the full diameter of the Earth is experienced as shown in Figure 61. This is an extreme case since the power consuming functions of the CubeSat happen in eclipse. In Figure 61, β^* is the angle at which the eclipse begins, and R_E is the radius of the Earth. For this mission $\beta = 0°$ is selected in order to take into account the most extreme case for the power consuming functions. Thus according to Figure 66 the fraction of time in eclipse is .38 (38%) or 35.9 minutes. Table 20 summarizes the orbital information for the daughter satellite.

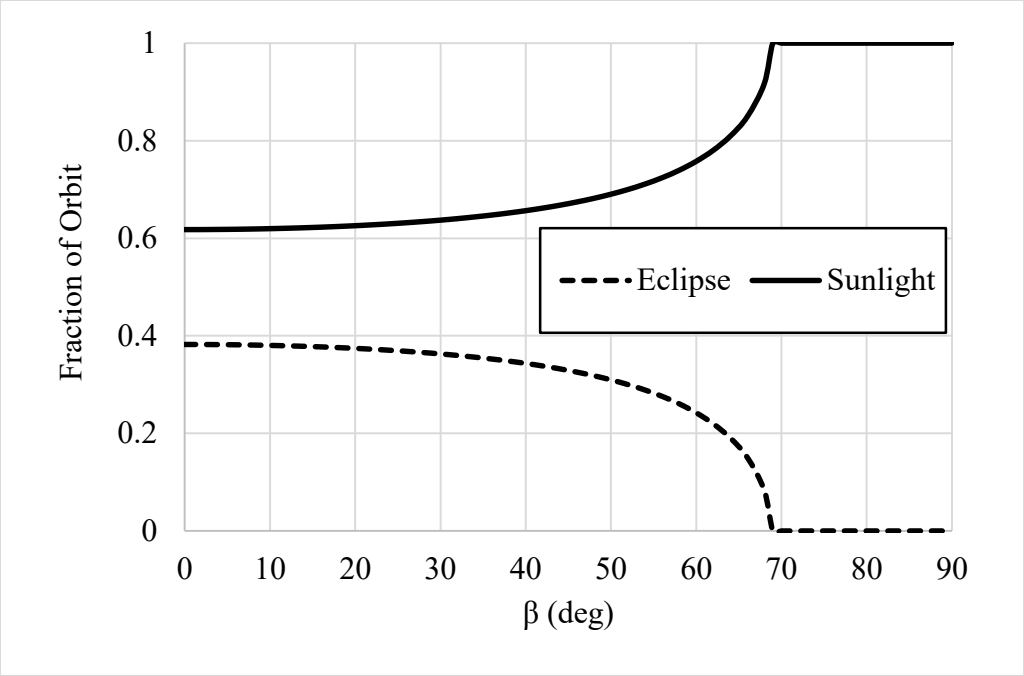

Figure 60. Day and eclipse periods for h = 500 km.

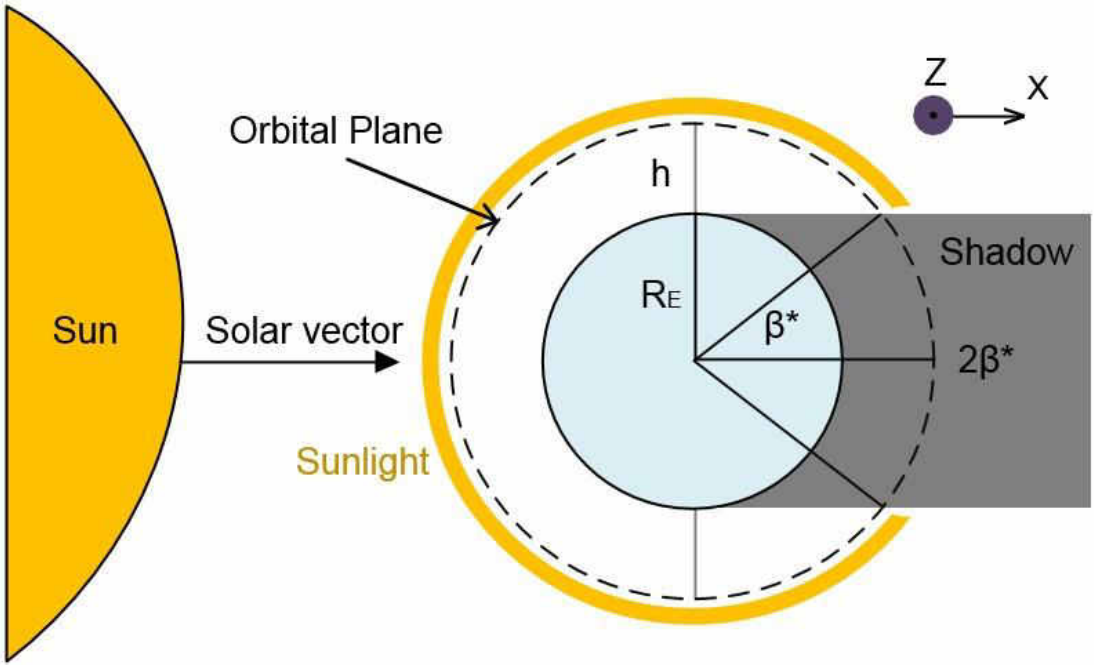

Figure 61. Looking down at the orbital plane for $\beta = 0°$.

Table 20. Orbital Characteristics.

Altitude (h)	500 km
Period (T)	~94.4 min
Eccentricity (e)	0 (circular orbit)
Velocity (v)	7.62 km/s
Inclination (i)	97.4°
Beta angle (β)	0°
Eclipse duration (T_E)	35.9 min
Sunlight duration (T_S)	58.5 min

5.3.4.3 Close Proximity Mission Requirements

Before going through the analysis of the EPS, we have to understand how unique and challenging in-space power beaming can be. In fact, in order to keep both satellites in a relative geometry (*i.e.* close proximity), we need to overcome the differential drag effect. This drag effect is caused by various effects, such as:

- Different initial conditions after the separation from the P-POD (or other launch container) and the HPGU deployment.
- Different satellite velocities resulting from different masses.
- Different atmospheric density and decay rate due to differences in orbit radius and density distribution.
- Different attitude motion causing the spacecraft cross-sectional area and thus the atmospheric drag to vary.

For the mission requirement of proximity operation to work, a propulsion system is necessary. It is assumed that the propulsion system will be employed during the orbital lifetime of the daughter satellite in order to control the orbit (altitude and plane change) and the speed. This will allow for formation flying between both the power transmitting spacecraft and the power reception spacecraft.

Propellantless propulsion systems, for example, seem to be an excellent choice. However, they have limited application to CubeSats and nano-sized satellites due to the lack of flexibility (e.g. high-temperature is created to obtain superconductivity for the electromagnetic coils that cannot be handled by the CubeSat's structure). Electric propulsion systems, on the other hand, represent a viable solution for a potential nanosatellite propulsion solution. Current CubeSat designs offer too little power for many electric propulsion concepts but some, like the micro-electrospray thrusters, can work within the power range of nano-sized satellites.

For the proposed mission, a micro-electrospray thruster from BUSEK [97] has been chosen. Based on the data sheet a total volume of 1U is needed for the thruster, its associated electrical circuitry and the propellant tank. At this time of technological advancements in propulsion systems, 2U architecture is the minimum architecture for CubeSats in which can be integrated with a propulsion system. For this mission, a 3U CubeSat form factor is considered as in Figure 62. The 3U size is large enough to allow enough space for the propulsion system (1U), the avionics, the energy storage unit, the reaction wheels, and the payload. It is also small enough to fit into the standard 3U P-POD or potentially larger spacecraft for launch.

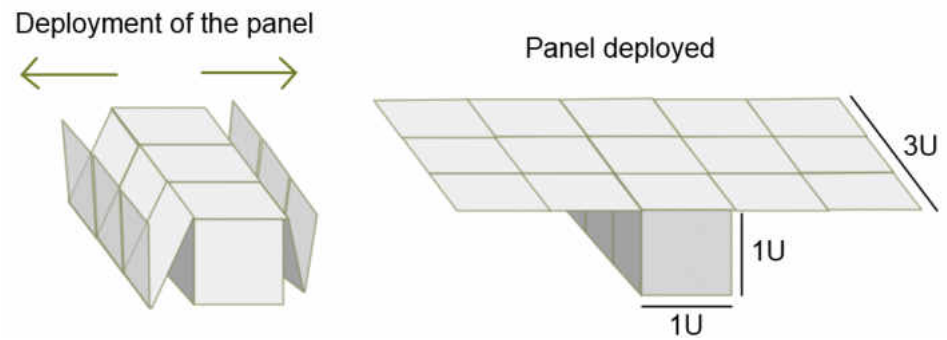

Figure 62. Configuration of a 3U CubeSat and array deployment mechanism.

5.3.4.4 Experimental Portion of the Mission

The proposed experiment plans to beam microwave power from a power transmitting mother satellite to a power receiving daughter satellite while in the eclipse part of their close proximity orbit. This experiment builds upon the previous work of Bergsrud, et al. [13], aimed at building an experimental spacecraft equipped with HPGU/HPSU in order to study the possible benefits of this future spacecraft design for a potentially new space environment where both microwave and solar energy sources may be available to harness. The proposed experiment also offers opportunity to establish performance data for super capacitors or the new lithium ion capacitors, rectenna material/components, etc. in the space environment. McSpadden, et al. [34] listed related experiments that can be done for a mission such as is proposed.

One calculated result from Bergsrud, et al., [13] is for an altitude of 500 km the power density of the microwave beam coming from a GEO-SSPS is 205 W/m^2 (20.5 mW/cm^2). Therefore, 20.5 mW/cm^2 should be the power density (p_d) at the interface of the proposed rectenna array. Power density received at the center of the receiving location as defined by Brown and Eves [51] in equation (16). The assumption here is that

the mother satellite has a parabolic dish as its power transmitting antenna [14, 91] (see Figure 61 and Figure 62.).

To get a sense of the relationship between p_d, d, P_t, and D we first solve (16) for d to obtain:

$$d = D\sqrt{\frac{p_d 4\lambda^2}{\pi P_t}} \tag{25}$$

Then varying D we obtain values of d as shown in Figure 63 for different values of P_t. Figure 63 reveals two phenomena. First, as P_t increases d decreases for the same separation distance. This is explained as lower P_t levels require a larger area in order to obtain the same p_d level. Second, as the separation distance increases the diameter of the transmitter increases. This is explained by the fact that in order to maintain the same p_d over distances the size of d must increase.

Taking this information a step further in order to achieve optimum power density transfer we refer to equation (18) to obtain a general equation for the aperture-to-aperture transmission efficiency based on a Gaussian profile scenario.

Based on Figure 62, we know that an area for the rectenna array is A_r = 1500 cm^2 (0.15 m^2). Solving for D in equation (18), using the output d from equation (25) for P_t = 100 W, and using Fig. 2 in Brown and Eves [51] to select τ = 2.5 (100% power density transfer efficiency) we generate Figure 64. Figure 64 is used to help to get a sense of aperture areas, and distances for the mother and daughter spacecraft. Bergsrud, et al. [13] showed that the rectenna array part of a HPGU can be used to decrease the mass of the PGU by increasing the area of the lighter rectenna part while simultaneously decreasing

the heavier PV part while obtaining the same power level. Because of this, $A_t = 0.21$ m^2 was also plotted in Figure 64.

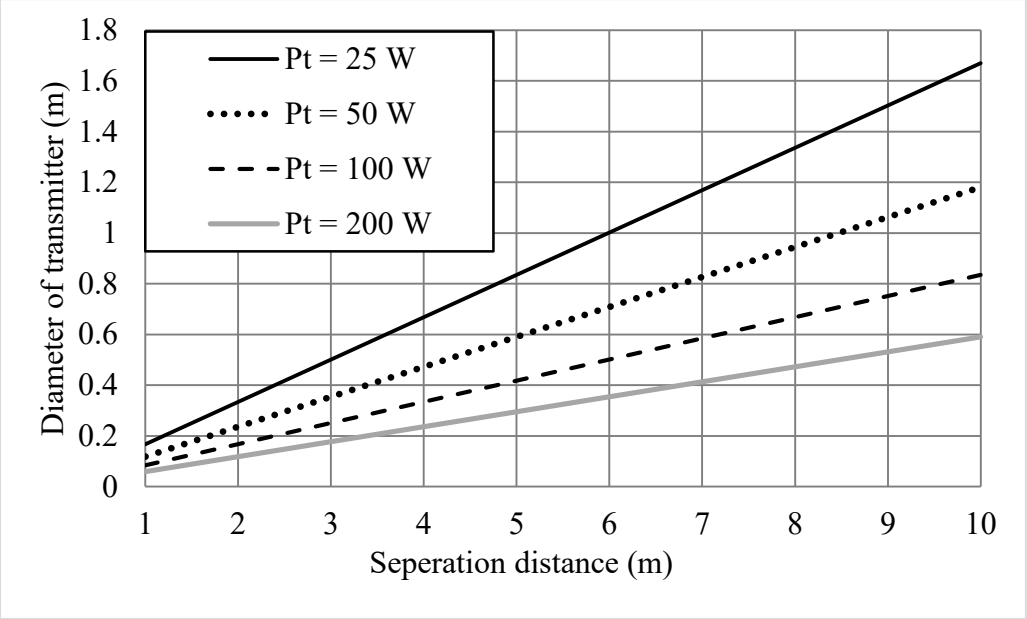

Figure 63. Diameter of transmitter as a function of *D*.

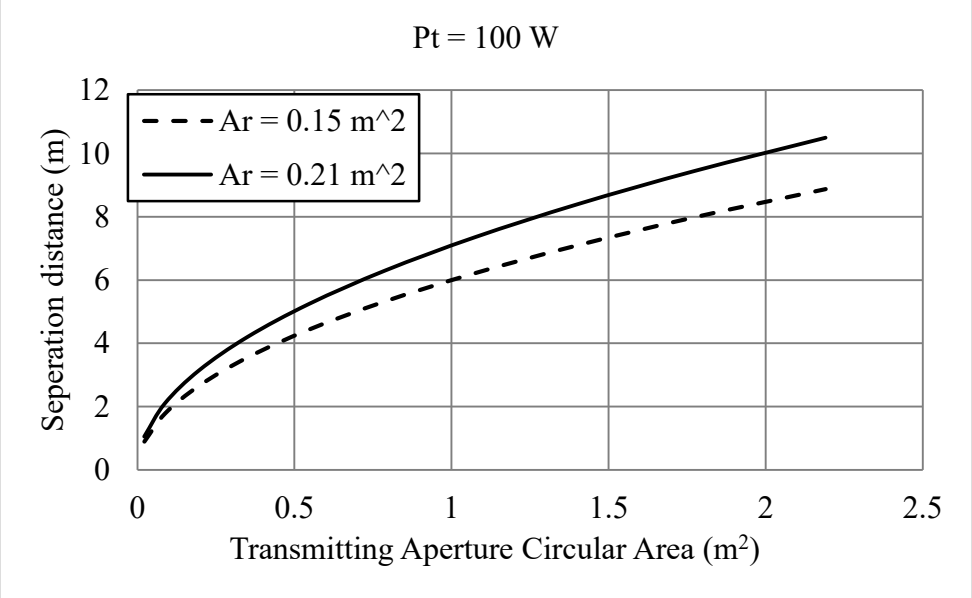

Figure 64. Separation distance as a function of A_t for 100% power density transfer efficiency.

Next referring to Table 6 from McSpadden and Mankin [56] we derive Table 21 for efficiency estimations. Using these efficiency assumptions for P_t = 25, 50, 100, and 200 W the DC power P_{DC} = 15, 30, 60, and 120 W. Rectenna efficiency estimation of 74% (0.74) came from the section 5.4 for RF-to-DC conversion efficiency calculation.

Table 21 Efficiency calculations.

Source of Inefficiency	Efficiency
Collection efficiency	0.92
Rectenna random failures	0.99
RF filter insertion loss	0.89
Rectenna efficiency	0.74
Rectenna Array Efficiency	0.60

The rectified power (P_{DC}) from the rectenna array will be stored in a lithium ion capacitor (LIC) or super capacitor (SC). The LIC offers higher specific power compared to the LIB [68, 98]. This is important for a power beaming scenario because the microwave power (P_t) can be delivered to the spacecraft at a reduced time since charging rate of a LIC is faster than charging rate of LIB. Moreover, the LIC offers a higher specific energy compared to a SC. This is important because more energy can be stored per mass. This is an interesting research question, however, it is outside the scope of this research.

5.3.4.5 Daughter Satellites Electrical Power System

The proposed EPS consists of a HPGU, HPSU, and the power conditioning and distribution unit (PCDU). Figure 65 shows a functional block diagram of the proposed EPS. A HPGU and HPSU is proposed using two power paths. Path 1 represents the main power path, and Path 2 represents the experimental power path. This section walks through the design of the proposed HPGU.

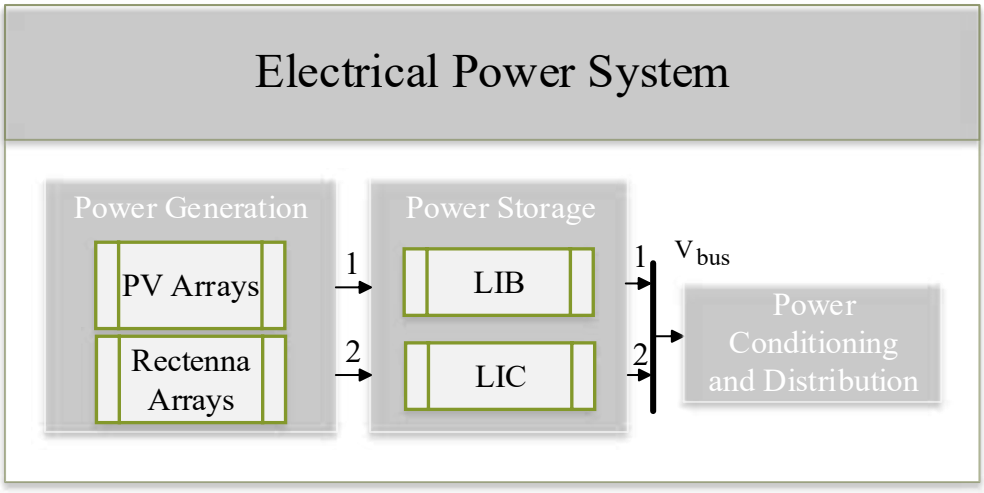

Figure 65. Functional block diagram of EPS. Path 1 represents the main power path and Path 2 represents the experimental power path.

5.3.4.5a Hybrid Power Generation Unit

This work proposes a stacked HPGU for a power receiving daughter satellite that has two functions. The first function is the role of the PV part of the HPGU as the primary power source for the spacecraft to harvest solar energy during the daylight part of the satellites orbit. The second function is for the rectenna part of the HPGU to collect and convert microwave energy from the mother satellite for experimental purposes.

1) Power Budget

In order to determine how much power is needed for satellite operations, a power budget is established based on the power requirements of each subsystem. There are two

steps to follow in order to establish the power budget. First, we calculate how much power is used by the satellite subsystems, including losses. Then we calculate the power produced by the solar cells.

Table 22 lists the different subsystems of the satellites in order to establish a power budget. The average power of ~22.00 Whr was calculated for a complete orbit. Table 23 breaks down the power demand for the satellite in daylight and eclipse.

To calculate the power that has to be supplied by the solar array while in sunlight period, we introduce the following equation:

$$P_{SA} = \frac{\frac{P_d T_d}{X_d} + \frac{P_e T_e}{X_e}}{T_d} \tag{26}$$

where

- P_{SA} is the power needed to be generated by the solar arrays.
- P_e and P_d are the power loads during eclipse and daylight, P_e = 8.4 W and P_d = 13.0 W.
- T_e and T_d are the time each orbit spends in eclipse and daylight, T_e = 36 min. and T_d = 58.5 min.
- X_d is the efficiency of power transfer from the solar arrays to the loads (typical value is X_d = 0.85 for DET [66]).
- X_e is the efficiency of power transfer from the solar arrays to the battery pack and then from the battery pack to the loads (typical value is X_e = 0.65 for DET [66]).

Table 22 Estimated power requirements for the 3U CubeSat.

Subsystem	Peak Current Use (mA)	Voltage Bus (V)	Peak Power Consumption (W)	Time of use (min)	Energy Use (Wh)	Hardware
Use during complete orbit						
OBC*	87.0	3.3	0.20	95.0	00.32	Cube Computer.
ADCS!	1320 6.0	5.0 5.0	6.60 0.03	95.0 95.0	10.50 00.05	3 MAI-400 reaction wheels (440 mA each). 3 Magnetic torquer Gyroscope ADXRS450
Use during Sunlight period of orbit						
TT&C#	-	5.0	1.55 (TX), 0.2 (RX)	59.0	1.72	Transceiver
Use during Eclipse period of orbit						
Propulsion	-	-	15.000	36.0	9.000	BET-1mN Busek Electrospray Thruster System
Energy Use Total					**22.00**	

*On-board processing (OBC) or Command and Data Handling	Receives commands from the ground, passes them to the appropriate components/payloads, and collects/stores data.
!Attitude Determination and Control (ADC) or Attitude Control System (ACS)	Determines the orientation of the spacecraft in space.
#Telemetry, Tracking, and Command (TT&C) or RF communications	Provides radio link between the spacecraft and the ground

Table 23. Periods in orbit.

Period	Energy Use (Wh)
During sunlight	8.4
During eclipse	13.0

Therefore, the amount of power that must be produced by the solar array is about P_{SA} = 22.00 W. The total power calculation seems to align with Janson [67], where microsatellites in the 10-100 kg mass range have a 26-120 W array. Next we select a solar cell in order to determine the solar PV array requirements in order to generate the 22.00 W of power.

2) Solar Cell Selection and Power Output Estimation

Triple junction GaAs cells have become the standard for most space applications, due to their higher collection efficiency and suitability for use in high radiation environments [66]. Spectrolabs' 29.5% efficient NeXt Triple Junction (XTJ) Solar Cell [99] was compared with Azurspace 30% efficient Triple Junction GaAs (3G30C) advanced Solar Cell [100]. The choice came to the 3G30C type because of its higher Beginning-of-Life (BoL) and End-of-life (EoL) efficiencies as seen in Table 24. Development for a four-layer GaAs cell type is under way with a theoretical maximum efficiency of 50% [101].

Table 24. Solar cell efficiency comparison.

Cell type	3G30 (Azurspace)	XTJ (Spectrolab)
Begin-of-life efficiency[1]	29.8%	29.5%
End-of-life efficiency after 15 years in GEO orbit[1]	28.1%	26.6%

[1]Measured at 1353 W/m^2, and 28°C.

Therefore, the estimated power output, P_o, with the Sun normal to the surface of the cells is $P_o = 0.298 \times 1{,}368\ W/m^2 = 408\ W/m^2$, where 1,368 W/m^2 is the *solar constant*. The solar cell efficiency gives us an ideal solar cell output performance per unit area, e.g. P_o.

3) Determination of the power output and array size

Next, we must determine the realistic power production capability of the manufactured solar array. The fact is that an assembled solar array is less efficient than single cells due to design inefficiencies, shadowing and temperature variations. The collective of these variations is referred to as *inherent degradation*, I_d. We will assume a nominal total inherent degradation of 0.72 [66]. The values of I_d, P_o, and β are used to estimate the beginning-of-life power per unit area by:

$$P_{BOL} = P_o I_d \cos\beta . \tag{27}$$

Thus the beginning-of-life power per unit area is calculated to be about 294 W/m^2. Next, we must consider the factors that degrade the solar array's performance during the mission, such as radiation, micrometeoroid strikes, thermal cycling in and out

of eclipses and material outgassing [66]. To calculate the *life degradation*, L_d, the following equation is used:

$$L_d = (1 - D)^L \tag{28}$$

where D is the degradation per year (D = 0.5%) and L is the satellite lifetime in years (L = 1 year mission). Thus, L_d = 0.995 (99.5 %) and the end-of-life power is calculated from

$$P_{EOL} = P_{BOL} L_d \,. \tag{29}$$

Therefore, the array's performance per unit area at end-of-life is P_{EOL} = 292.5 W/m^2.

The solar-array area, A_{sa}, required to support the spacecraft's power requirement, P_{sa}, is found from

$$A_{sa} = P_{sa} / P_{EOL} \,. \tag{30}$$

The resulting solar-array is about 0.08 m^2. These calculations have assumed the worst case scenario.

4) PV and Rectenna Array Configuration

Based on the calculated result for the required solar array area, it is evident that the proposed deployable array, as seen in Figure 66 and Figure 67, will have 9 panels (dark pink) dedicated for the PV part of the 3U CubeSat's HPGU. The rectenna array part of the HPGU will consist of 15 panels where 9 of the 15 panels are the stacked HPGU configuration. In the stacked HPGU configuration, the PV array is on top of the rectenna array.

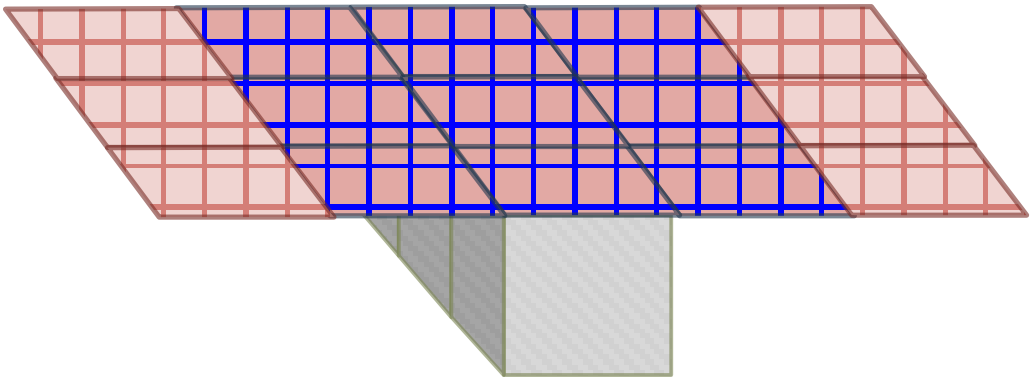

Figure 66. HPGU configuration for experimental 3U CubeSat.

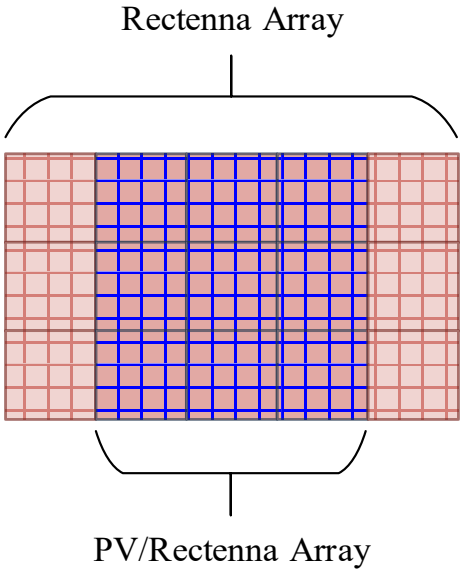

Figure 67. Top view of a HPGU configuration.

5.4 Printed Rectenna Design for In-Space Power Reception

The rectifying antenna or rectenna is the technology that collects/harvests the microwave energy and converts it into usable DC power. The LEO space environment poses challenging design considerations for the rectenna equipped on the daughter satellite, such as out-gassing, large temperature variations, and the effects of oxygen on materials. This chapter will highlight some of these LEO environmental challenges and offer possible design solutions to overcome these challenges in terms of the materials used and design approaches.

The trade-off between optimizing for the conditions of space is a reduction in RF-to-DC efficiency. This chapter gives a detailed understanding and process toward rectenna element design with an emphasis for in-space application. Careful design directions and clear understanding is essential in order to achieve high RF-to-DC conversion efficiency results with the rectenna. This chapter is organized as follows: First, an antenna design study including thermal analysis; second, material and component analysis and selection specifically for space application; third, theory of rectenna operation; fourth, coplanar stripline theory and design; fifth, CPS-to-Klopfenstein Taper back-to-back transition design and measurement; and sixth, proposed experimental measurement setups, are presented.

5.4.1 Antenna Design Study

Antennas designed for space application and for the rectenna part of the HPGU must be small, have low mass, and be highly efficient. A microstrip antenna design seems a suitable option. The electromagnetic behavior of a microstrip antenna is strongly influenced by the feeding technique and is governed by a number of factors [102]: (i) transfer of efficient power between the radiating structure and feed structure, (ii) minimization of spurious radiation and its effect on radiation pattern, and (iii) suitability of the feed for array applications.

Different types of microstrip feeding techniques are seen in Figure 68. Some advantages and disadvantages of these feeding techniques are seen in Table 25. In an array the probe-fed mechanism can lead to more points of failures, and therefore, decrease reliability. Thus, the probe-fed option is eliminated. The antenna feeding mechanism that seems to satisfy the aforementioned factors best is an aperture coupled

feeding technique. This non-contacting feeding method offers at least four degrees of freedom in the design [103], it minimizes spurious radiation, and avoids vertical elements and soldering (thus increasing the reliability, which is important for space applications).

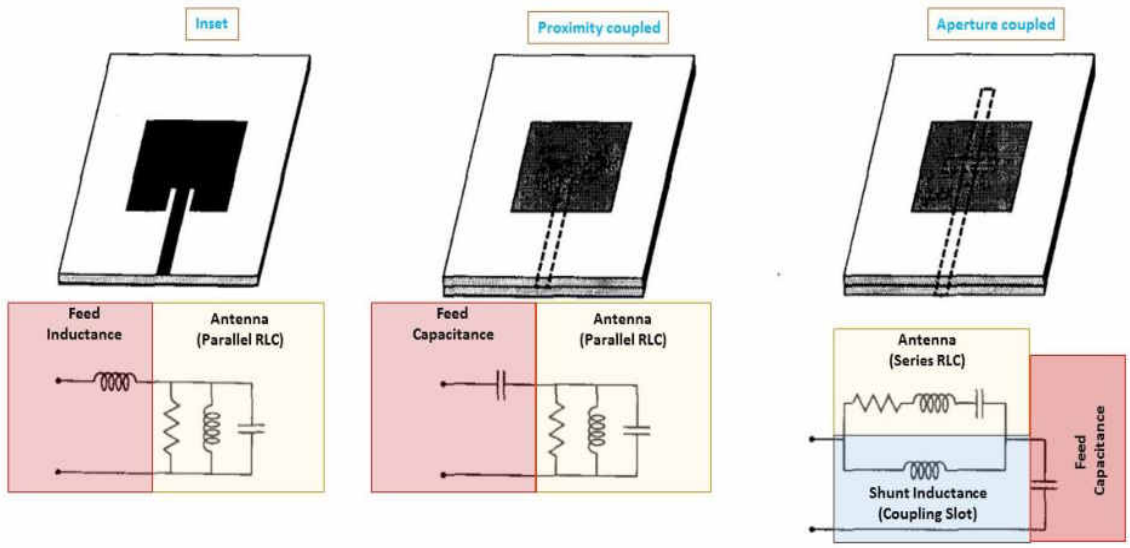

Figure 68. Microstrip antennas and feeding mechanisms [103].

An aperture-coupled antenna was designed using CST-MWS, as seen in Figure 69. This work investigated a multi-layered PCB aperture-coupled antenna design at fundamental frequency of 5.8 GHz, having a layered topology from top to bottom layer as; antenna, the first substrate layer, bondply/prepeg, ground plane with apertures, the second substrate layer, and the feeding network.

The antenna model incorporated change in dielectric constant as a function of change in temperature for a combination of different material layers and slot designs. The material for antenna substrate was either 6002 or 5880LZ and the material for the feed line substrate was 4360G2. The two slot designed were rectangular and dogbone. The results showed that the 6002 material with dogbone slot performed the best in terms of

Table 25. Microstrip antenna feed techniques advantages and disadvantages.

Technique	Advantages	Disadvantages
Microstripline (BW 2-5%)	Simplicity in design – one degree of freedom.	Suffer from BW/feed radiation trade-off. Spurious feed radiation.
Coaxial Probe (BW 2-5%)	Simplicity in design – one degree of freedom.	Suffer from BW/feed radiation trade-off. Array configuration – reduced reliability.
Proximity Coupling (BW 13%)	At least two degrees of freedom. Reduced spurious feed radiation. No via connectors .	Fabrication is more difficult.
Aperture Coupling (BW 10-20%)	At least four degrees of freedom. Reduced spurious feed radiation. No via connectors.	Multilayer fabrication required. Large back lobe.

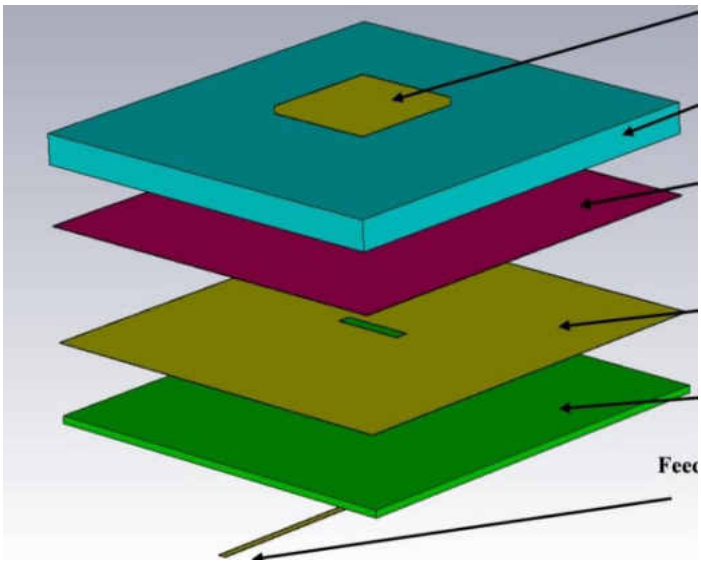

Figure 69. Aperture coupled antenna design in CST MWS.

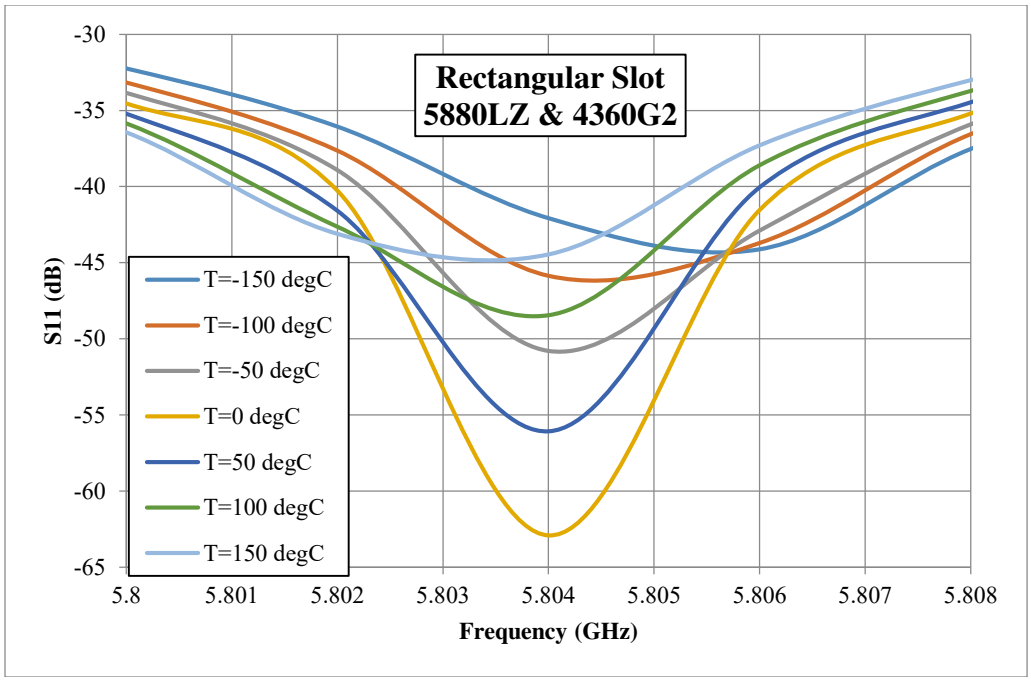

Figure 70. Rectangular slot antenna using 5880LZ as antenna layer and 4360G2 as feed line layer.

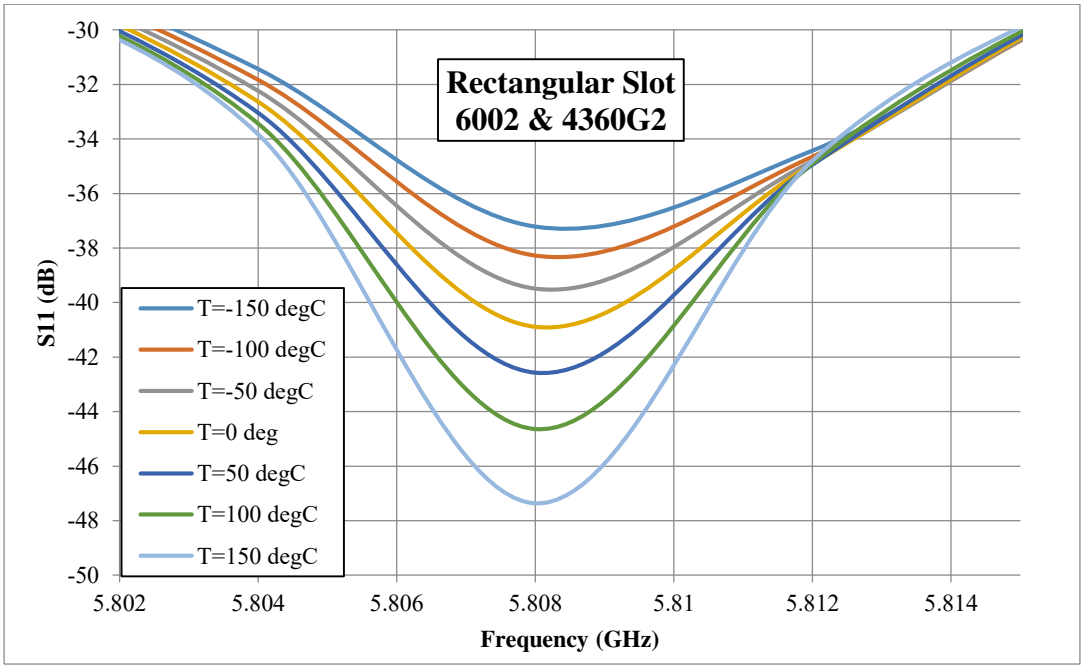

Figure 71. Rectangular slot antenna using 6002 as antenna layer and 4360G2 as feed line layer.

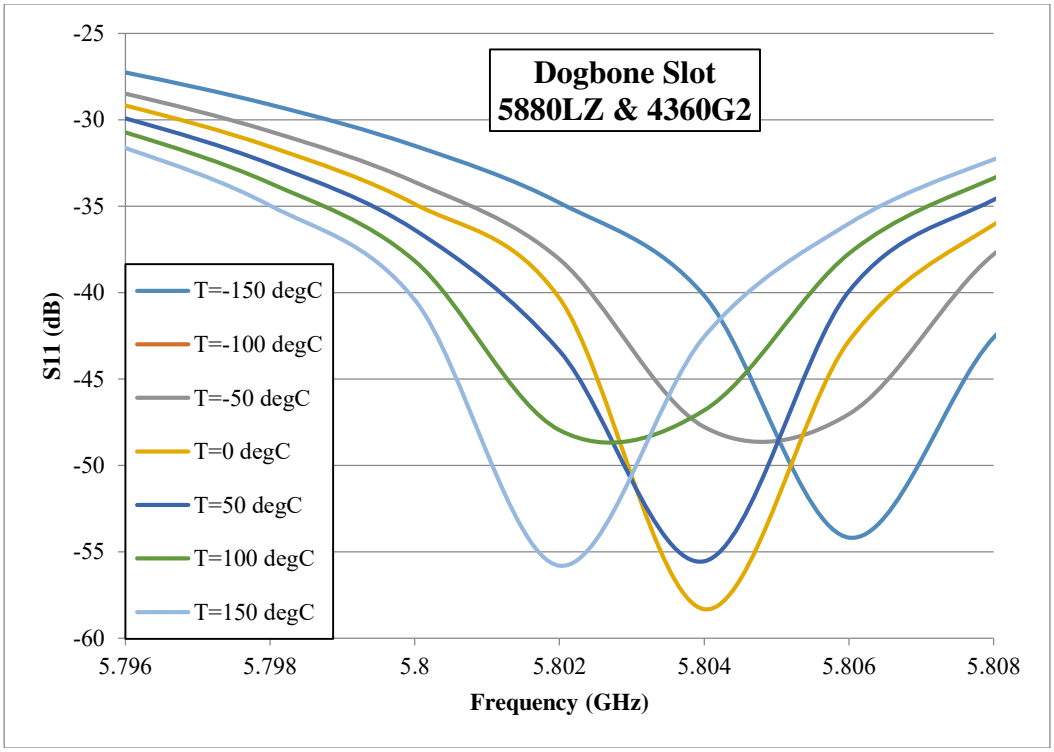

Figure 72. Dogbone slot antenna using 5880LZ as antenna layer and 4360G2 as feed line layer.

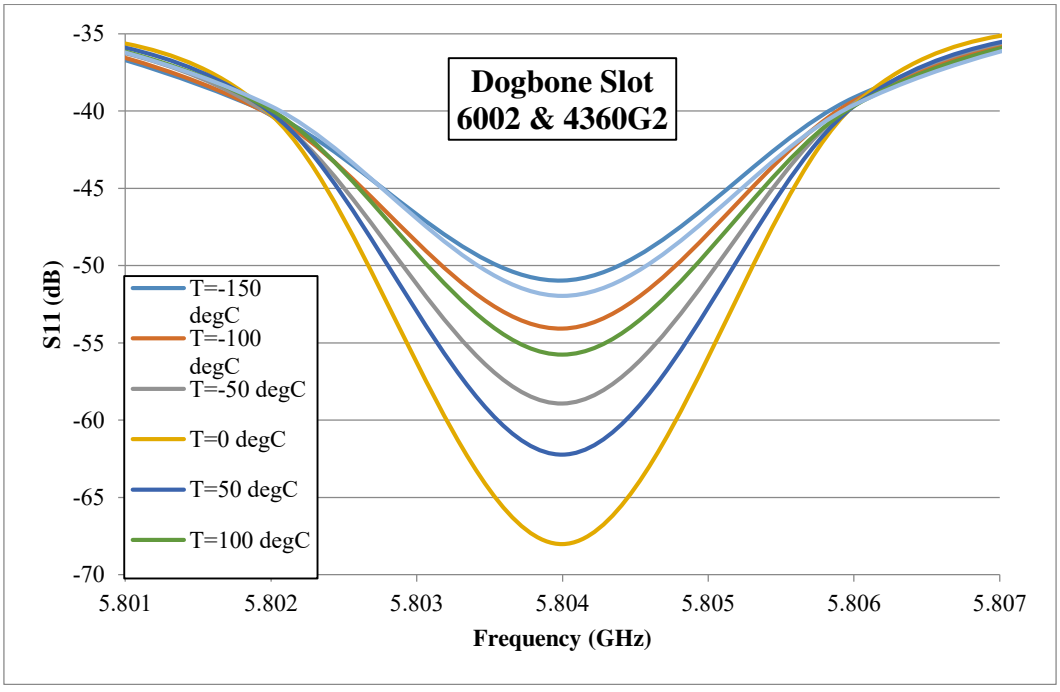

Figure 73. Dogbone slot antenna using 6002 as antenna layer and 4360G2 as feed line layer.

stability of the resonant frequency as seen in Figure 70 - Figure 73. These results matched the expectations based on the material data sheets thermal stability ratings of materials.

The issue with the aperture coupled fed antenna is the complexity of the multi-layer design as Table 25 indicated. Another factor was that the aperture-coupled fed antenna will have greater feed loss compared to the other techniques [104]. In fact, according to a study done by Pozar and Kaufman [104] the microstrip line-fed showed a much lower loss compared to the aperture coupled mechanism. Thus, one of the best candidate antennas for this application the microstrip line-fed antenna. Therefore, further research was conducted and the conclusion was a dual rhombic loop antenna (DRLA) with a CPS feed technique as seen in Figure 18 is a good choice. The DRLA offers high gain. Additionally, integrating it with a filter and rectifier circuit through the CPS structure is convenient and efficient. The DRLA was designed and simulated using ANSYS Ansoft HFSS. However, the antenna needs to be simulated with a filter design as the filter will couple to the antenna and change its properties.

The point to take away from this section is that microstrip antennas are a good choice for the rectenna part of the proposed HPGU. Features that must be met in the design of the antenna is circular polarization capability, high gain, broad beam, and the suitability for antenna array. The DRLA offers all these features and should be pursued further as the design of choice.

5.4.2 Material and Component Selection for Space Application

Spacecraft's in LEO face many challenges and so do the antennas/rectennas installed on the spacecraft's. First, antennas designed for space application equipped on a modern small satellites must be low profile, have low mass, be highly efficient and

reliable, and be low cost. Moreover, the antenna and material must be able to perform well over a wide temperature variation, typically from -150℃ to 150℃ [6]. The material must also be able to handle the effects of atomic oxygen for LEO missions and pass outgassing requirements from the vacuum environment.

For selecting material and components this work considers: (1) outgassing and (2) operating under a large range of thermal variations. In a vacuum environment, trapped or absorbed gas (from manufacturing or from curing laminates) can evolve causing the material to lose volatile mass particles that may act as contaminants to other surfaces and can harm the satellite [78]. For example, the particles can condense onto optical elements, thermal radiators, solar cells or antenna elements, thus obscuring them and decreasing their performance. All materials used for space flight applications should satisfy the outgassing requirements recognized by space agencies. Contamination requirements are usually expressed in terms of total mass loss (TML) and collected volatile condensable materials (CVCM)s [78]. In general, materials with TML over 1.0% or CVCM over 0.10% should be avoided in spacecraft applications [72].

For LEO environment atomic oxygen strongly interacts with materials to form oxygen bonds with atoms on the exposed surface [105]. Depending on the chemical reaction in place, atomic oxygen can result in the erosion of materials, surface oxidation or gradual conversion of silicones to high-modulus silica [105]. One method to reduce the effect of atomic oxygen on thin polymers and increase their durability is based on the use of coatings, generally made of SiO_2, Al_2O_3, and indium tin oxide, Ge, Si, Al and Au. Up to 100 nm of sputtering of vapor deposited protective coatings is generally used [105]. The analysis for coating the rectenna array is left for future research.

Another concern for electronic circuits in space is the impact of the large swings in temperature (typically, -150℃ to 150℃ for modern small satellites in LEO [106]) which can alter the PCB material's characteristics. PCB materials affected by changes in temperature, which in-turn can influence the performance of microwave circuits fabricated on PCB materials such as shifting of the operating frequency. This work considers coefficient of thermal expansion (CTE) and thermal coefficient of dielectric constant ($TC\varepsilon_r$) as influencing the PCB circuit performance. CTE is a measure of the dimensional changes in the material as a function of temperature and should be considered in the material selection for uniform expansions in the X, Y, and Z directions. $TC\varepsilon_r$ is a change in the dielectric value of the substrate as a function of temperature.

For this work, Rogers Corporation PCB materials were analyzed considering thermal and outgassing characteristics. Table 26 and Table 27 list the results of this comparison and Figure 74 plots εr as a function of temperature for the different PCB materials. Based on this information it is evident that RT/Duroid 6002 material is the most stable over the temperature range of interest. Moreover, RT/Duroid 6002 has a uniform CTE in the X and Y directions. These results conclude RT/Duroid 6002 as the selected PCB material of choice for space rectenna element design.

The diode component selected for this design is Yokowo GaAs Schottky Barrier Diode (YSD110). YSD110 has a storage temperature range from -55℃ to 125℃. The GaAs material of the diode fits in the confines of a LEO space mission. However, temperature control methods would have to be employed on the rectennas to ensure operational reliability. This is outside the scope of this work but an interesting question to

Table 26. Material from Rogers Corporation compared for dielectric constant, loss tangent, and outgassing.

Material Material	ε_r	Tanδ	Outgassing TML (%)	CVCM (%)
5880LZ	1.96	0.0019	0.01	0.01
6002	2.94	0.0012	0.02	0.01
4003C	3.55	0.0021	0.06	0.00
4360G2	6.15	0.0038	0.13	0.021
3010	10.2	0.0022	0.02	0.025
2929 Bondply	2.94	0.0030	0.42	0.02

Table 27. Material from Rogers Corporation comparing thermal coefficient of dielectric constant, coefficient of thermal expansion, and thermal conductivity.

Material	TCε_r (ppm/℃)	CTE (ppm/℃) (X,Y,Z)	Thermal Conductivity (W/m/K)
5880LZ	+22	44, 43, 41.5	0.33
6002	+12	16, 16, 24	0.60
4003C	+40	10, 12, 32	0.71
4360G2	-131	13, 14, 28	0.75
3010	-280	13, 11, 16	0.95
2929 Bondply	-6	50, 50, 50	0.40

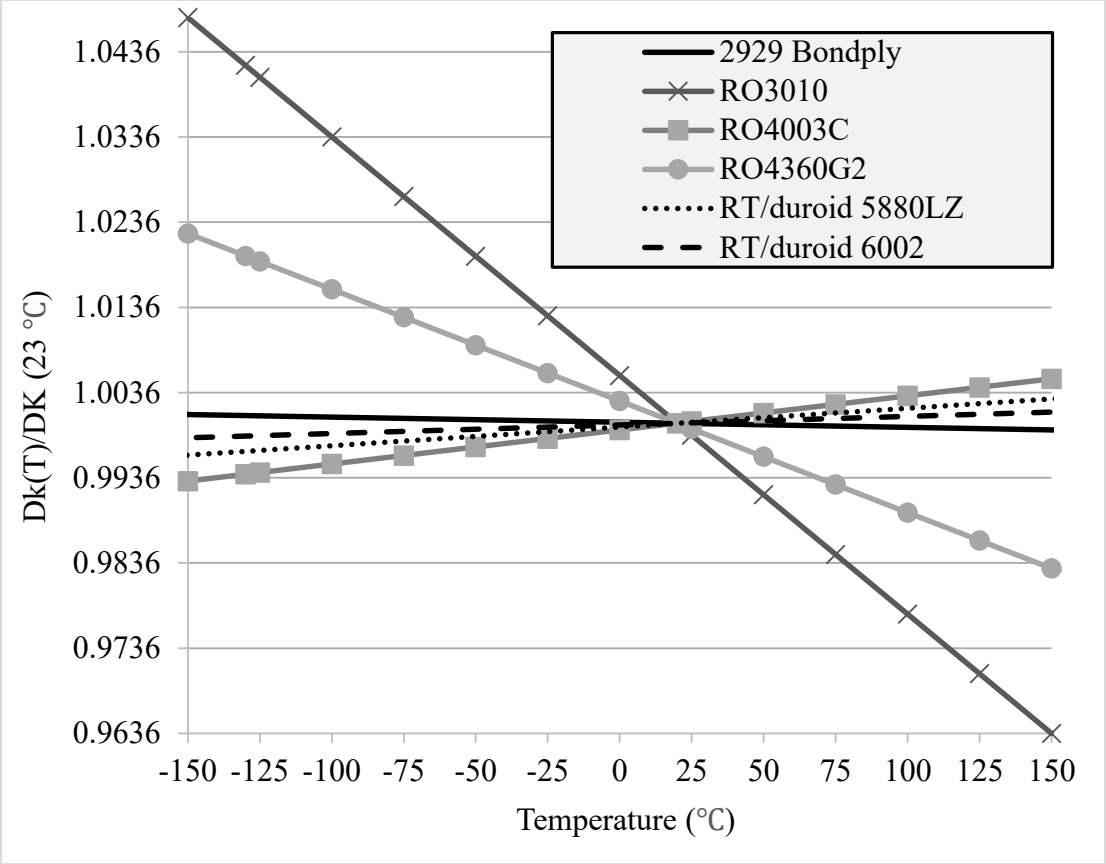

Figure 74. Change in dielectric constant as a function of temperature. The less rate of change over the temperature range the more stable the material is and thus less influence on affecting electrical performance of the circuit. Room temperature is set as 23 ℃.

answer in future research. The capacitor selected to filter RF signals before it reaches the load is Dielectric Laboratories broadband (1MHz-20GHz) DC block (C08BLBB1X5). This capacitor also has a storage temperature range between -55℃ and 125℃. However, in order to determine the capacitors electrical performance for space application it must go through rigorous testing in both the space environment and on Earth. Thus for this thesis the capacitor (C08BLBB1X5) has not been tested for the space environment.

5.4.3 Deeper Understanding of Material Properties

After material selection it is important to understand insertion loss or total loss. Insertion loss is the amount of power lost between two points in a circuit. Losses can take the form of:

1. Dielectric loss
    a. Dissipation factor or Loss Tangent (Tanδ) that an electromagnetic wave experiences while traveling in part through the substrate material
2. Conductor loss
    a. Dominated by conductor properties
        i. Conductor width
        ii. Surface roughness
        iii. Skin effects
3. Radiation loss – energy on the circuit that is lost by radiating away from the circuit and into the surrounding environment (e.g. impedance mismatches)
4. Leakage loss – this is very small and can be ignore

The rectenna's RF-to-DC conversion efficiency performance is higher with a thinner substrate thickness and with a lower dielectric constant substrate value. This combination achieves higher impedance values which leads to increased RF-to-DC conversion efficiency as is shown in Section 5.4.4.1. In addition, the rectenna structure as a whole benefits from the thinner substrate and lower dielectric constant values through a decrease in generated heat, decreased weight and decreased dielectric losses. These benefits are all positive for being equipped on a spacecraft. However, the trade-off is strength. A thicker substrate will provide the strength needed in the rectenna design to

better withstand against the phenomena's of getting into space and while operational in space. However, it impacts the RF-to-DC conversion efficiency level due to restricting to low power input levels due to low resistive values selected to obtain optimal RF-to-DC conversion efficiency.

It is also important to recognize the effects of skin depth and copper conductor thickness. Skin depth is defined by:

$$\delta = \sqrt{\frac{2\rho}{2\pi f \mu}} \tag{31}$$

where ρ is the bulk resistivity (or 1/σ, where σ is the conductivity), f is the frequency, and μ is the permeability. At 5.8 GHz frequency, bulk resistivity for annealed copper measured at 20 ℃ is $\rho = 1.72 \times 10^{-8}\ \Omega \cdot m$ and permeability of copper is $\mu = \mu_0 \mu_r = \left(4\pi \times 10^{-7}\right)\left(0.999991\right) = 12.5663 \times 10^{-7}\, Hm^{-1}$. Taking this a step further by incorporating electrical resistivity and changes to temperature defined by:

$$\rho(T) = \rho_0 \left[1 + \alpha\left(T - T_0\right)\right] \tag{32}$$

where α is the temperature coefficient of resistivity ($\alpha = 0.00393 K^{-1}$), resistivity of annealed copper at room temperature (T_0 = 0 ℃), and $\rho_0 = \rho = 1.72 \times 10^{-8} \Omega \cdot m$. Equation (32) is a linear approximation. To minimize conductor loss while simultaneously minimizing the amount of metallic material flanking the dielectric, the conductor thickness should be greater than approximately 3-5 skin depths [107] as shown in Figure 81.

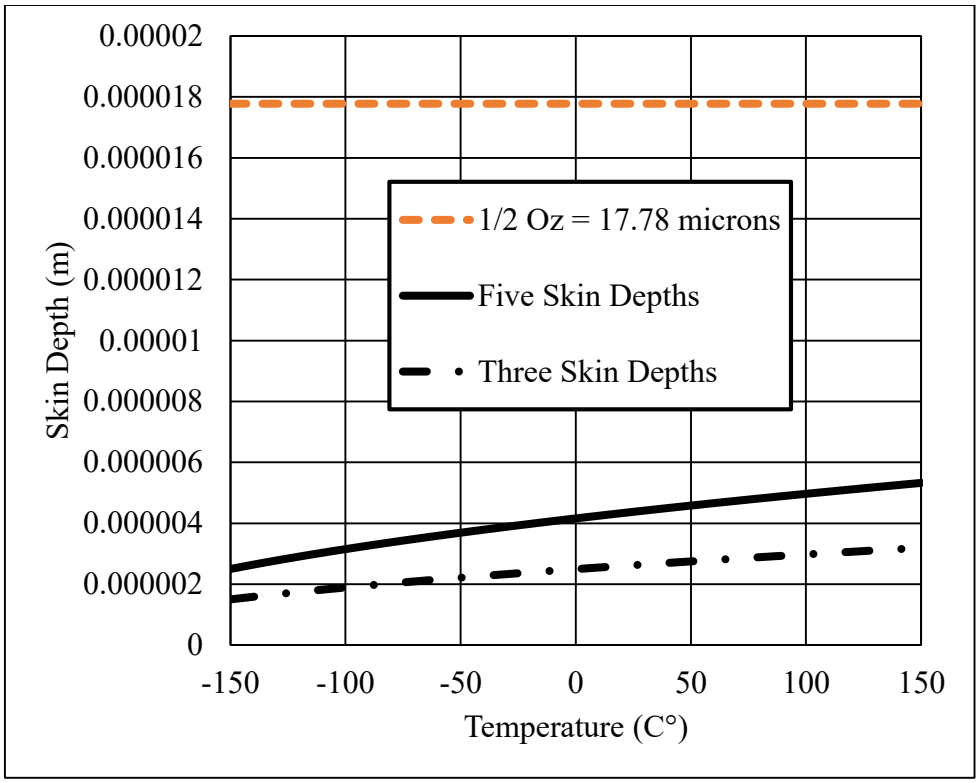

Figure 75. Figure shows skin depth as a function of temperature.

5.4.4 Rectenna Operation Theory

An example of a rectenna configuration is shown in Figure 76. The antenna receives and captures the electromagnetic wave that is transformed into a RF signal that travels along a conductor passing through a filter (in this example a LPF), onto the diode where harmonic frequencies are bounced back towards the LPF and are suppressed or filter out, and DC power continues forward on the other side of the diode to the DC bypass filter (capacitor) that smooths out the DC ripples, and finally the DC signal reaches the load.

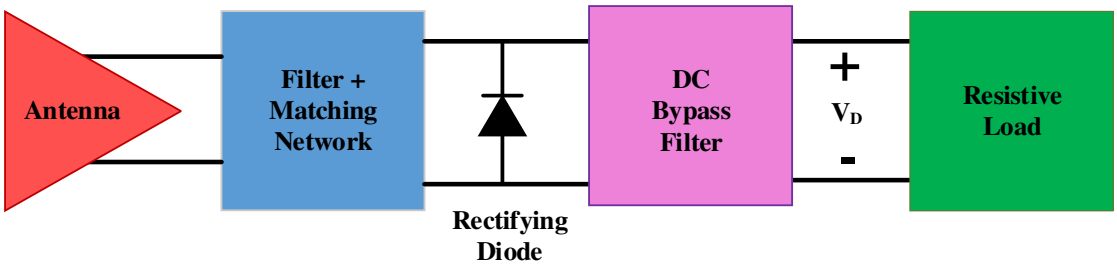

Figure 76. Example of rectenna configuration.

According to Strassner and Chang [37] when designing an efficient rectenna element one should begin with the characterization of the diode's nonlinear electrical behavior since the design of the other rectenna parts depends directly upon the diode's performance. In fact, it has been shown [7, 9, 108] that the diode's RF-to-DC conversion efficiency (η_D) is the key part in the rectenna element that determines the rectenna's performance.

The diode has two sources of nonlinearity: conductive and reactive. The conductive nonlinearity in the *I(V)* (current and voltage) curves and the reactive nonlinearity in the *C(V)* (capacitance and voltage) curves are evident. The nonlinearity is caused by the diodes voltage dependent capacitance, dispersion due to the periodicity, and the dissipation due to the finite conductivity of the conductor and series resistance of the diode [109]. Diodes are typically modeled according to the nonlinear relationship of the *I(V)* curve as seen in Figure 83 [69]. Valenta and Durgin [69], characterized this diode *I-V* curve into three major regions of operation: (1) the region below the reverse breakdown voltage (V_{br}) where the diode is reversed biased and will conduct in the reverse direction; (2) the region between V_{br} and the turn-on voltage V_T where the diode is off and only a small leakage current will flow, and; (3) the region above V_T where the diode is forward biased and current flows proportionally to the voltage.

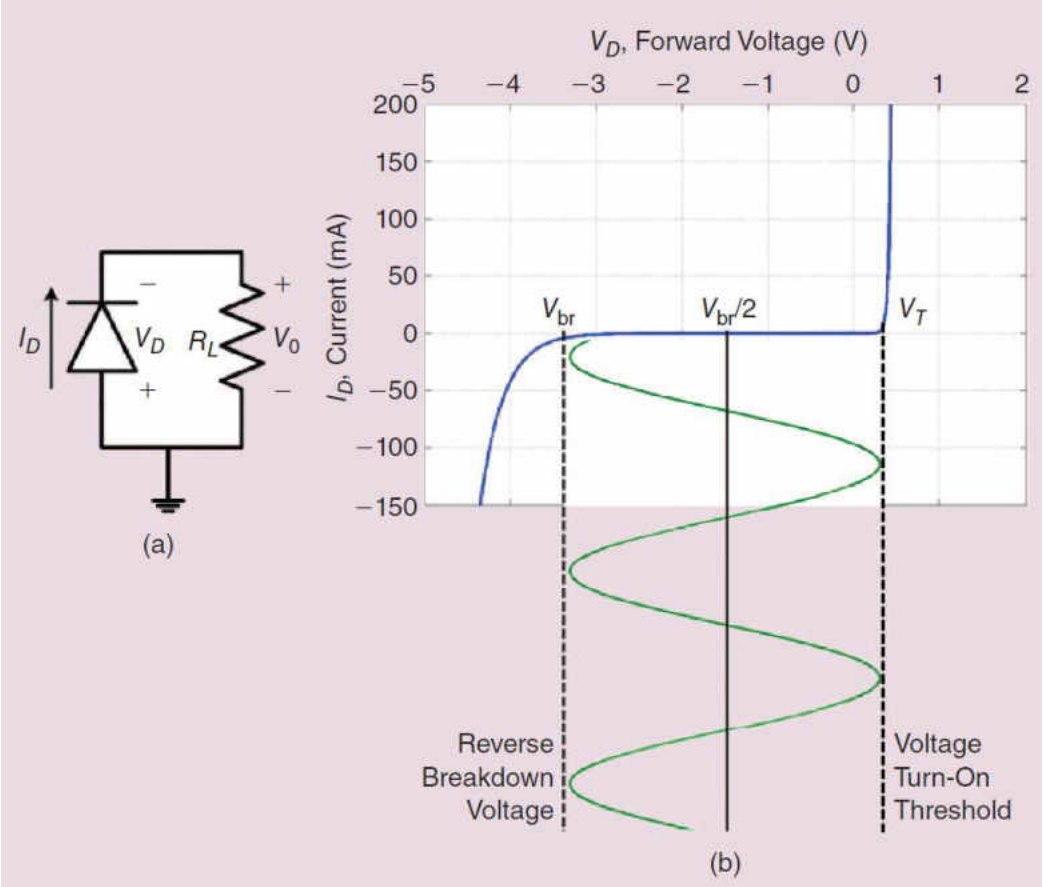

Figure 77. Typical diode I-V curve with annotated breakdown and turn-on voltages. (a) assumes all reactive elements have been tuned out, and sufficient RF power exists across the diode to generate a dc voltage across the output resistor R_L. Figure used from [69] with permission.

Actually, the voltage across the diode $V_{o,dc}$ is limited by the reverse breakdown voltage according to

$$V = \frac{V_{br}}{2}. \tag{33}$$

If the peak-to-peak voltage is larger than this value, the waveform will exceed the breakdown voltage and the dc level will no longer increase. Therefore, the maximum DC power P_{dc} is limited by

$$P_{dc,\max} = \frac{V_{br}^2}{4R_L}. \tag{34}$$

This limitation is understood through Figure 84. The load resistance R_L, which guarantees the maximum efficiency for applications operating near V_{br} is typically 1.3-1.4x the diode input resistance [7]. Beyond $P_{dc,max}$ limitation the breakdown voltage effect takes over, thus, decreasing the diode RF-to-DC conversion efficiency and ultimately the rectenna element's RF-to-DC conversion efficiency [69].

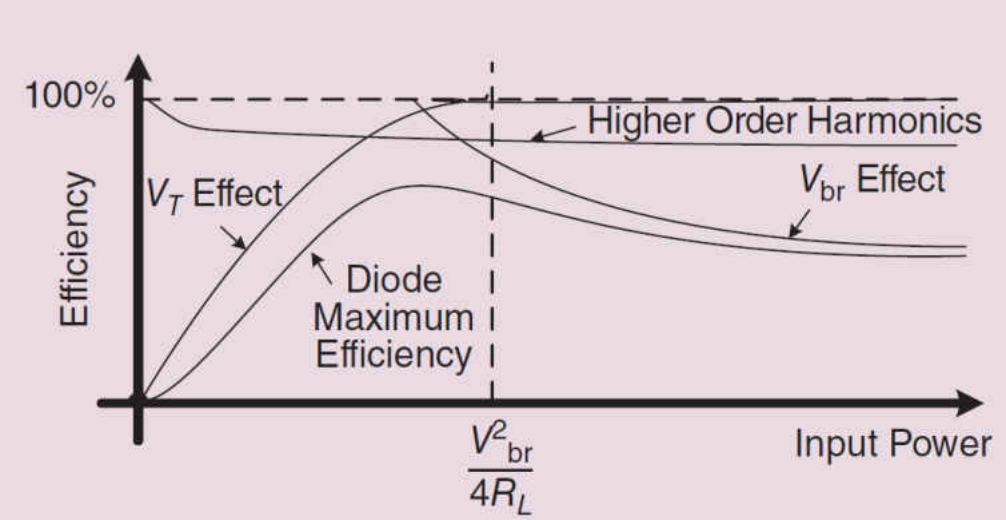

Figure 78. General relationship between the efficiency and losses in microwave energy conversion circuits as a function of input power. Figure from [69] with permission. At low powers, the efficiency is limited by the input signal ability to surpass the diode turn-on threshold voltage. As the power continues to increase, the efficiency will increase along with harmonics. At higher power, the diode reverse breakdown voltage limits the efficiency. A maximum conversion efficiency occurs between these points.

Figure 79 shows a simplified rectifier circuit and equivalent circuit of the Schottky diode. The diode model consists of a series resistance R_s, a nonlinear junction resistance R_j described by its *IV* characteristics, and a nonlinear junction capacitance C_j. A DC load resistor is connected in parallel to the diode along a DC path represented by a

dashed line to complete the dc circuit. The symbol Γ represents the reflected signal from the diode back to the generator.

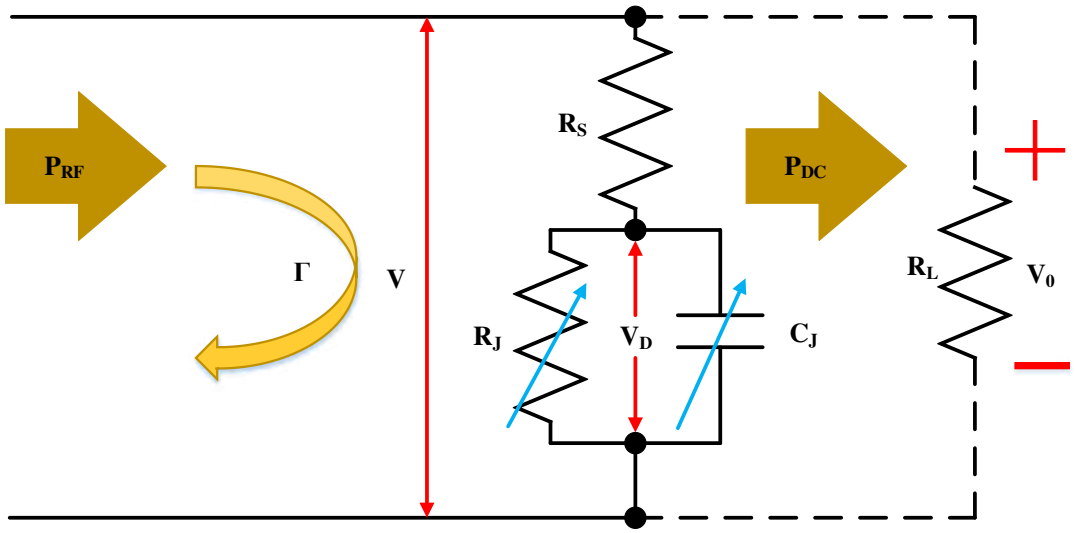

Figure 79 Equivalent rectifiying circuit model. In this circuit, the RF current to be rectified passes only through the solid part of the circuit, while the DC travels along the dashed path.

A diode model described by Yoo and Chang [8] and expanded by McSpadden, *et al*., [7] to account for varying input power levels was used to predict the rectenna diode's behavior. This model depends only on the diode's electrical parameters and microwave circuit losses at the fundamental frequency of operation. Harmonic effects are not included. To derive these expression, Figure 80 helps view the rectification cycle.

The diode junction waveform can be expressed as

$$V = -V_0 + V_1 \cos(\omega t)$$
$$V_d = \begin{cases} -V_{do} + V_{d1} \cos(\omega t - \phi), & \text{if diode is off} \\ V_{bi}, & \text{if diode is on} \end{cases} \tag{35}$$

where V_o is the output self-bias DC voltage across the resistive load and V_1 is the peak voltage amplitude of the incident microwave signal. Biasing in electronics is the method of establishing predetermined voltages or currents at various points of an

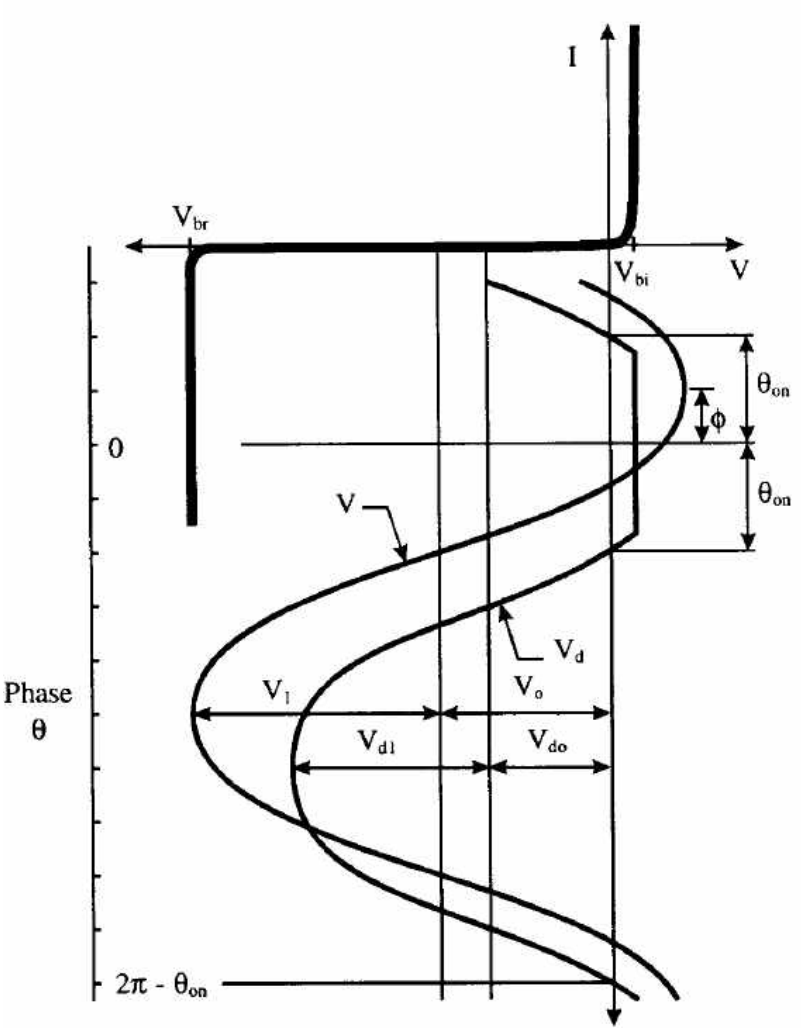

Figure 80. Rectification cycle represented by the input fundamental and diode junction voltage waveforms impressed on the diode IV curve. This model assumes there are no losses in the harmonics and $\theta=\omega t-\phi$. Figure is used with permission from [7].

electronic circuit for the purpose of establishing proper operating conditions in electronic components. As the incident power increases, the output DC voltage becomes more reversed biased [7]. V_{do} and V_{d1} are the DC and fundamental frequency components of the diode junction voltage, and V_{bi} is the diode's built-in voltage in the forward bias region. Also in Figure 80 the forward-bias turn-on angles θ_{on} of V_d and the phase

difference ϕ between V and V_d. θ_{on} is a dynamic variable dependent on the diode's input power and is determined by

$$\tan\theta_{on} - \theta_{on} = \frac{\pi R_s}{R_L\left(1+\frac{V_{bi}}{V_0}\right)} \tag{36}$$

This transcendental equation should be solved iteratively. McSpadden, *et al.* [7] applied Kirchoff's voltage law to the diode's equivalent circuit model in order to derive a closed-form equation for the diode's efficiency and input impedance as

$$\eta_D = \frac{1}{1+A+B+C} \tag{37}$$

where

$$A = \frac{R_L}{\pi R_s}\left(1+\frac{V_{bi}}{V_o}\right)^2\left[\theta_{on}\left(1+\frac{1}{2\cos^2\theta_{on}}\right)\right] \tag{38}$$

$$B = \frac{R_s R_L C_j^2 \omega^2}{2\pi}\left(1+\frac{V_{bi}}{V_o}\right)\left(\frac{\pi-\theta_{on}}{\cos^2\theta_{on}}+\tan\theta_{on}\right) \tag{39}$$

$$C = \frac{R_L}{\pi R_s}\left(1+\frac{V_{bi}}{V_o}\right)\frac{V_{bi}}{V_o}\left(\tan\theta_{on}-\theta_{on}\right) \tag{40}$$

and ω is the angular frequency ($2\pi f$). The junction capacitance is defined as

$$C_j = C_{jo}\sqrt{\frac{V_{bi}}{V_{bi}+|V_o|}} \tag{41}$$

where C_{jo} is the diode's zero bias junction capacitance. The diode's input impedance is expressed as

$$Z_D = \frac{\pi R_s}{\cos\theta_{on}\left(\frac{\theta_{on}}{\cos\theta_{on}}-\sin\theta_{on}\right)+j\omega R_s C_j\left(\frac{\pi-\theta_{on}}{\cos\theta_{on}+\sin\theta_{on}}\right)} \tag{42}$$

And finally the diodes input resistance is given as

$$R_D = \frac{\pi R_s}{\cos\theta_{on}\left(\frac{\theta_{on}}{\cos\theta_{on}} - \sin\theta_{on}\right)} \tag{43}$$

Similar to efficiency, the diode's input resistance is also a dynamic variable dependent on the input microwave power. MATLAB code has been written to calculate the various characteristics of the diode component as will be shown next.

5.4.4.1 Diode Analysis

Four GaAs Flip Chip Schottky Barrier Diodes: (1) MA-COM (MA4E1317); (2) Aeroflex/Metalics (MGS801A), (3) Aeroflex/Metalics (MGS801), and; (4) Yokowo (YSD110) and four GaAs Beam Lead Schottky Diodes: (1) Avago (HSCH-5312); (2) Avago (HSCH-5310); (3) Avago (HSCH-5330), and; (4) Avago (HSCH-5332) were used for a comparison analysis.

Table 28 shows the aforementioned diodes' Spice parameters. Plugging these values into equations (39), (45) and (46) we obtain calculated diode's real and imaginary impedance values as a function of load resistance as seen in Figure 87 and Figure 88, respectively.

From Figure 88 and Table 28, it is clear that low C_{jo} values of MA4E1317 and YSD110 result in low diode reactance change as a function of load resistance. The importance of the low C_{jo} value is understood through equations (44), (40), and (42). Basically, the greater C_{jo} the lower the diodes efficiency, and vise-versa.

Table 28. Spice parameters and operating temperatures for various diodes.

Model	Typ. V_F (V)	Typ. V_{Br} (V)	Typ. C_{Jo} (pF)	Typ. R_S (Ω)	Operating Temperature (°C)
MA4E1317	0.70	7.0	0.020	4	-65 to +125
MGS801A*	0.68	6.0	0.055	5	-65 to +150
MGS801*	0.70	6.2	0.044	7	-65 to +150
HSCH-5312* (med)	0.65	5.0	0.13	9	-65 to +175
HSCH-5310* (med)	0.65	5.0	0.09	13	-65 to +175
HSCH-5330* (Low)	0.5	5.0	0.09	13	-65 to +175
HSCH-5332* (Low)	0.5	5.0	0.13	9	-65 to +175
YSD110	0.70	10.0	0.030	5	-55 to +125
Test Conditions	I_F = 1 mA	I_R = 10 μA	0V at 1 MHz	10 mA or 5 mA*	

Now in order to determine diode efficiency in equation (40), a resistive load value needs to be selected. The selection of R_L is determined from the characteristic impedance value of the coplanar stripline ($Z_{o,CPS}$). Coplanar stripline is analyzed in detail next. In the analysis of the coplanar stripline the only parameter that changed was the gap (S) between the two conducting lines as shown in Figure 86. The other parameters were set as: W = 2.1 mm, t = 35.56 μm, h = 0.254 mm (10-mils), and the air gap = 10.85 mm (~0.21 λ_o). The gap was set based on the diode components inner dimensions. Each diode had slightly different gap lengths, as listed in Table 29. The characteristic impedance of the coplanar stripline was determined by simulations using Ansoft HFSS. Those results

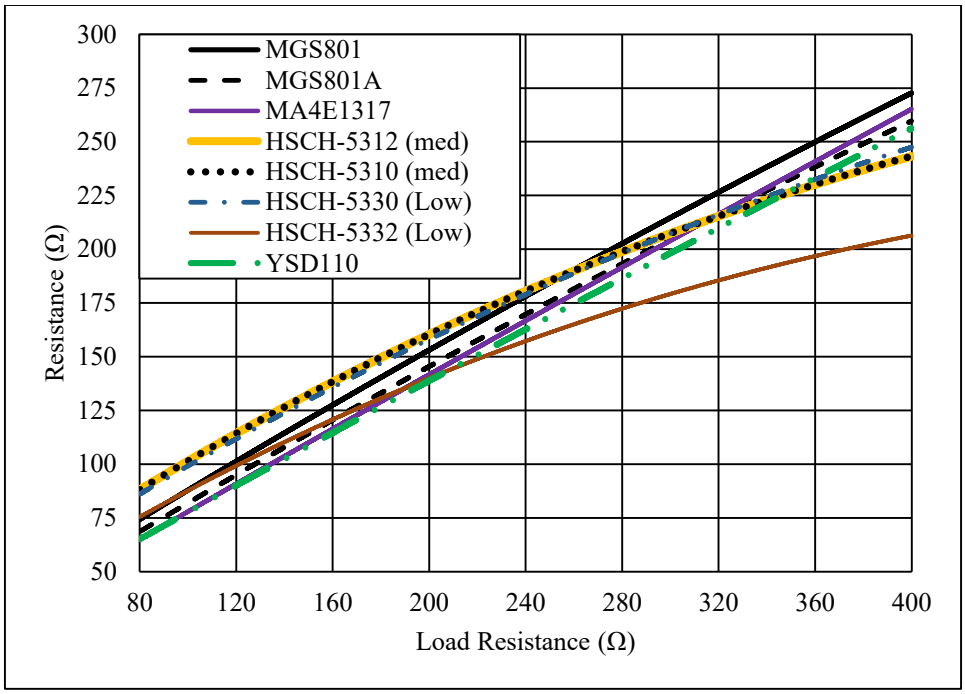

Figure 81. Different diode's resistance as a function of load resistance.

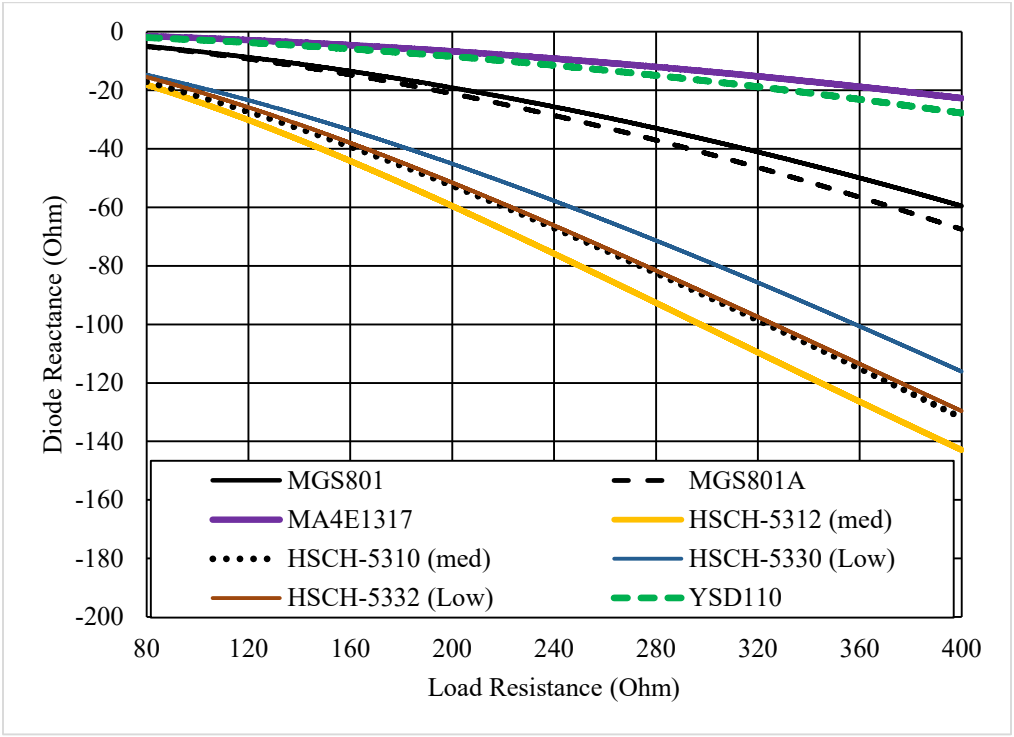

Figure 82. Different diodes reactance as a function of load resistance.

are also listed in Table 29. Setting $Z_{o,CPS}$ = diode resistance value from Figure 87, we can match R_L for each diode case, as listed in Table 29. The reason $Z_{o,CPS}$ = diode resistance value, is because the matching reduces loss and therefore maintains high efficiency.

The load resistance values R_L calculated for each diode was then plugged into equations (41)-(43) to solve equation (40). Maximum input power level across the diode was determined by:

$$P_{dc,\max} = \frac{V_{br}^2}{4R_L}. \tag{44}$$

The calculated RF-to-DC rectification efficiency results are seen in Figure 89. From Figure 89 it is evident that YSD110 allows for the greatest amount of input power at a high efficiency for both low input power levels as well as high input power levels. With a lower dielectric constant material YSD110 has ~80% RF-to-DC rectification efficiency.

Relating the results of Figure 89 to the Spice parameters from Table 28, we can determine that in order to obtain the highest RF-to-DC rectification efficiency, R_S and V_F need to be low, and V_{br} needs to be high. Having low R_S means the power transferred beyond rectification process remains high. Having low V_F means less energy is needed to overcome the barrier, and therefore, more power is transferred beyond the rectification process. Having high V_{br} means it takes greater power levels to reach the reverse breakdown voltage level as defined by $V_{o,\mathrm{DC}} = V_{br}/2$ across the diode, and therefore, higher power levels are injected into the circuit for rectification as defined by equation (47). Next the coplanar stripline and focuses on designing the rectenna using YSD110 are presented.

Table 29. Various diodes and their resulting matched resistive load for highest efficiency.

Diode	S (mm)	$Z_{o,CPS}$ (Ω)	R_L (Ω)	$P_{dc,max}$
MA4E1317	0.200	100.0	134.3	125
MGS801A	0.305	112.0	146.5	88
MGS801	0.305	112.0	136.2	106
HSCH-5312 (med)	0.250	107.4	131.7	76
HSCH-5310 (med)	0.250	107.4	109.3	103
HSCH-5330 (low)	0.250	107.4	113.1	99
HSCH-5332 (low)	0.250	107.4	134.8	75
YSD110	0.200	100.0	136.0	180

The diode used in this rectenna circuit, YSD110, has Spice parameters; R_S = 5 Ω, C_{jo} = 0.03 pF, V_{bi} =0.7 V, and breakdown voltage V_{br} = 10 V. The load resistance (R_L) was selected to be 136 Ω. For this load resistance, the diodes impedance is Z_D = 136 – j4.5 Ω at 5.8 GHz and the maximum DC voltage across the diode is limited to $V_{br}/2$ = 5.0 V, as shown in Figure 84. The reactance part of Z_D is tuned out through placing a shorted stub capacitor a distance from the diode where the line length distance matches to +j4.5 Ω. Figure 85 shows the effects of diode voltage on diode impedance. The diode resistance at 5.0 V is 136 Ω. A CPS transmission line structure was used as the mechanism to transfer power between the rectennas parts. The CPS characteristic impedance $Z_{o,CPS}$ = 100 Ω. By selecting R_L so that R_D matches to $Z_{o,CPS}$ eliminates RF

mismatch at the diode, thus maintaining high RF-to-dc conversion efficiency. The CPS structure and analysis will be detailed next.

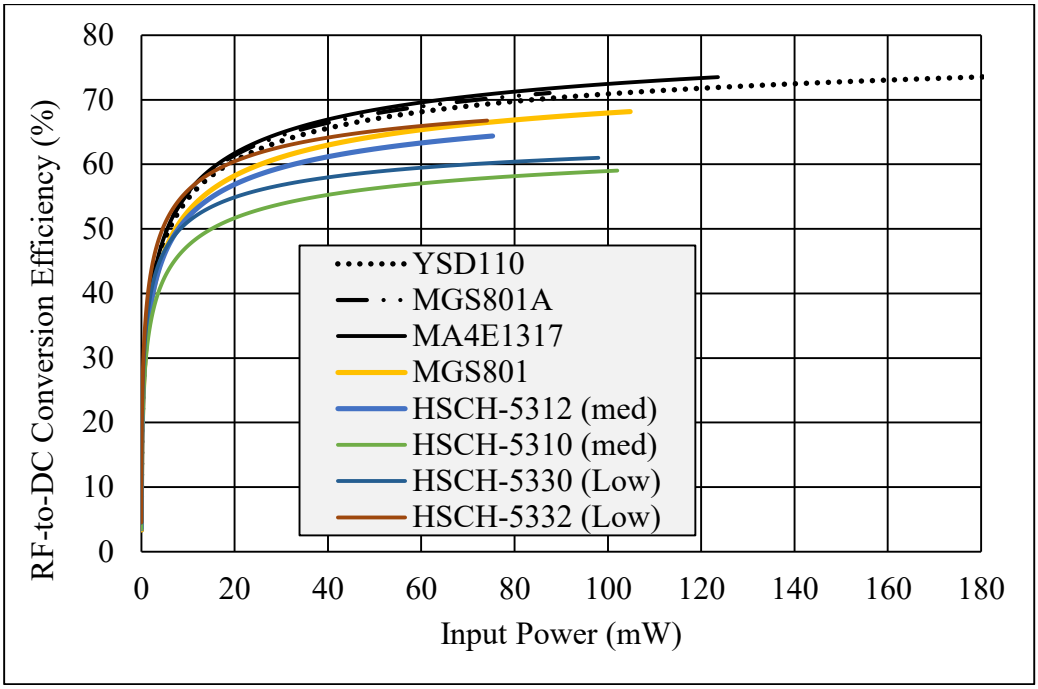

Figure 83. Calculated RF-to-DC rectification efficiency as a function of input power.

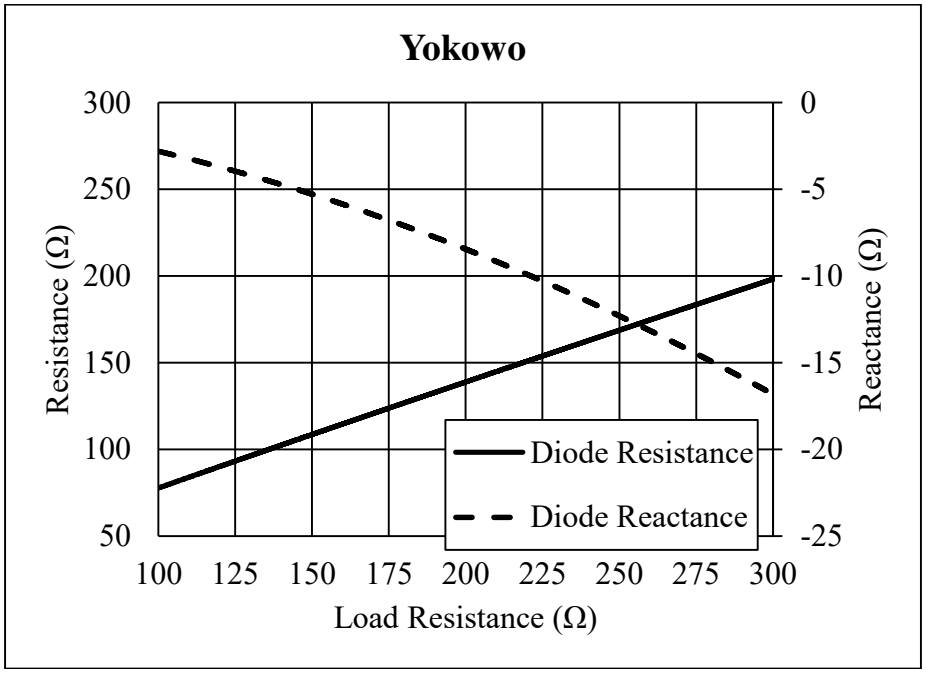

Figure 84. Calculated diode (YSD110) impedance versus load resistance for V_D = 5.0 V.

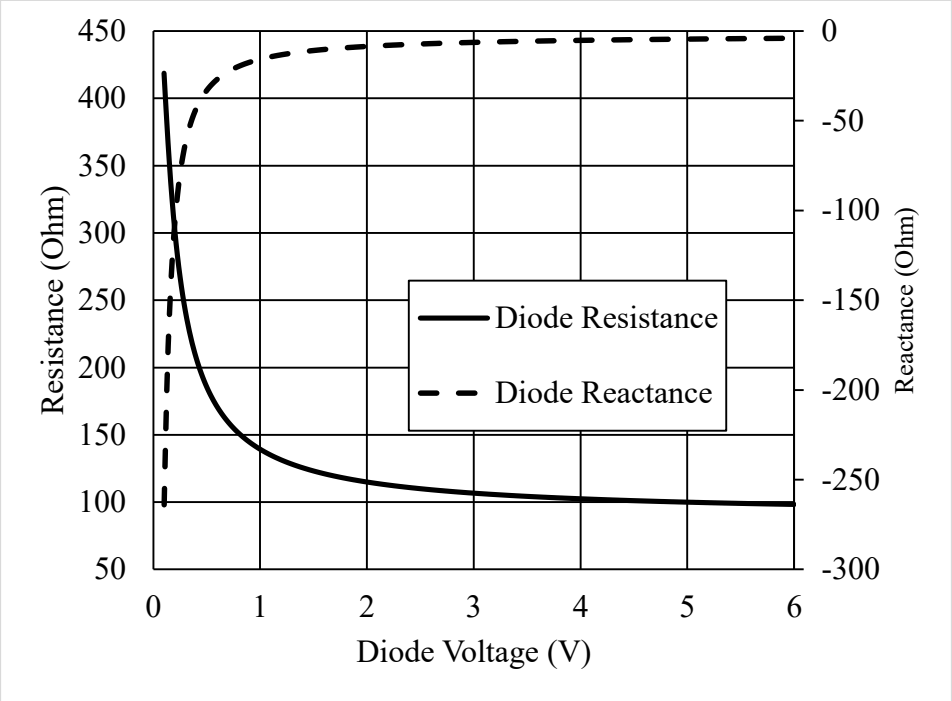

Figure 85 Calculated diode (YSD110) impedance as a function of diode voltage for R_L = 136 Ω.

5.4.5 Coplanar Stripline Theory and Design

A coplanar stripline (CPS) structure, as seen in Figure 86, is chosen as the technique to transfer power efficiently between the different parts of the rectenna systems. The parameters for CPS include; dielectric constant of the substrate (ε_r), thickness of the substrate (h), thickness of conductors (t), width of the conducting strips (W), and gap between the conducting strips (S). CPS structure is a balanced transmission line with a topology consisting of two parallel conducting lines that reside on the same plane. Naturally, CPS offers advantages over the microstrip line mainly through the option to mount lumped (active or passive) components in shunt or series configurations with ease as well as eliminating the need to drill holes through the substrate to reach the ground plane [110]. Moreover, it is easier to realize high line impedances with CPS than with coplanar waveguide.

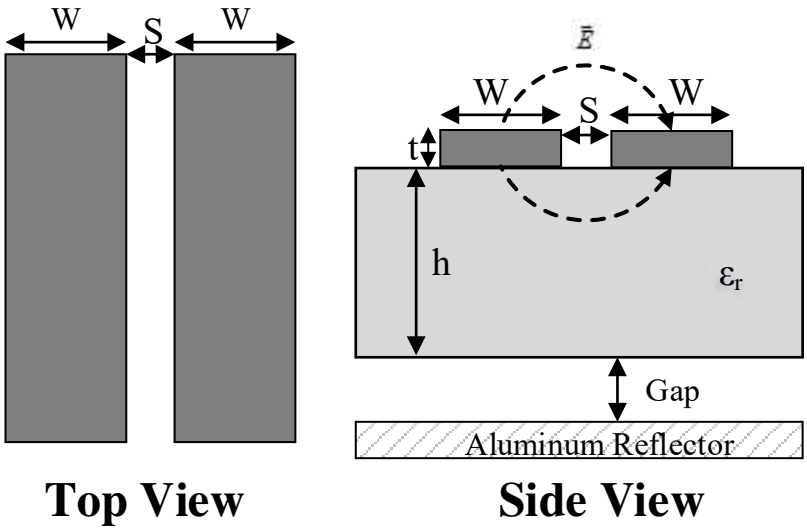

Figure 86. Top and side view of a CPS structure with parameters.

The substrate material chosen for this design is Rogers RT/Duroid 6002. This substrate material was chosen based on its thermal stability/tolerance compared to the other materials as was presented previously. The diode component selected for this design is Yokowo GaAs Schottky Barrier Diode (YSD110). YSD110 has a storage temperature range from -55℃ to 125℃. The GaAs material of the diode fits in the confines of a LEO space mission. However, the diode component must go through rigorous testing in both the space environment and on Earth to validate its reliability. The capacitor selected to filter RF signal before it reaches the load is Dielectric Laboratories broadband (1MHz-20GHz) DC block (CO8BLBB1X5). This capacitor also has a storage temperature range between -55℃ to 125℃. However, in order to determine the capacitors electrical performance for space application it must go through rigorous testing in both the space environment and on Earth. The rigorous testing of diode and capacitor is outside the scope of this work.

To achieve high RF-to-DC conversion efficiency the real impedance part of Z_D and the impedance of the CPS $Z_{o,CPS}$ structure should be matched. If these are not matched then the rectennas RF-to-DC conversion efficiency suffers. The following parameters of the CPS structure determine $Z_{o,CPS}$; material (RT Duroid 6002), gap (S) between the striplines, width (W) of each stripline, metal thickness (t) of the copper cladding, and height (h) of the substrate. The gap was set to S = 0.2 mm based on the inner package dimension of the diode component (YSD110) and the width of the striplines were set to W = 2.1 mm based on the outer packaged dimension of the capacitor component (C08BLBB1X5). Metal thickness was chosen to be t = 35.56 μm and height of the substrate was h = 0.254 mm (10-mils).

5.4.6 CPS Characteristic Impedance

CPS is a balanced transmission line where its characteristic impedance cannot be measured directly. Therefore modeling and analytical calculations (closed form expressions) are implemented.

For a symmetric CPS with infinitely thick substrate the effective dielectric constant (ε_{eff}) and characteristic impedance (Z_0) are found using [110]:

$$\varepsilon_{re} = \frac{\varepsilon_r + 1}{2} \tag{45}$$

$$Z_0 = \frac{120\pi}{\sqrt{\varepsilon_{re}}} \frac{K\left(k_1\right)}{K^{'}\left(k1\right)} \tag{46}$$

where

$$\frac{K\left(k\right)}{K^{'}\left(k\right)} = \frac{\pi}{\ln\left[2\left(1+\sqrt{k^{'}}\right)\Big/\left(1-\sqrt{k^{'}}\right)\right]} \tag{47}$$

$$k_1 = \frac{a}{b} = \frac{S}{S+2W} \tag{48}$$

$$k' = \sqrt{1-k^2}\ . \tag{49}$$

For a symmetric CPS with a finite thick substrate's ε_{eff} and Z_0 are found using [111]:

$$\varepsilon_{eff} = 1 + \frac{\varepsilon_r - 1}{2} \frac{K\left(k'\right) K\left(k_1\right)}{K\left(k\right) K\left(k_1'\right)} \tag{50}$$

$$k_1 = \sinh\left(\pi a/2h\right) / \sinh\left(\pi b/2h\right) \tag{51}$$

$$Z_0 = \frac{120\pi}{\sqrt{\varepsilon_{eff}}} \frac{K\left(k\right)}{K\left(k'\right)} \tag{52}$$

Another formula to calculate a symmetric CPS with a finite thick substrate from [110]:

$$\varepsilon_{eff} = 1 + \frac{\varepsilon_r - 1}{2} \frac{K'\left(k_{10}\right)}{K\left(k_{10}\right)} \frac{K\left(k_1\right)}{K'\left(k_1\right)} \tag{53}$$

$$k_{10} = \tanh\left(\frac{\pi}{4}\frac{a}{h}\right) \Big/ \tanh\left(\frac{\pi}{4}\frac{b}{h}\right) \tag{54}$$

$$Z_0 = \frac{120\pi}{\sqrt{\varepsilon_{eff}}} \frac{K\left(k_1\right)}{K'\left(k_1\right)} \tag{55}$$

The values of Z_0 and ε_{eff} obtained previously are valid for infinitesimally thin metallic strip conductors. But in practice, the metallization has a finite thickness t that affects the characteristics. Z_0 and ε_{eff} accounting for conductors with a metallic thickness ($t \neq 0$) are calculated from [110]:

$$Z_0\left(\varepsilon_r\right) = \frac{Z_{0a}}{\sqrt{\varepsilon_{eff}}} \tag{56}$$

$$Z_{0a} = 120\pi \frac{K\left(k_{1e}\right)}{K^{'}\left(k_{1e}\right)} \tag{57}$$

$$k_{1e} = \frac{S_e}{S_e + 2W_e} \tag{58}$$

$$S_e = W + \Delta \tag{59}$$

$$S_e = S - \Delta \tag{60}$$

$$\frac{\Delta}{t} = \frac{1}{\pi}\left(5.188 + \left\{0.9959 + 8.0808\times10^{-4}\left[\frac{b}{t}\right]\right\}\ln\left[\frac{4\pi W}{t}\right]\right) \tag{61}$$

$$\varepsilon_{eff} = \frac{C_1\left(t\right) + C_2\left(\varepsilon_r\right)}{C_1\left(t\right) + C_2\left(\varepsilon_r = 1\right)} \tag{62}$$

$$C_1 = \frac{\varepsilon_0}{2}\frac{K^{'}\left(k_{1e}\right)}{K\left(k_{1e}\right)} \tag{63}$$

$$C_2 = \frac{\varepsilon_0\varepsilon_r}{2}\frac{K^{'}\left(k_{1e}\right)}{K\left(k_{1e}\right)} \tag{64}$$

where $C_1(t)$ is the line capacitance for the upper-half region with nonzero conductor thickness, and $C_2(\varepsilon_r)$ is the capacitance for the lower-half region of coplanar line with the given dielectric configuration. However, for the latter case of metallic thickness ($t \neq 0$) the conditions that have to be met are:

$$0.1 \le S \le 0.9,\ 0.05 \le W \le 0.45 \text{ and } 0.3 < S < 0.8,\ 0.05 < W < 0.35.$$

Two cases: (1) a symmetric CPS with infinitely thick substrate, and (2) symmetric CPS with a finite thick substrate's were calculated for Z_0 and ε_{eff}, and compared with simulated results from ANSYS Ansoft HFSS. Case (3) is not included in this comparison because the conditions of the equations are not met. The results of these comparisons are

seen in Table 30. Notice that the values calculated used the equations proposed by Bahl are closer to the simulated values. The simulation model in ANSYS Ansoft HFSS was setup in a vacuum environment.

Two substrate materials from Rogers Corporation were used to analyze the effect on Zo,CPS and εeff,CPS due to different values of εr. Selected substrate materials from Rogers Corporation include: RT/Duroid 5870 εr = 2.33, and RT/Duroid 6002 εr = 2.94. The other design parameters are: h =10-mils, t = 35.56 μm, S = 0.2, and W = 2.1 mm. The results of this comparison are found in Table 31.

As is seen in Table 31 the lower dielectric constant material (RT/Duroid 5870) provides a higher impedance value. As was mentioned previously, the higher impedance value has benefits in terms of RF-to-DC rectification efficiency for the rectifier structure. Although, as we showed previously, RT/Duroid 6002 material is more suitable for space application.

Table 30. Calculated and simulated $Z_{o,CPS}$ and $\varepsilon_{eff,CPS}$ results at 5.8-GHz frequency for the CPS structure.

	$Z_{o,CPS}$ (Ω)			$\varepsilon_{eff,CPS}$ (F/m)		
Method	S = 0.2 mm	S = 0.25 mm	S = 0.305 mm	S = 0.2 mm	S = 0.25 mm	S = 0.305 mm
Ghione	116.2	122.5	128.7	1.3	1.28	1.27
Bahl	111.3	117.9	124.5	1.41	1.38	1.36
ANSYS	104.8	110.8	118.5	1.49	1.46	1.44

*material = RT/Duroid 6002, ε_r = 2.94 F/m, h =10-mils, t = 0 μm, and W = 2.1 mm.

Table 31. Simulated results for CPS structure using ANSYS Ansoft HFSS.

	$Z_{o,CPS}$ (Ω)		$\varepsilon_{eff,CPS}$ (F/m)	
Material	5870	6002	5870	6002
ANSYS	105.5	100	1.33	1.47

To achieve high RF-to-DC conversion efficiency the real impedance part of Z_D and $Z_{o,CPS}$ structure should be matched. If these are not matched then the rectennas RF-to-DC conversion efficiency suffers. The following parameters of the CPS structure determine $Z_{o,CPS}$; material (RT Duroid 6002), gap (S) between the striplines, width (W) of each stripline, metal thickness (t) of the copper cladding, and height (h) of the substrate. The gap was set to S = 0.2 mm based on the inner package dimension of the diode component (YSD110) and the width of the striplines were set to W = 2.1 mm based on the outer packaged dimension of the capacitor component (C08BLBB1X5). Metal thickness was t = 35.56 μm and height of the substrate was h = 0.254 mm (10-mils).Figure 92 shows the CPS structure with dimensions.

Figure 93 shows the simulated $Z_{o,CPS}$ results for the CPS structure using ANSYS Ansoft HFSS version 16.0 for air region. At 5.8 GHz $Z_{o,CPS}$ = 100 Ω for a 10-mil-thick substrate with an aluminum reflector placed ~10.85 mm (0.21 λ_o) behind the CPS structure referenced from the lower part of the copper conductors. Notice the effect that substrate thickness has on $Z_{o,CPS}$. This is important because the higher $Z_{o,CPS}$ the higher R_L, and thus, the greater RF-to-DC efficiency can be reached. Another interesting analysis is the effect of copper cladding thickness on $Z_{o,CPS}$, as shown in Figure 94. As

can be seen the thicker t is, the lower $Z_{o,CPS}$ becomes. The opposite phenomena occurs for $\varepsilon_{eff,CPS.}$ Both of these occurrences are validated correctly according to [110].

Another study done through simulation by ANSYS Ansoft HFSS on the CPS structure was the total attenuation. Losses considered in this analysis are conductor (α_c) and dielectric (α_d) losses. Total attenuation ($\alpha_c + \alpha_d$) was simulated with the following fixed parameters: f = 7 Ghz, W = 2.1 mm, h = 0.508 mm, and t = 35.56 μm. The separation distance S between the CPS lines was used as the variable to determine total attenuation of the CPS structure. Figure 95 plots total attenuation and $Z_{o,CPS}$ as a function of separation between the strips (S). It is seen that the higher the characteristic impedance of CPS the lower the transmission-line attenuation achieved. This information can be useful for selecting design parameters [112].

The relationship between diode and CPS structure has been presented in Section 5.4.6. Section 5.4.7-5.4.9 expands the rectenna design to the next stage by providing a detailed development of a CPS back-to-back Klopfenstein taper transition. The CPS back-to-back Klopfenstein taper transition is a vital tool in the CPS rectenna design process as it allows all systems in the rectenna to be appropriately measured with low loss.

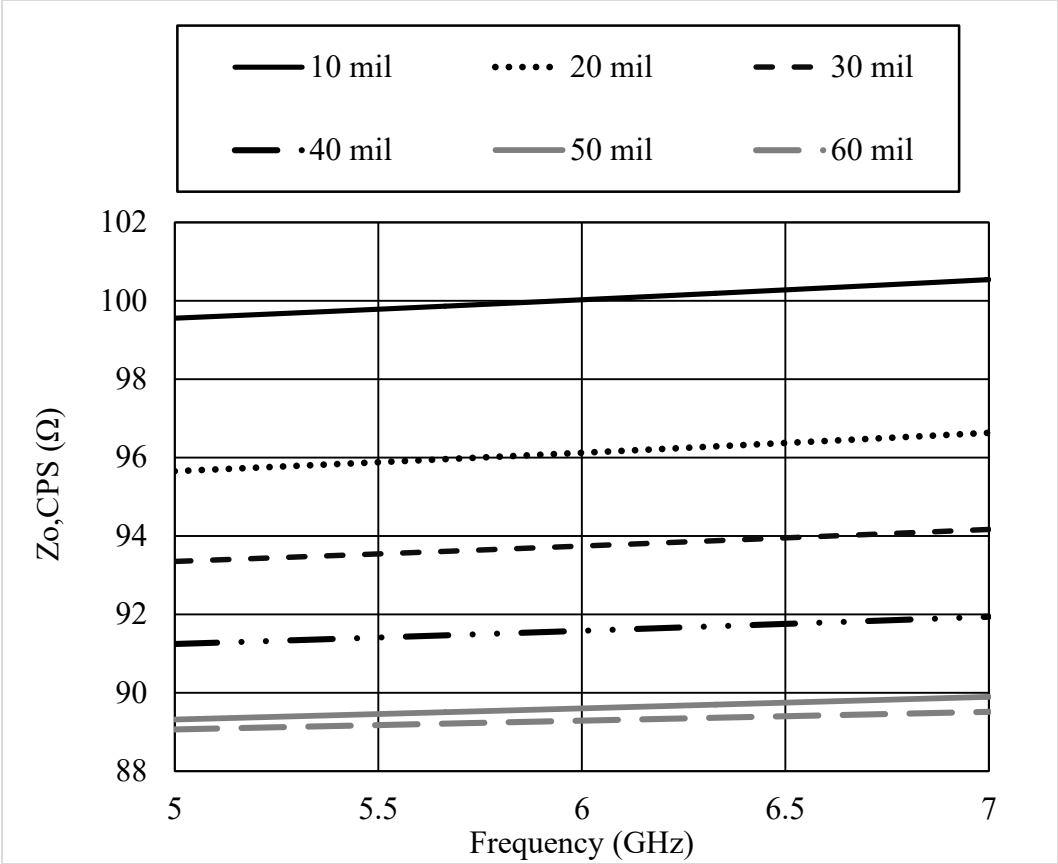

Figure 87. Simulated results of $Z_{o,CPS}$ as a function of h while fixing S = 0.2 mm, W = 2.1 mm, and t = 35.56 um for RT/Duroid 6002.

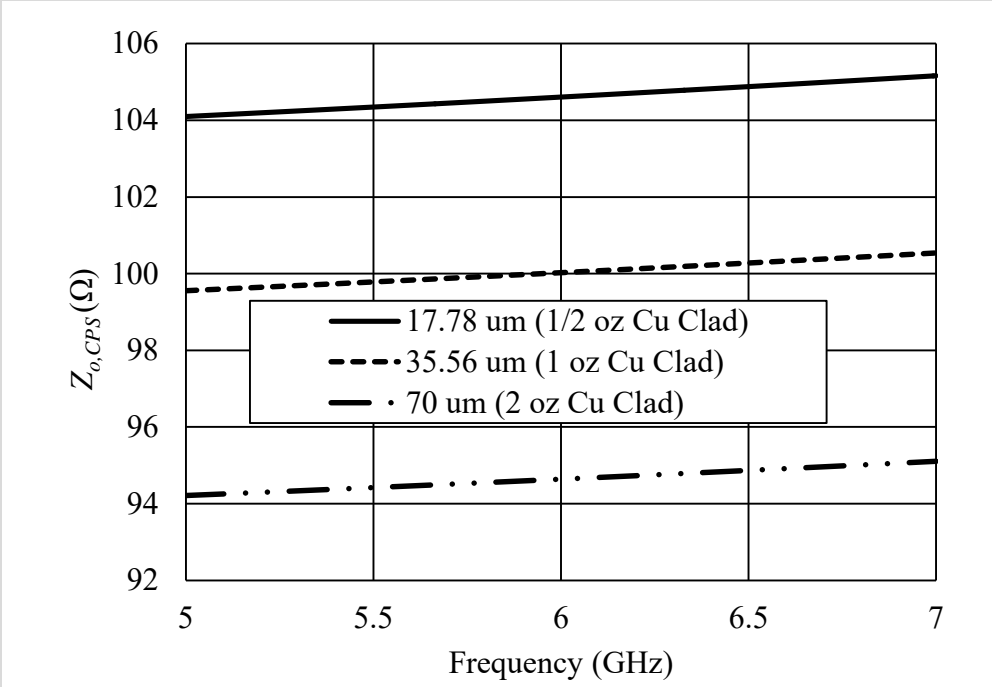

Figure 88. Simulated results of $Z_{o,CPS}$ as a function of t while fixing S = 0.2 mm, W = 2.1 mm, and h = 10-mils for RT/Duroid 6002.

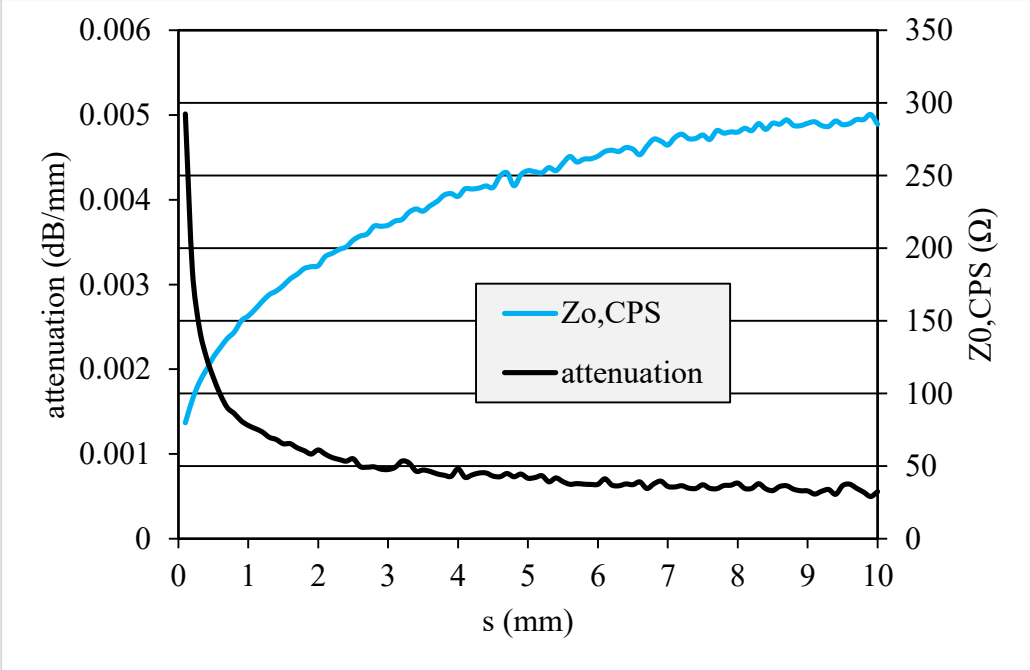

Figure 89 Total attenuation ($\alpha_c + \alpha_d$) as a function of separation width (s) at 7-GHz.

5.4.7 Design of CPS-to-Klopfenstein Taper Back-to-Back Transition

In choosing an impedance matching technique the objective was to design for high efficiency at 5.8 GHz. The Chebyshev transformer optimizes bandwidth at the expense of passband ripple [113]. Like the stepped-Chebyshev matching transformer, the response of the Klopfenstein taper has equal-ripple lobes versus frequency in its passband. Moreover, for a given taper length (greater than a critical value), the Klopfenstein impedance taper has been shown to be optimum in the sense that the reflection coefficient is minimum over the passband [113]. Alternatively, for a maximum reflection coefficient specification in the passband, the Klopfenstein taper yields the shortest matching section [113]. The Klopfenstein taper is derived from a stepped Chebyshev transformer as the number of sections increases to infinity, and is analogous to the Taylor distribution of antenna array theory [113].

The logarithm of the characteristic impedance variation for the Klopfenstein taper is given by

$$\ln Z(z) = \frac{1}{2}\ln Z_0 Z_L + \frac{\Gamma_0}{\cosh A} A^2 \phi(2z/L - 1, A) \qquad \text{for } 0 \le z \le L, \tag{65}$$

where the function is $\phi(z, A) = -\phi(-z, A) = \int_0^z \frac{I_1\left(A\sqrt{1-y^2}\right)}{A\sqrt{1-y^2}} dy, \qquad \text{for } |z| \le 1$ (66)

where $I_1(z)$ is the modified Bessel function. The value A is found from

$$A = \cosh^{-1}\left(\frac{\Gamma_0}{\Gamma_m}\right) \tag{67}$$

where Γ_m is the maximum ripple in the pass band and Γ_0 is the reflection coefficient at zero frequency defined by

$$\Gamma_0 = \frac{Z_L - Z_0}{Z_L + Z_0} \tag{68}$$

In the Section 5.4.6 we found the characteristic impedance of the CPS to be Z_0 = 96 Ω for RT/Duroid 6002 material with h = 20-mils, t = 35.56 μm, S = 0.2 mm, and W = 2.1 mm. Due to manufacturing difficulties a thicker substrate than the 10-mils was used.

A parametric study was conducted on the following parameters:

1. Total length of taper defined by lowest cutoff frequency f_{Low} = 3 GHz
2. The maximum ripple, Γ_m = 0.01 (i.e., 1%)
3. Radius of radial stub, R
4. Length of each segment, L

The Klopfenstein taper with 10 impedance steps is shown in Figure 96. With a maximum ripple Γ_m = 0.01 and 10 design points along the curve, we derive the impedance information for the Klopfenstein taper with feed Z_{fed} = 50 Ω and Z_{CPS} = 96 Ω. Length and width as a function of impedance are seen in Figure 91 and Figure 92, respectively. Those values are also presented in Table 32. The calculated frequency response in dB and linear scaling of this Klopfenstein taper is seen in Figure 99 and Figure 100, respectively.

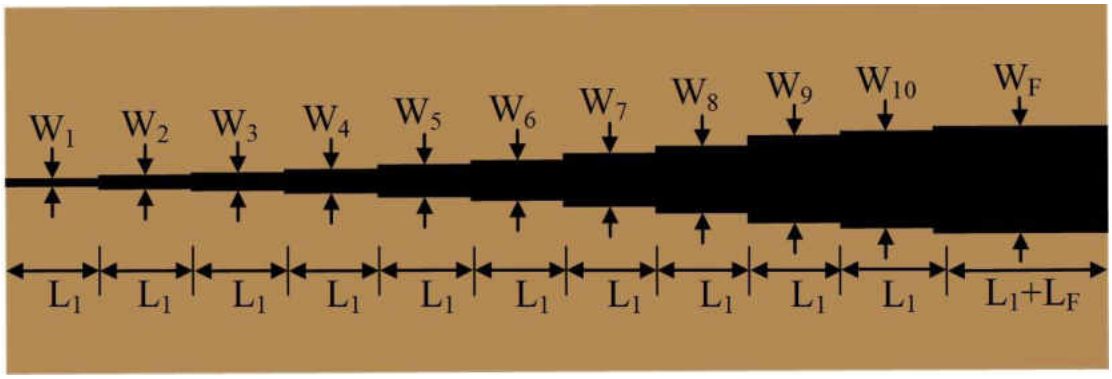

Figure 90. Klopfenstein taper with 10 impedance steps.

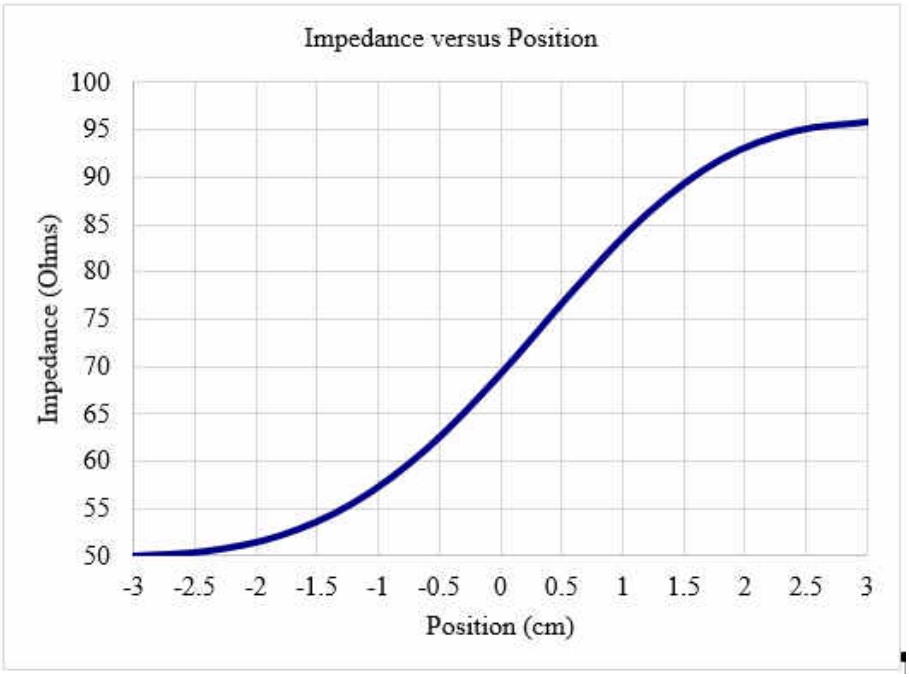

Figure 91. Impedance as a function of length for the Klopfenstein taper for 10 design points along the curve.

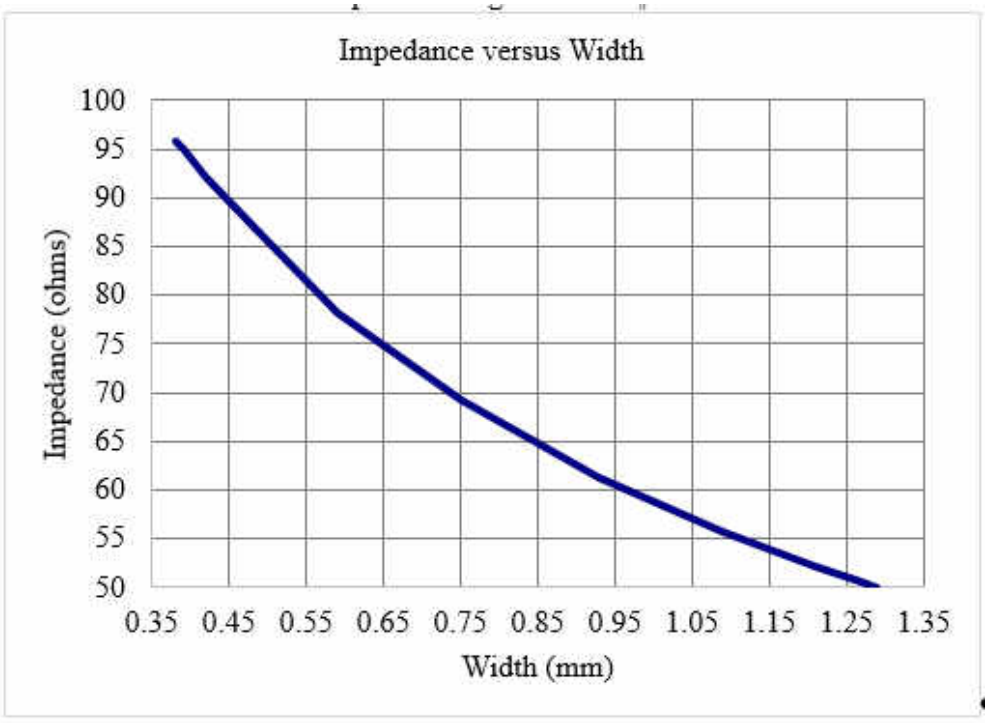

Figure 92. Impedance as a function of width for the Klopfenstein taper for 10 design points along the curve.

The next design was integrating the Klopfenstein taper with the CPS structure as shown in Figure 95. The field rotation was accomplished with a radial stub with radius R = 5.5 mm, and angle θ = 80°. Each width ($W_1, \ldots, W_F$) was used from Table 32. The length $L_1 \sim$= 4 mm, and L_F = 4 mm to provide additional length for end launch connector.

Table 32. The impedance as a function of length (z) and width (W) for 10 step sizes. Based on the impedance output from the taper design for each step, an online "Microstrip Line Calculator" from em:talk was used to calculate the width of the strip to obtain that impedance.

z (normalized)	z (cm)	Z0 (Ω)	W (mm)
-1	-3.0	50.050	1.29
-0.8	-2.4	50.564	1.27
-0.6	-1.8	52.199	1.21
-0.4	-1.2	55.654	1.09
-0.2	-0.6	61.392	0.93
0.0	0	69.282	0.75
0.2	0.6	78.186	0.59
0.4	1.2	86.248	0.49
0.6	1.8	91.956	0.42
0.8	2.4	94.930	0.39
1.0	3.0	95.904	0.38

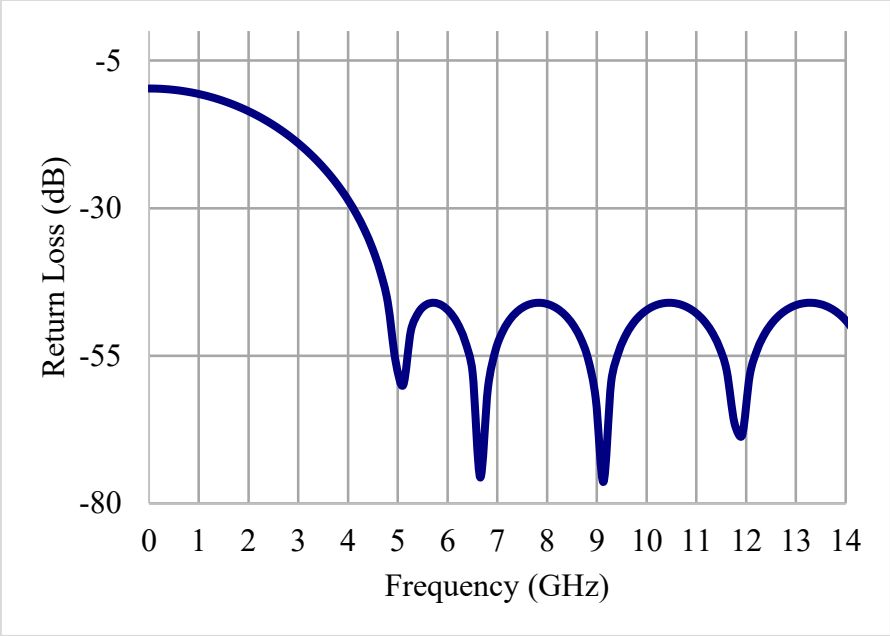

Figure 93. Calculated frequency response of Dolph-Tchebycheff transmission line taper in dB scale.

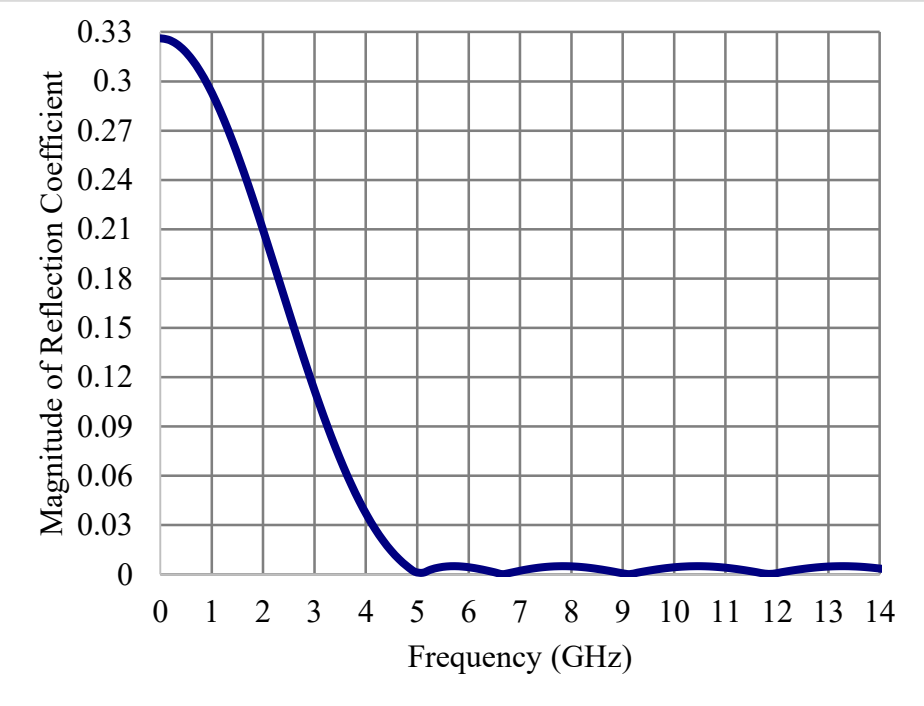

Figure 94. Calculated frequency response of Dolph-Tchebycheff transmission line taper in linear scale.

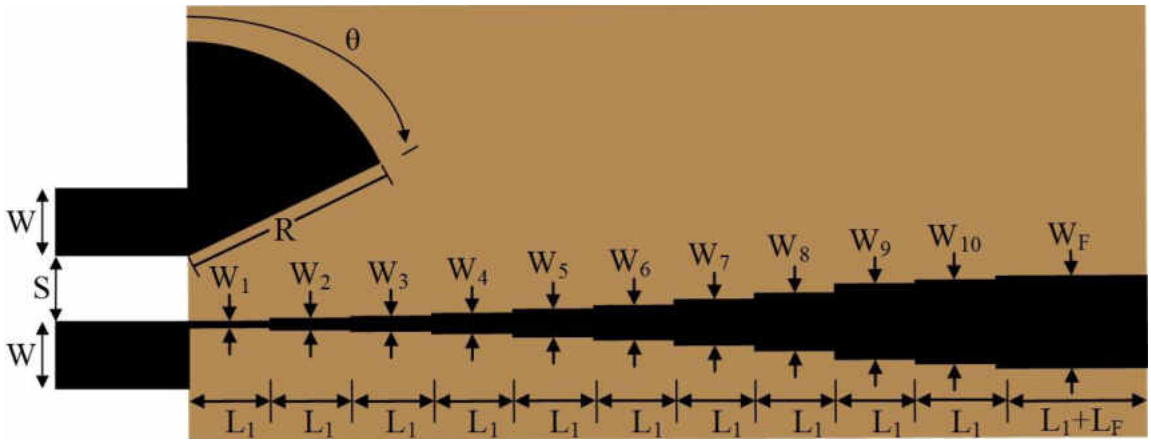

Figure 95. Klopfenstein Taper-to-CPS Transition. Transition of electric field was accomplished with a radial stub.

5.4.8 Manufacturing and Fabrication Process

Many challenges presented themselves for the manufacturing and fabrication processes. The first challenge was transferring the designs from the software's (CST MWS or ANSYS Ansoft HFSS) to the mill machine. One problem was transferring all the design information from ANSYS to the mill machine. Several avenues were explored including transferring the ANSYS software first to AutoCad software, and then to the mill machine. Also, a free trial program was installed with AutoCad to generate Gerber files. Still the complete design information was not transferred to the mill machine. The designs were re-made in CST Microwave Studio. CST Microwave Studio has an export file option that directly converts the simulation design into a Gerber file which can be read by the mill machine program.

The next task was the manufacturing of the designs. Many sample boards were delivered from Rogers Corporation for trial and error with settings on the mill machine. The conclusion is that for the super high frequency designs the milling process currently is non-repeatable.

After months of trial and error with dry etching the design from the mill machine, the decision was to do the best job in the dry etch aimed at minimizing the passes over the material that seemed to be damaging the thin substrate material. Figure 96 shows the top and bottom layer of a PCB after dry etching. Notice the remaining copper that was not removed from the milling process. In order to remove the copper wet etching is to be done. First black finger nail polish was applied over the copper design as indicated in Figure 103. The finger nail polish is put on to protect the PCB design from acid in the

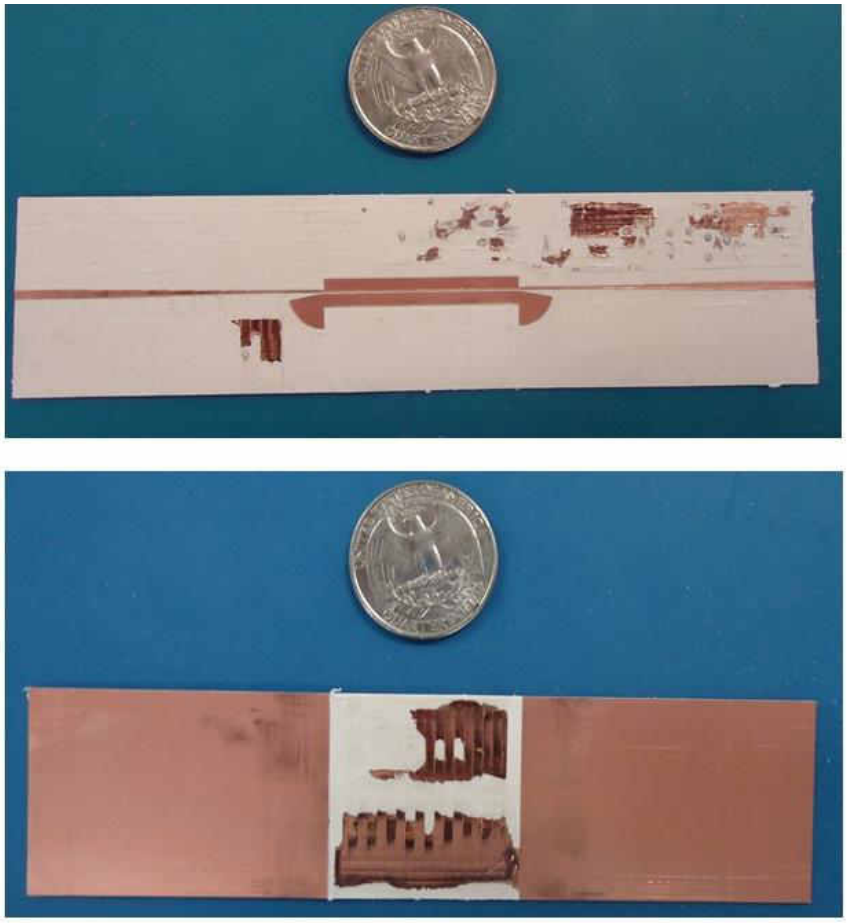

Figure 96. Top and bottom layers of PCB after dry etching.

Figure 97. Finger nail polish applied to the PCB design.

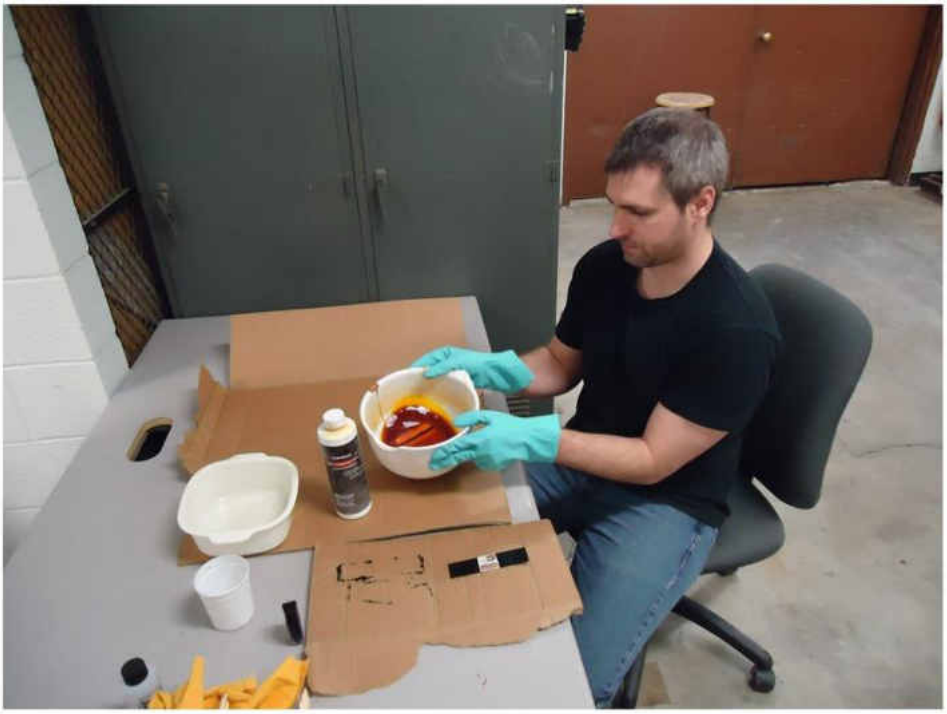

Figure 98. Wet etching the PCB design with acid.

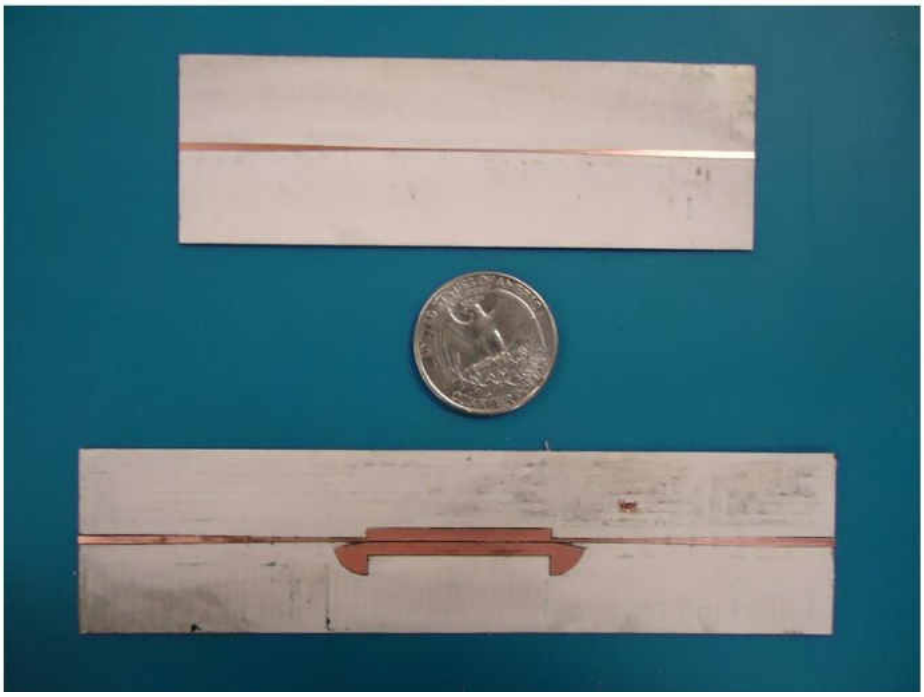

Figure 99. Results of wet etch process.

wet etch process. After the finger nail polish dried the next step was to immerse the PCB in acid solution, as seen in Figure 104. After about 20-30 minutes of rolling the PCB around in the acid the PCB was removed and the PCB was placed in water in order to dilute/clean the acid off the PCB. After the acid was removed with water then finger nail polish remover was used to remove the finger nail polish. The final results of the wet etch process are seen in Figure 105.

Fabrication and assembly of the design was done next. The topology of all pieces to construct the two designs can be seen in Figure 106. First two aluminum block were secured to the aluminum reflector. This was down by drilling holes and then tapping out the threads for the screws. Next a layer of bondply was laid down on top of the aluminum reflector followed by the foam material. A heat gun was used to heat up the bondply while simultaneously putting pressure on the foam. After around 30 minutes the foam and

aluminum structures were bonded. Next another layer of bondply was placed on top of the foam followed by the PCB. Again a heat gun was used with pressure about 30 minutes until the PCB and the Foam/aluminum structures were bonded. Finally, the SMA connectors were placed in alignment with the feeding part of the design and mounting holes were marked with paint. Holes were drilled in the aluminum block and the screw threads were tapped out. The SMA connector was then mounted on the design and soldiered. The PCB was then ready for testing as shown in Figure 101.

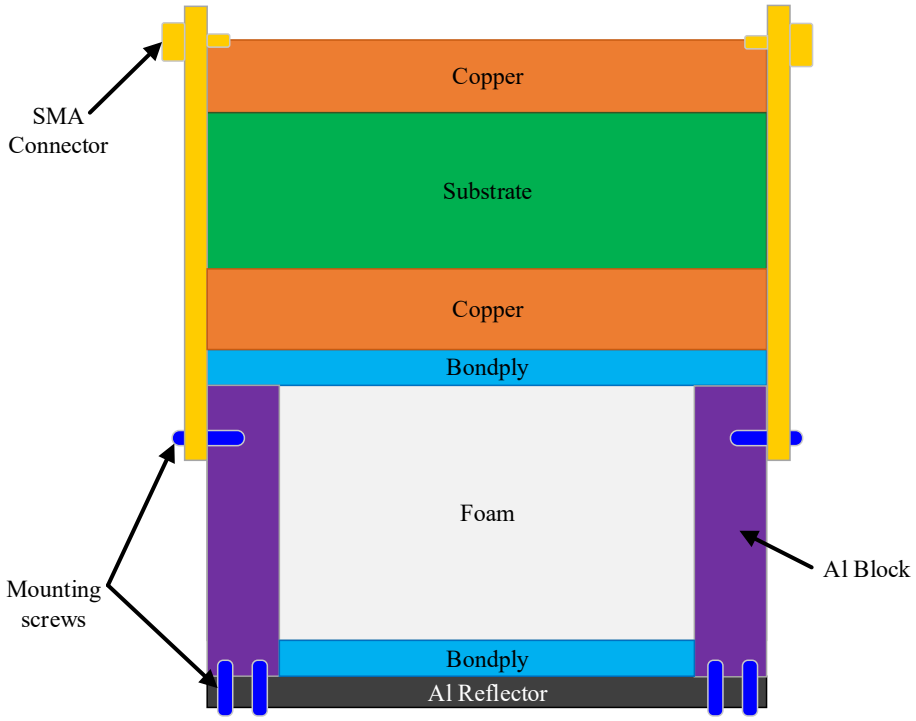

Figure 100. Topology of the super high frequency circuit designs. Not to scale.

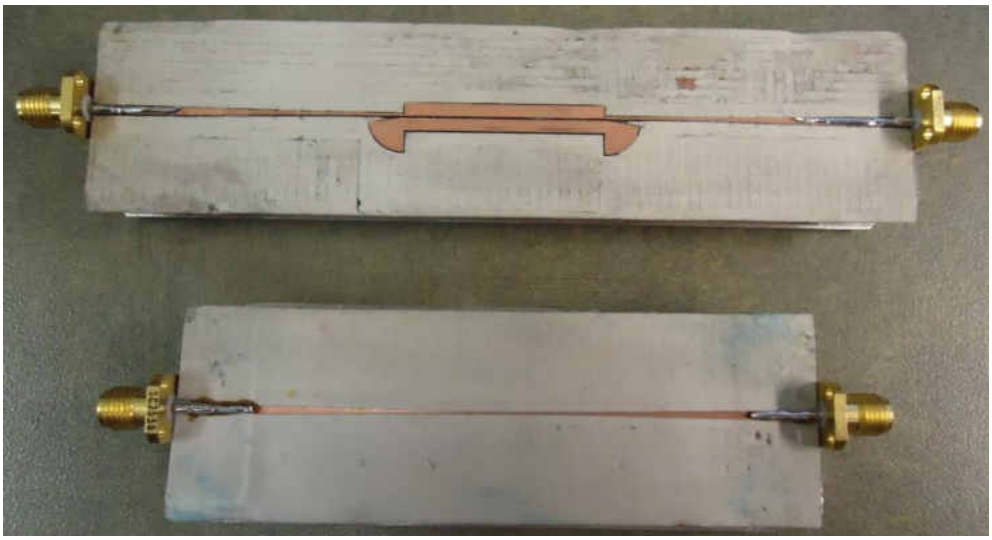

Figure 101. Assembled PCB's ready for testing.

5.4.9 Simulation and Measurment Results of Back-to-Back Klopfenstein Taper

In order to measure the taper a back-to-back configuration needs to be used. First, electromagnetic software tools, CST Microwave Studio and ANSYS Ansoft HFSS, were used to simulate the back-to-back taper. The designs from the simulation model were manufactured, assembled, and measured. The simulated and measured results of the back-to-back Klopfenstein taper configuration are compared in Figure 102.

5.4.10 Simulated and Measured Klopfenstein Taper-to-CPS Back-to-Back Transition

In order to measure the Klopfenstein taper-to-CPS a back-to-back configuration needs to be used. First, electromagnetic software tools, CST Microwave Studio and ANSYS Ansoft HFSS, were used to simulate the back-to-back taper. The designs from the simulation model were than manufactured, assembled, and measured. The simulated and measured results of the back-to-back Klopfenstein taper configuration is shown in Figure 109. Low reflection loss (S_{11}) – means that the system is well matched and little energy is

sent back. Low insertion loss (S_{21} close to 0dB) is achieved at the frequency of interest i.e., 5.8 GHz, which means that as the energy travels through the design there is low loss.

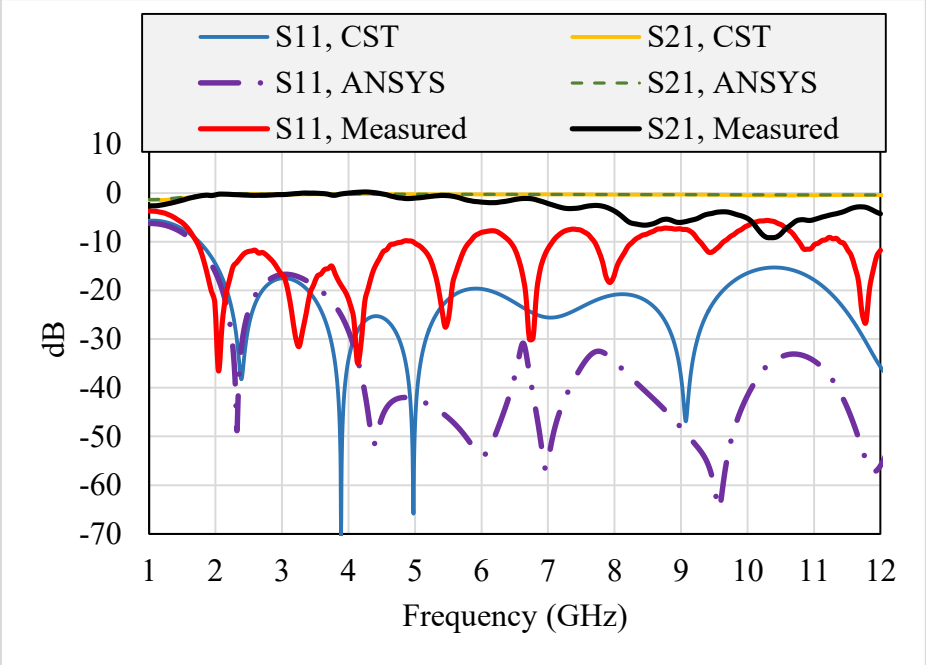

Figure 102. Simulated and measured results of the back-to-back Klopfenstein Taper.

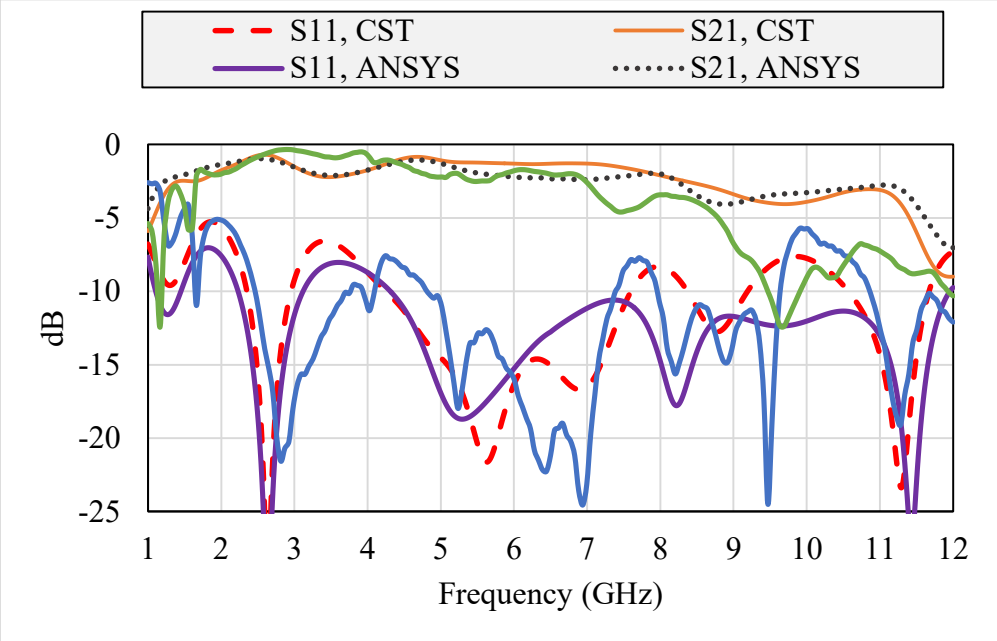

Figure 103. Simulated and measured results of the Klopfenstein Taper-to-CPS Back-to-Back Transition.

5.4.11 Proposed Rectenna Experimental Measurement Setups

This experimental setups to test the rectenna are proposed in Figure 110 – Figure 113.

The experiment proposed in Figure 107 allows a single rectenna element to be tested in an environment with minimized radiation interference. The waveguide chamber is a unique experimental setup for testing a single cell rectenna element that may closely provide the elements performance characteristics if it were in an array. Moreover, the proposed temperature control design would allow changing the temperature inside the waveguide in order to inflict temperature changes on the rectenna element and to measure the changes in DC output.

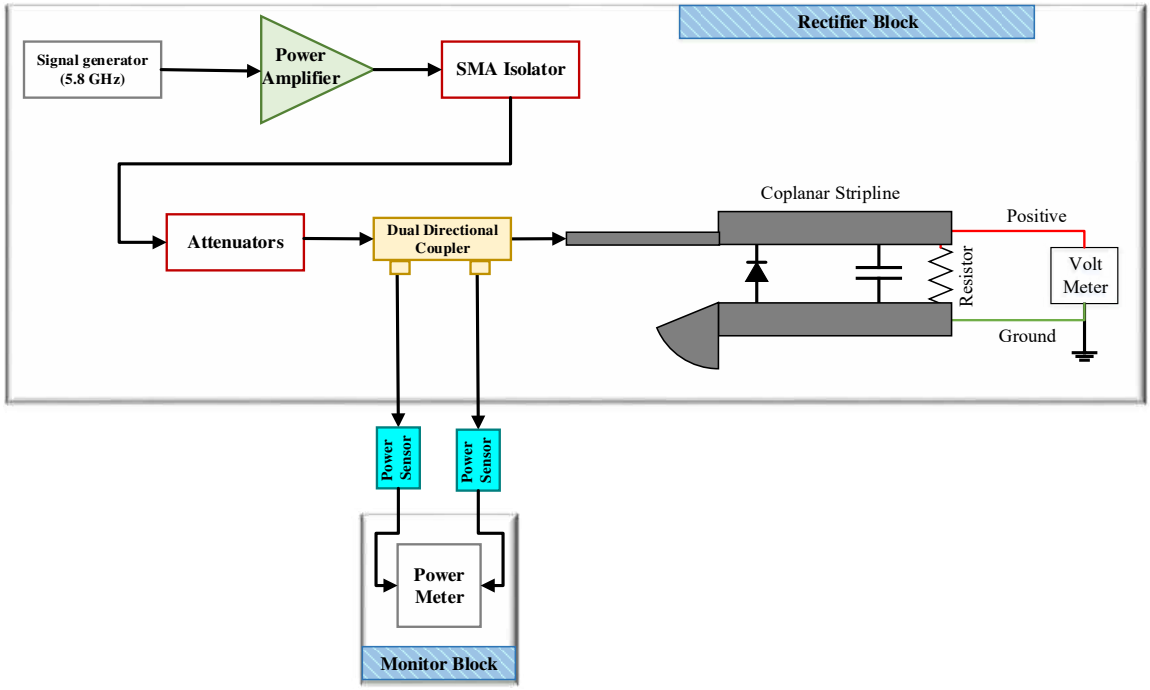

Figure 104. Proposed measurement setup to measure RF-to-DC rectifier conversion efficiency.

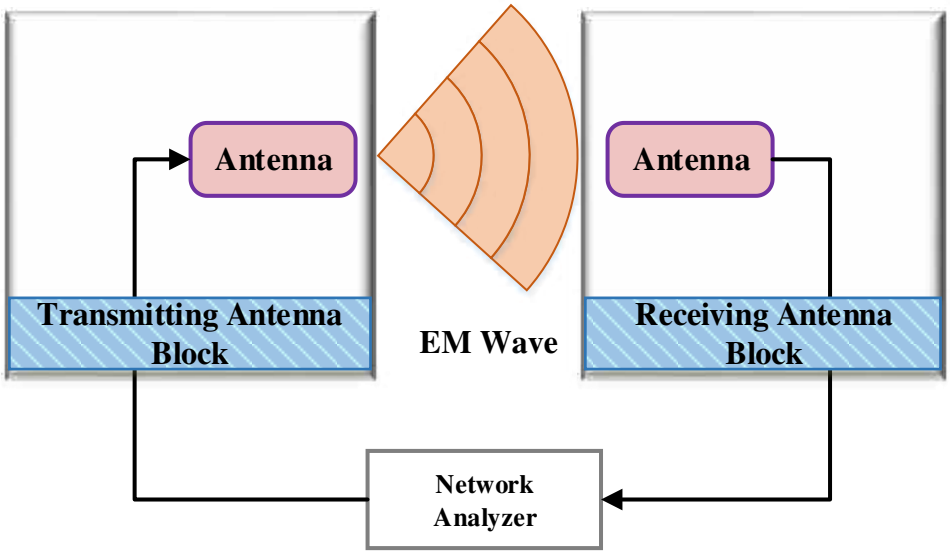

Figure 105. Proposed measurement setup to measure antenna gain and polarization properties.

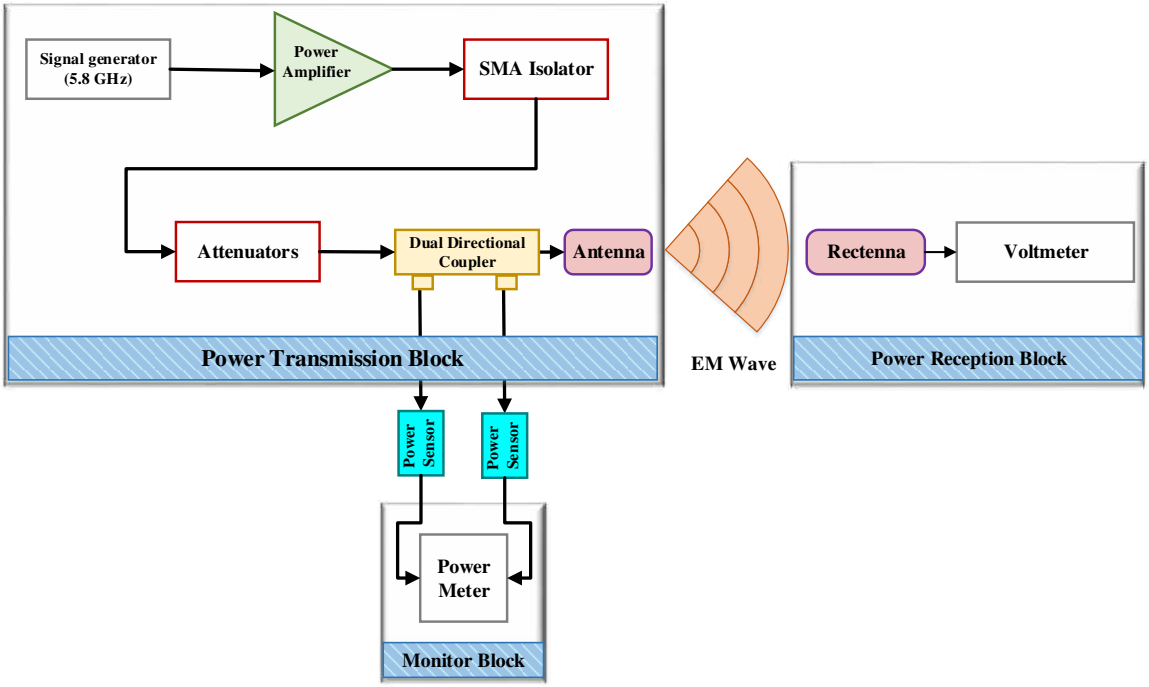

Figure 106. Measurement setup to measure RF-to-DC rectenna efficiency.

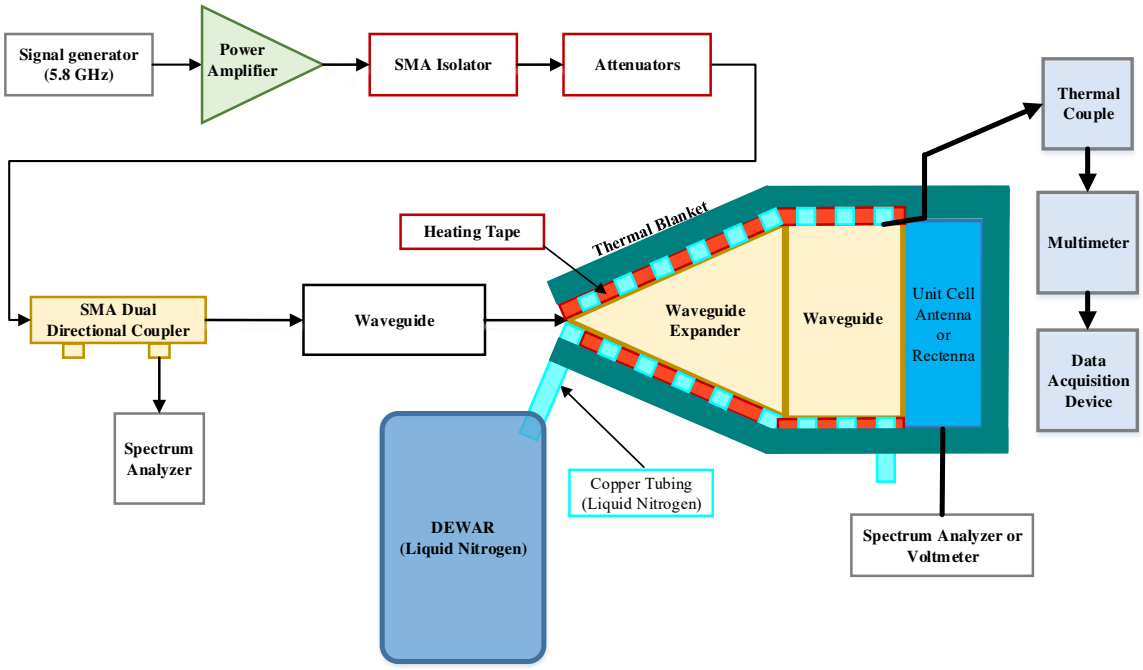

Figure 107. Proposed measurement setup to measure unti cell rectenna in a waveguide chamber with temperture controled environment.

CHAPTER VI

RESULTS AND DISCUSSION

One day GEO-SSPS may transmit microwave power from GEO to Earth almost indefinitely year round. The microwave beam would be a source of EMI to satellites. This work looked at the microwave beam not as a source of EMI but as a source of additional power (with solar) for satellites in space. Therefore, the following hypothesis was put forth: "satellites orbiting below GEO equipped with a rectenna array to harvest RF energy transmitted from a GEO-SSPS offer benefits in terms of satellite mass reduction, increased mission longevity, and increased mission flexibility."

In pursuing this question the term "power beam medium" was introduced. The power beam medium was defined as the volume of energy that stretched from a GEO-SSPS to a rectenna array on Earth for a static power beam medium scenario, or the volume of energy that stretched from a GEO-SSPS to lower orbiting spacecraft for a dynamic power beam medium scenario. A rectenna array and stacked hybrid PV/rectenna array to be equipped on spacecraft as alternative power generation systems compared to a conventional PV array were explored to find out whether such systems could benefit from future GEO-SSPS power beams. The analysis showed that the stand-alone rectenna array system could not benefit in the scenario of a fixed power beam medium for two reasons: (1) the energy density is not enough and (2) the charging periods are too short,

which will not allow enough energy to be stored. Increased exposure time is needed for such a system to work.

It was proposed that a phased array antenna system to be integrated with the GEO-SSPS that can track and beam power to lower orbiting satellites or for GTO assist via a pilot beam signal. The stacked hybrid PV/rectenna array system fits well with this dynamic power beam medium scenario. This stacked hybrid system allows flexibility in the area of the arrays where the heavier solar PV array can be reduced, thus reducing the mass of the EPS while simultaneously increasing the lighter rectenna array's area to accommodate for the solar array's degradation effect. Also, since the rectenna array system outlives the PV array system, the former corresponds to increased mission life. Moreover, if in the future there are many SSPSs, then greater mission flexibility could be obtained through this power on-demand or re-fueling option.

Two new types of energy generation systems were investigated to be equipped on future spacecraft: (1) rectenna array and (2) stacked hybrid PV/rectenna array. These new concepts were compared to a conventional PV array system in terms of area, mass, component life, and efficiency. Moreover, cost was compared between a solar EPS and rectenna EPS. Ultimately, it seems likely that a reduction in power generation unit mass can be accomplished through the proposed hybrid power generation system. Future work would need to map out a global environment of SSPSs to more fully comprehend the benefits of this system. Additionally, future work would be needed to investigate the hybrid power storage system considered in this paper, a system that may also lead to mass savings and increased overall mission performance.

This work provided numbers for what satellites could experience from the GEO-SSPS power beam for LEO and MEO environments in terms of power density and Airy disk. Such considerations are important so that future advancements in GEO-SSPS concepts can offer solutions/products to future LEO and MEO spacecraft to mitigate electromagnetic interference. From this analysis, it appears that there is a distinct savings in EPS mass from the hybrid PV/rectenna array system, which ultimately leads to reduced satellite mass and, hence, launch cost.

In order to practically realize the analytical findings of the stacked hybrid PV/rectenna array with a dynamic power beam medium scenario, the second part of this dissertation answers the following hypothesis: "modern small satellites can be used as technology demonstrators for the proposed stacked hybrid PV/rectenna array PGU." Modern small satellites offer a much reduced cost and development schedule compared to conventional satellites.

To address the second hypothesis a novel mission utilizing two modern small satellites was designed where a smaller power receiving daughter satellite sits inside a larger power transmitting mother satellite during launch. Once in orbit and separated from the launch vehicle the daughter satellite is ejected away from the mother satellite and both satellites deploy their respective power receiving or power transmitting hardware. The two satellites utilize the concept of close proximity operations during the mission life.

Several improvements of the original mission design concept were presented, such as, incorporating a propulsion unit, utilizing the concept of close proximity operations, and equipping the daughter satellite with a HPGU. This proposed mission

concept of utilizing modern small satellites as MWPT technology demonstrators offers many advantages over previous mission concepts such as the ISY-METS, space shuttle, and ISS. The advantage of this work over the existing concepts is the greater flexibility in mission options such as mission duration, frequency, power level, payload design, and aperture-to-aperture distances.

After the mission was mapped out the dissertation worked toward the design of the two spacecraft electrical power systems with MWPT payloads. The objective of the EPS designs was to begin to design out what needs to go into the mother and daughter spacecraft's to push the proposed mission closer to reality. The mother satellite would be equipped with power transmitter as its payload. Both vacuum and solid state devices were considered as well as different antenna designs. The design of the daughter satellites EPS focused on a HPGU. The HPGU design calculated a power budget from off-the-shelves parts, and sized the PV arrays accordingly.

The rectenna array was then considered. It was found that planar antennas are a good fit for this application due to their low mass and low profile. At first an aperture-coupled fed antenna seemed a good design choice. However, due to its multi-layer complexities and higher fed loss this antenna was not investigated further. Required antenna features were listed as circular polarization capability, high gain, wide band, and capable of integrating into an array. The antenna design of choice was the dual rhombic loop antenna with CPS feeding technique.

Five different substrate materials from Rogers Corporation were analyzed in which the PCB rectenna would be designed on. The factors that were compared included thermal stability, low dielectric constant, and out-gassing characteristics. Rogers

RT/duroid 6002 was the best option. Also, for assembling of the proposed rectenna Rogers 2929 Bondply and Evonik Foams, Inc. 71HERO were analyzed for the same factors. Rogers 2929 bondply does not pass the out-gassing test.

Analysis on nine different diodes was presented in order to determine the highest RF-to-DC conversion efficiency. All other parts of rectenna are designed based on the electrical behavior of the diode component. Yokowo diode was chosen because it offered superior performance compared to the other diodes compared. Part of the diode analysis supplied diode impedance information as a function of load resistance. This information is used to match up the coplanar stripline's impedance with the real impedance of the diode component. Also, the imaginary part of the diode would be used to determine the placement of the shunt capacitor from the diode in order to cancel out the imaginary part of the impedance.

Analysis of the coplanar stripline (CPS) was conducted using ANSYS Ansoft HFSS software tool. These studies also found that the greater the separation gap between the two striplines of the CPS the lower the total attenuation and the higher the impedance of the structure. All these CPS studies are important design parameters because they help in the design process in achieving the highest RF-to-DC conversion efficiency objective.

Design of a back-to-back Balun transition structure was also completed. The back-to-back Balun transition structure is a tool that allows correct feeding of the CPS designs (antenna + filter, rectifier, and rectenna). A novel CPS-to-Klopfenstein taper back-to-back transition was designed. Simulated and measured results were compared and were in agreement.

CHAPTER VII

CONCLUSIONS

In conclusion to this work three main objectives were reached. The first objective of this research pursued the design and analysis of a power beam medium and its possible benefits for future satellites as an additional source of power in the space environment. Future advancements in this area should consider a tapered amplitude coming from the transmitter of the GEO-SSPS. A tapered amplitude may offer a wider coverage range for the dynamic power beam medium scenario. Also, to advance the satellite re-fueling research area a software tool such as Systems Tool Kit (STK) should be used to design both SSPS and lower orbiting satellite orbits. This way a four dimensional space environment can be visualized more easily. Another study to advance this research area is to consider sub-arrays from various SSPS to share the power supplied to other satellites, beam safety techniques for the dynamic power beam medium, satellite servicing plan, etc.

The second objective of this research pursued a mission design concept using a pair of modern small satellites as MWPT technology demonstrators. Using a program such as STK can help in visualizing the mission profile more easily and accurately. A list of different missions should be considered relative to what MWPT technologies need to be validated. The third objective pursued the design of a space rectenna array part of the HPGU to be equipped on a power receiving daughter satellite as an experimental

payload. The space rectenna array system design is a topic for future research. This includes testing the rectenna array performance under the conditions of space. This includes integrating the PV array with the rectenna array and testing the performance of each array simultaneously under the conditions of space. Ultimately, research in the design for both a transmitting and a receiving satellite needs to be implemented.

REFERENCES

[1] N. J. C. Tech. (2015). *Global Climate Change: Vital Signs of the Planet*. Available: http://climate.nasa.gov/

[2] C. J. A. Bradshaw and B. W. Brook, "Human population reduction is not a quick fix for environmental problems," *National Academy of Sciences,* vol. 111, Nov. 18 2014.

[3] P. E. Glaser, "Power from the Sun: Its Future," *Science,* vol. 162, pp. 857-861, November 22 1968.

[4] R. H. Dietz, G. D. Arndt, J. W. Seyl, L. Leopold, and J. S. Kelley, "Satellite Power System. Concept development and evalutation program, power transmission and reception. Technical summary and assessment," July 1981.

[5] J. C. Mankins and J. Howell, "Overview of the space solar power exploratory research and technology program," presented at the 35th Intersociety Energy Conversion Eng. Conf., Las Vegas, NV, 2000.

[6] S. Gao, K. Clark, M. Unwin, J. Zackrisson, W. A. Shiroma, J. M. Akagi*, et al.*, "Antennas for Modern Small Satellites," *Antennas and Propagation Magazine, IEEE,* vol. 51, pp. 40-56, 2009.

[7] J. O. McSpadden, F. Lu, and K. Chang, "Design and experiments of a high-conversion-efficiency 5.8-GHz rectenna," *Microwave Theory and Techniques, IEEE Transactions on,* vol. 46, pp. 2053-2060, 1998.

[8] T. W. Yoo and K. Chang, "Theoretical and Experimental Development of 10 and 35 GHz Rectennas," *IEEE Transaction on Microwave Theory and Techniques,* vol. 40, pp. 1259-1266, 1992.

[9] B. Strassner and K. Chang, "5.8-GHz circularly polarized rectifying antenna for wireless microwave power transmission," *Microwave Theory and Techniques, IEEE Transactions on,* vol. 50, pp. 1870-1876, 2002.

[10] J. A. Layzer, *The Environmental Case: Translating Values Into Policy*. Washington, DC: CQ Press, a division of Congressional Quarterly Inc, 2005.

[11] *worldometers*. Available: http://www.worldometers.info/world-population/#pastfuture

[12] NASA. (2015). *Global Climate Change: Vital Signs of the Planet*. Available: http://climate.nasa.gov/effects/

[13] C. A. M. Bergsrud, R. Bernaciak, S. Chaieb, and J. Casler, "Rectenna Array Equipped on Satellites," *Journal of Spacecraft and Rockets,* vol. 0, pp. 1-14, 2016.

[14] C. Bergsrud and J. Straub, "A space-to-space microwave wireless power transmission experiential mission using small satellites," *Acta Astronautica,* vol. 103, pp. 193-203, 2014.

[15] T. Valone, *Harnessing the Wheelwork of Nature Tesla's Science of Energy*. Kempton, Illinois: Adventures Unlimited Press, 2002.

[16] J. C. Maxwell, *A Dynamical Theory of the Electromagnetic Field* vol. 155: Royal Society Transactions, 1865.

[17] W. C. Brown, "The history of power transmission by radio waves," *IEEE Transactions on Microwave Theory and Techniques,* vol. MTT-32, pp. 1230-1242, September 1984.

[18] H. Hertz, *Electric Waves-Research on the Propagation of Electric Action with Finite Velocity Through Space*. New York: Dover Publications, Inc., 1962.

[19] H. Boot and J. Randall, "Historical notes on the cavity magnetron," *IEEE Trans. Electron Devices,* vol. 23, July 1976.

[20] W. Brown, "Rectification," in *Microwave Power Engineering: Generation, Transmission, Rectification*. vol. 1, E. Okress, Ed., ed New York, New York: Academic Press Inc., 1968, pp. 273-276.

[21] W. Brown, "A survey of the elements of power transmission by microwave beam," *IRE International Convention Record,* vol. 9, pp. 93-106, 1961.

[22] W. C. Brown, "Experiments involving a microwave beam to power and position a helicopter," *IEEE Trans. Aerospace Electron System,* vol. 5, pp. 692-702, Sept. 1969.

[23] W. C. Brown, R. H. George, N. I. Heenan, and R. C. Wonson, "Microwave to DC Converter," United States of America Patent 3,434,678, 1969.

[24] W. C. Brown, "The history of the development of the rectenna," in *Rectenna Session of the SPS Microwave Systems Workshop*, LyndonB. Johnson Space Center, Houston, Texas, 1980, pp. 271-280.

[25] P. E. Glaser, "Method and Apparatus for Converting Solar Radiation to Electrical Power," United States of America Patent 3,781,647, 1973.

[26] C. Bergsrud, R. Bernaciak, B. Kading, J. McClure, J. Straub, S. Shahukhal*, et al.*, "Nano SSP Satellite," *Online Journal of Space Communication,* 2014.

[27] J. Schlesak, A. Alden, and T. Ohno, "SHARP rectenna and low altitude flight trials," in *IEEE Global Telecommun.*, New Orleans, LA, USA, 1985.

[28] H. Matsumoto, N. Kaya, M. Fuyita, T. Fujtwara, and T. Sato, "Microwave lifted airplane experiment with active phased array antennas," *Kyoto University, Kyoto, Japan, MILAX,* 1995.

[29] N. Kaya, H. Matsumoto, S. Miyatake, I. Kimura, M. Nagatomo, and T. Obayashi, "Nonlinear interaction of strong microwave beam with the ionosphere MINIX rocket experiment," *Space Solar Power,* vol. 6, 1986.

[30] H. Matsumoto and T. Kimura, "Nonlinear excitation of electron cyclotron waves by a monochromatic strong microwave: Computer simulation analysis of the MINIX results," *Space Solar Power Review,* vol. 6, pp. 187-191, 1986.

[31] M. Nagatomo, N. Kaya, and H. Matsumoto, "Engineering aspect of the microwave ionosphere nonlinear interaction experiment (MINIX) with a sounding rocket," *Acta Astronautica,* vol. 13, pp. 23-29, 1986.

[32] R. Akiba, K. Miura, M. Hinada, H. Matsumoto, and N. Kaya, "ISY-METS Rocket Experiment," Japan Aerospace Exploration Agency1993.

[33] N. Kaya, H. Kojima, H. Matsumoto, M. Hinada, and R. Akiba, "ISY-METS rocket experiment for microwave energy transmission," *Acta Astronautica,* vol. 34, pp. 43-46, 1994.

[34] J. McSpadden, F. E. Little, M. B. Duke, and A. Ignatiev, "An in-space wireless energy transmission experiment," in *Intersociety Energy Conversion Engineering Conference*, Washington, D.C., 1996.

[35] G. P. Barnhard, "Space-to-Space Power Beaming," presented at the International Space Development Conference, Los Angeles, California, 2014.

[36] G. P. Barnhard, "Unbundling space power systems to foster applications of space-to-space power beaming," presented at the IAC, Toronto, Canada, 2014.

[37] B. I. Strassner and K. Chang, "Microwave Power Transmission: Historical Milestones and System Components," *IEEE,* pp. 1379-1396, 2013.

[38] B. Strassner and K. Chang, "Highly efficient C-band circularly polarized rectifying antenna array for wireless microwave power transmission," *Antennas and Propagation, IEEE Transactions on,* vol. 51, pp. 1347-1356, 2003.

[39] S. S. Bharj, R. Camisa, S. Grober, F. Wozniak, and E. Pendleton, "High Efficiency C-Band 1000 Element Rectenna Array for Microwave powered Applications," presented at the IEEE MTT-S International Microwave Symposium Digest, 1992.

[40] S. Adachi and Y. Sato, "Microwave-to-dc conversion loss of rectenna," *Space Solar Power Rev.,* vol. 5, pp. 357-363, 1985.

[41] Y.-J. Ren and K. Chang, "5.8 GHz circularly polarized dual-diode rectenna and rectenna array for microwave power transmission," *IEEE Trans. Microw. Theory Tech.,* vol. 51, pp. 1495-1502, Apr. 2006.

[42] H. Sun, Y. X. Guo, M. He, and Z. Zhong, "Design of a high-efficiency 2.45-GHz rectenna for low-input-power energy harvesting," *IEEE Trans. Antennas and Wireless Prop. Letters,* vol. 11, 2012.

[43] J. T. Sun, X. X. Yang, T. Yoshimasu, and X. M. Sun, "Bow-Tie Loop Printed Antenna with High Gain and Broad Beam Width for 5.8Ghz Rectenna Application," in *Circuits and Systems for Communications, 2008. ICCSC 2008. 4th IEEE International Conference on*, 2008, pp. 312-314.

[44] X. M. Sun, Y. Y. Gao, X. X. Yang, and H. H. Wang, "A High Gain Printed Dual-Loop Antenna Fed by CPS with Broad Beam," in *Microwave Conference, 2008 China-Japan Joint*, 2008, pp. 450-453.

[45] T. Wen-Hua and K. Chang, "Wide-band microstrip-to-coplanar stripline/slotline transitions," *Microwave Theory and Techniques, IEEE Transactions on,* vol. 54, pp. 1084-1089, 2006.

[46] R. N. Simons, N. I. Dib, and L. P. B. Katehi, "Coplanar stripline to microstrip transition," *Electronics Letters,* vol. 31, pp. 1725-1726, 1995.

[47] S. Young-Ho and K. Chang, "A wideband coplanar stripline to microstrip transition," *Microwave and Wireless Components Letters, IEEE,* vol. 11, pp. 28-29, 2001.

[48] M. Tanaka, Y. Suzuki, K. Araki, and R. Suzuki, "Microstrip antenna with solar cells for microsatellites," *Electronics Letters,* vol. 31, pp. 5-6, 1995.

[49] K. Niotaki, A. Collado, A. Georgiadis, S. Kim, and M. Tentzeris, "Solar/Electromagnetic energy harvesting and wireless power transmission," *Proceedings of the IEEE,* vol. 102, pp. 1712-1722, November 2014.

[50] M. Zawadzki and J. Huang, "Integrated RF antenna and solar array for spacecraft application," in *Phased Array Systems and Technology, 2000. Proceedings. 2000 IEEE International Conference on*, 2000, pp. 239-242.

[51] W. C. Brown and E. E. Eves, "Beamed microwave power transmission and its application to space," *Microwave Theory and Techniques, IEEE Transactions on,* vol. 40, pp. 1239-1250, 1992.

[52] G. A. Landis, "Solar Power From Space: Separating Speculation from Reality," presented at the XXIth Space Photovoltaic Research and Technology Conference, Cleveland, OH, 2009.

[53] C. A. Balanis, *Antenna Theory*, 3rd ed. Hoboken, New Jersey: John Wiley & Sons, Inc., 2005.

[54] Global Positioning System (GPS) 2F Satellite [Online]. Available: http://www.losangeles.af.mil/library/factsheets/factsheet.asp?id=18670

[55] Global Positioning System (GPS) 2R/2R-M Satellite [Online]. Available: http://www.losangeles.af.mil/library/factsheets/factsheet.asp?id=18671

[56] J. O. McSpadden and J. C. Mankins, "Space solar power programs and microwave wireless power transmission technology," *Microwave Magazine, IEEE,* vol. 3, pp. 46-57, 2002.

[57] J. W. Dankanich, C. Vassallo, and M. Tadge, "Space-to-space power beaming enabling high performance rapid geocentric orbit transfer," presented at the 51st Propulsion and Energy Forum, Orlando, FL, 2015.

[58] P. Jaffe and J. McSpadden, "Energy Conversion and Transmission Modules for Space Solar Power," *Proceedings of the IEEE,* vol. 101, pp. 1424-1437, 2013.

[59] C. Rodenbeck, S. J. Kokel, K. Chang, and F. Little, "Microwave Wireless Power Transmission with Retrodirective Beam Steering," in *2nd International Energy Conversion Engineering Conference*, ed: American Institute of Aeronautics and Astronautics, 2004.

[60] J. H. Saleh, D. E. Hastings, and D. J. Newman, "Spacecraft design lifetime," *Spacecraft and Rockets,* vol. 39, pp. 244-257, 2002.

[61] -, "AIAA assessment of NASA studies of space solar power concepts," American Institute of Aeronautics and Astronautics, Reston, VA2000.

[62] C. A. Hill, "Satellite battery technology: A tutorial and overview," *IEEE Aerospace and Electronic Systems Magazine,* vol. 26, pp. 38-43, 2011.

[63] M. R. Patel, *Spacecraft Power Systems*. Boca Raton, Florida: CRC Press, 2004.

[64] S. Y. Kim, J.-F. Castet, and J. H. Saleh, "Spacecraft electrical power subsystem: Failure behavior, reliability, and multi-state failure analyses," *Reliability Engineering & System Safety,* vol. 98, pp. 55-65, 2// 2012.

[65] M. Tafazoli, "A study of on-orbit spacecraft failures," *Acta Astronautica,* vol. 64, pp. 195-205, Jan.-Feb. 2009.

[66] J. K. McDermott, J. P. Schneider, and S. W. Enger, "Power," in *Space Mission Engineering: The New SMAD*, J. R. Wertz, D. F. Everett, and J. J. Puschell, Eds., ed Hawthorne, CA: Microcosm Press, 2011, pp. 641-662.

[67] S. W. Janson, "The Future of Small Satellites," in *Small Satellites: Past, Present, and Future*, H. Helvajian and S. W. Janson, Eds., ed Reston, VA: AIAA, 2008, pp. 771-814.

[68] T. Shimizu and C. Underwood, "Super-capacitor energy storage for micro-satellites: Feasibility and potential mission applications," *Acta Astronautica,* vol. 85, pp. 138-154, 2013.

[69] C. Valenta and G. Durgin, "Harvesting Wireless Power," *IEEE Microwave Magazine,* vol. 15, pp. 108-120, June 2014.

[70] -, "RT/Duroid 6002," Rogers Corporation2014.

[71] J. Coonrod, "Sending Circuit Materials Into Space," vol. 2014, ed. Online: Microwave Journal, 2014.

[72] -, "Low Outgassing Characteristics of Rogers Laminates Approved for Spacecraft Applications," R. Corporation, Ed., ed. Online, 2002.

[73] Y. Han, O. Leitermann, D. A. Jackson, J. M. Rivas, and D. J. Perreault, "Resistance compression networks for radio-frequency power conversion," *IEEE Trans. on Power Electronics,* vol. 22, pp. 41-53, Jan. 2007.

[74] J. McSpadden, "Rectenna cover for a wireless power receptor," ed: Google Patents, 2010.

[75] D. M. Pozar, "The active element pattern," *Antennas and Propagation, IEEE Transactions on,* vol. 42, pp. 1176-1178, 1994.

[76] N. Amitay, J. S. Cook, R. G. Pecina, and C. P. Wu, "On mutual coupling and matching conditions in large planar phased arrays," *IEEE G-AP Internat\'l Symp. Digest,* pp. 150-156, 1964.

[77] M. C. Casey, R. A. Gigliuto, J. M. Lauenstein, E. P. Wilcox, A. M. Phan, H. Kim, *et al.*, "Destructive Single-Event Failures in Schottky Diodes," NASA Goddard Space Flight Center, Greenbelt, MD2013.

[78] L. Boccia and O. Breinbjerg, "Antenna Basics," in *Space Antenna Handbook*, W. A. Imbriale, S. Gao, and L. Boccia, Eds., ed The Atrium, Sourthern Gate, Chichester, West Sussex, United Kingdom: John Wiley & Sons, Ltd, 2012, pp. 1-35.

[79] G. Warwick, "DARPA's Phoenix Would Harvest Dead Satellites," *Aviation Week.com,* 2013.

[80] J. C. Mankins, *The Case for Space Solar Power*. Houston, TX: The Virginia Edition, Inc., 2014.

[81] J. W. Lee, Y. K. Anguchamy, and B. N. Popov, "Simulation of charge-discharge cycling of lithium-ion batteries under low-earth-orbit conditions," *Power Sources,* pp. 1395-1400, Sept. 2006.

[82] W. Ley and R. Roder, "Electrical Power Supply," in *Handbook of Space Technology*, W. Ley, K. Wittmann, and W. Hallmann, Eds., ed United Kingdom: John Wiley and Sons, 2008.

[83] D. F. Everett, "Overview of Spacecraft Design," in *Space Mission Engineering: The New SMAD*, J. R. Wertz, D. F. Everett, and J. J. Puschell, Eds., ed Hawthorne, CA: Microcosm Press, 2011, pp. 397-438.

[84] E. Bashevkin, J. Kenahan, B. Manning, B. Mahlstedt, and A. Kalman, "A Novel Hemispherical Anti-Twist Tracking System (HATTS) for CubeSats," 2012.

[85] R. Emrick. (2015, April) IMS2015 Special and Focus Sessions. *IEEE Microwave Magazine*. 28-30.

[86] C. P. S. University. (2015, 4/6). *CubeSat Design Specification Rev 13*. Available: http://www.cubesat.net/images/developers/cds_rev13_final2.pdf

[87] M. Swartwout, "The first one hundred cubesats: A statistical look," *Journal of Small Satellites,* vol. 2, pp. 213-233, Dec. 2013.

[88] R. M. Crook, "NPS Cubesat Launcher Design, Process and Requirements," Masters of Science, Naval Postgraduate School, Monterey, California, 2009.

[89] DoD, "Secondary Payload Planner's Guide For Use On The EELV Secondary Payload Adapter," DoD Space Test ProgramJun 2009.

[90] C. Bergsrud, S. Chaieb, and S. Plathottam, "Realizing GEO-SSPS concepts with modern small satellites," *Acta Astronautica,* 2015.

[91] C. Bergsrud and S. Noghanian, "Investigating the design of a nano space solar power satellite," in *IEEE Antenna and Propagation*, Memphis, TN, 2014.

[92] P. Jaffe, "A Sunlight to Microwave Power Transmission Module Prototype for Space Solar Power," Doctor of Philosophy, Electrical and Computer Engineering, University of Maryland, College Park, Maryland, 2013.

[93] H. Hausman. (2008, January) Comparison of High Power Amplifier Technologies: TWTAs vs SSPAs. *Microwave Product Digest*. Available: http://www.mpdigest.com/issue/articles/2008/jan/miteq/default.asp

[94] A. Vladimir, *Orbital Mechanics*, 3 ed. Wright-Patterson Air Force Base, Ohio: AIAA, 2002.

[95] T. Logsdon, *Orbital Mechanics Theory and Applications*. New York: John Wiley and Sons, INC, 1998.

[96] R. Twiggs and B. Malphrus, "CubeSats," in *Space Mission Engineering: The New SMAD*, J. R. Wertz, D. F. Everett, and J. J. Puschell, Eds., ed Hawthorne, CA: Microcosm Press, 2011, pp. 803-828.

[97] B. S. P. a. Systems. (2012, Aug. 12). *Propulsion for CubeSats and NanoSats*. Available: http://www.busek.com/cubesatprop__main.htm

[98] M. Uno and K. Tanaka, "Spacecraft Electrical Power System using Lithium-Ion Capacitors," *IEEE Transactions on Aerospace and Electronic Systems,* vol. 49, pp. 175-188, 2013.

[99] Spectrolab, "29.5% NeXt Triple Junction (XTJ) Solar Cells," Boeing, Ed., ed, 2012.

[100] Azurspace, "30% Triple Junction GaAs Solar Cell," A. S. S. P. GMBH, Ed., ed, 2014.

[101] H. Oman, "Solar power from space new developments make it practical," *Aerospace and Electronic Systems Magazine, IEEE,* vol. 16, pp. 17-26, 2001.

[102] R. Garg, P. Bhartia, I. Bahl, and A. Ittipiboon, *Microstrip Antenna Design Handbook*. Norwood, MA: Artech House, Inc., 2001.

[103] D. M. Pozar, "Microstrip Antennas," *Proceedings of the IEEE,* vol. 80, pp. 79-91, January 1992.

[104] D. M. Pozar and B. Kaufman, "Comparison of three methods for the measurement of printed antenna efficiency," *Antennas and Propagation, IEEE Transactions on,* vol. 36, pp. 136-139, 1988.

[105] J. S. Prowald and L. S. Drioli, "Space Environment and Materials," in *Space Antenna Handbook*, W. A. Imbriale, S. Gao, and L. Boccia, Eds., ed The Atrium, Southern Gate, Chichester, West Sussex, United Kingdom: John Wiley & Sons, Ltd, 2012, pp. 106-132.

[106] S. Gao, M. Brenchley, M. Unwin, C. I. Underwood, K. Clark, K. Maynard*, et al.*, "Antennas for small satellites," in *Antennas and Propagation Conference, 2008. LAPC 2008. Loughborough*, 2008, pp. 66-69.

[107] L. G. Maloratsky, "Reviewing the basics of microstrip lines," *Microwaves and RF,* pp. 79-88, March 2000.

[108] Y. J. Ren and K. Chang, "5.8-GHz circularly polarized dual-diode rectenna and rectenna array for microwave power transmission," *Microwave Theory and Techniques, IEEE Transactions on,* vol. 54, pp. 1495-1502, 2006.

[109] I. M. A. Ireban, "Transmission Lines and Schottky Diode," Islamic University of Gaza.

[110] R. Garg, I. Bahl, and M. Bozzi, "Coplanar Lines: Coplanar Waveguide and Coplanar Strips," in *Microstip Lines and Slotlines*, 3rd ed Boston, MA: Artech House, 2013, pp. 347-432.

[111] G. Ghione and C. Naldi, "Analytical formulas for coplanar lines in hybrid and monolithic MICs," *Electronics Letters,* vol. 20, pp. 179-181, 1984.

[112] S. Young-Ho and C. Kai, "Coplanar stripline resonators modeling and applications to filters," *Microwave Theory and Techniques, IEEE Transactions on,* vol. 50, pp. 1289-1296, 2002.

[113] D. M. Pozar, "Impedance Matching and Tuning," in *Microwave Engineering*, 3 ed Hoboken, NJ: John Wiley & Sons, Inc., 2005, pp. 222-265.